5-2021

Numerical Modeling for Patch Antennas

Luis Mario Bres Castro
The University of Texas Rio Grande Valley

NUMERICAL MODELING FOR PATCH ANTENNAS

A Thesis

by

LUIS MARIO BRES CASTRO

Submitted to the Graduate College of
The University of Texas Rio Grande Valley
In partial fulfillment of the requirements for the degree of

MASTER OF SCIENCE

May 2021

Major Subject: Physics

NUMERICAL MODELING FOR PATCH ANTENNAS

A Thesis
by
LUIS MARIO BRES CASTRO

COMMITTEE MEMBERS

Dr. Volker Quetschke
Chair of Committee

Dr. Teviet Creighton
Committee Member

Dr. Hyeongjun Kim
Committee Member

May 2021

ABSTRACT

Bres, Luis M., Numerical Modeling for Patch Antennas. Master of Science (MS), May, 2021, 93 pp., 2 tables, 70 figures, 22 references.

This thesis will focus on creating a number of designs that will be tested in a simulation environment using an electromagnetic solver software called Computer Simulation Technology (CST) as well as we are going to develop our own model to be able to simulate more complex design due to the limitations of CST licensing. The simulations will help us optimize the parameters of gain-frequency allocation for future projects of antenna building. After doing a parametric study of a patch antenna we will develop a model for the return signal of a signal patch antenna, we will present four potential models. The first model is the circuit model for return signal, the second is the solutions of the wave equation that works with the geometry of the patch antenna, the third is the solutions of the wave equation but by using its correspondent eigien-values (on this variant we actually developed the patch antenna output return signal), and the fourth variant will be the implementation of the Wave Iterative Method. After doing this we will present a phased array iteration study in which we will show the radiation pattern of a single antenna, a 2x2, 3x3, 4x4, 5x5, 6x6, 7x7, and 8x8 phased array element. The purpose of this thesis is to develop our own model to simulate a patch antenna in order to decrease our dependence on commercial electromagnetic software.

DEDICATION

To my family:

You all have been there for me in my most adverse times and have always had my back, and also in my best most joyful moments as we have celebrated. To you I will always be thankful for the privilege of being part of our family.

ACKNOWLEDGMENTS

I am grateful for the guidance provided by my advisor Dr. Jenet, Dr. Quetschke and Dr. Creighton members of the CARA Executive Committe. Thanks to all of my research mates, Keeisi Caballero, Andrea Tellez, Louis Dartez, Suryarao Bethapudi, Keith Bolher, and Francisco Llamas for being in my journey and helping me around the way.

I thank the Department of Physics & Astronomy at the University of Texas Rio Grande Valley for providing the setting and support that allowed this work to be done and for providing me the undergraduate and graduate preparation for this thesis and my degree. Thanks to Project Space for the numerous scholarships provided so that I could continue pursuing my career.

TABLE OF CONTENTS

Page

LIST OF TABLES

Page

LIST OF FIGURES

CHAPTER I

INTRODUCTION

A patch antenna is an easy to print, low cost, element consisting of a patch, a substrate dielectric and a ground plane. These antennas are small working around the microwave frequencies, they emit radiation at a certain resonant frequency, and the practical applications for the patch antennas are for tracking and are heavily used in the telecommunications industry.

Patch antennas consist of a flat rectangular sheet (patch) of metal mounted over a larger sheet of a dielectric circuit board which is itself mounted over a ground copper plane of the same size. To design a high efficiency coaxial cable is necessary to consider the basic characteristics of the antenna. As seen on figures 1.1a and 1.1b the dimensions to be considered are the length and width of the patch (L_p , W_p, copper), height of the substrate material (h, substrate material), length and width of the conductive ground plane (L_g, W_g, copper), thickness of the patch ante conductive ground plane (t), radius of the cable or pin (r_i, copper), radius of the dielectric cover of the pin (r_o, Teflon), and radius of the conductive cover for the cable ($r_o + t$, copper).

To calculate these dimensions, it's necessary to rely on a set of equations specifically derived to build these type of antennas. The only input variables are the substrate height, the patch and ground plane thickness, the dielectric constant of the substrate, and the standard dimensions for the cable which in this case will be an SMP connector. Sub-Miniature push-on (SMP) Connectors are plug-in connectors for applications up to 40 GHz and the standard value of it's impedance is $50\,\Omega$.

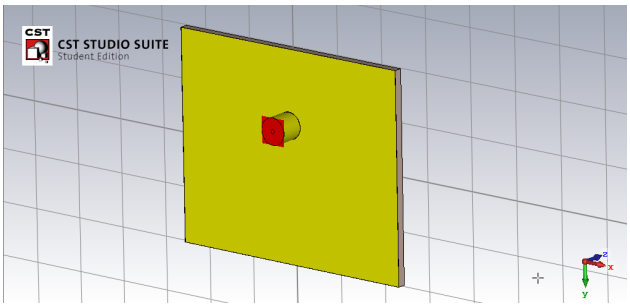

(a) Bottom view from the coaxial cable which is located at the bottom of the patch antenna (Generated from CST).

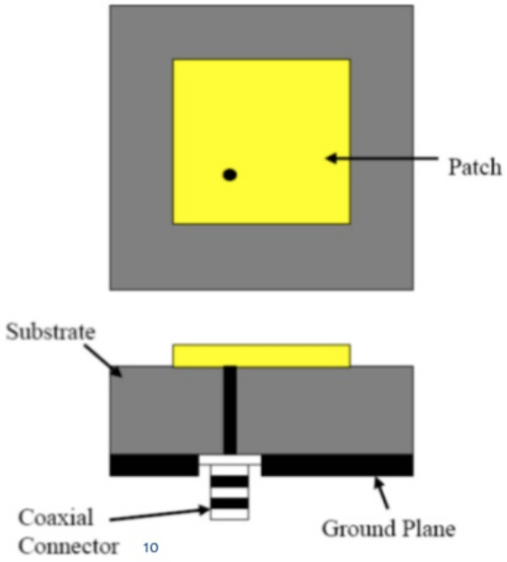

(b) Detailed structure of a patch antenna [14].

Figure 1.1: Geometrical look of patch antenna in Computer Simulation Technology (CST).

CHAPTER II

SIMULATION TECHNIQUES

2.1 Computer Simulation Technology

Most of the computed simulations are going to be generated from the software of Computer Simulation Technology (CST). CST is a licensed software that generates electromagnetic solutions of different types of antennas. All of the related literature can be generated and simulated using this software. Some physical testing to antennas is going to be done using a 2.25 GHz coaxial cable patch antenna with a Rohde Schwarz FSH3-Spectrum Analyzer that works from 100 kHz to 3 GHz.

2.2 Transmission Line Model

A rectangular micro-strip patch antenna can be defined by its principal parameters like width W, length L and substrate thickness h which creates an array of two radiating narrow apertures separated by a distance. Because of this we can derive a transmission line model based on the solutions of a circuit model that is dependent on the low impedance Z_c, a transmission line length of l and a characteristic impedance Z_0 with a propagation constant determined by the antenna dimensions. In this model we are going to rely on these parameters in order to have a return loss plot based on the circuit configuration of the antenna.

2.3 Cavity Model

This model analyzes the geometrical properties of the patch antenna, it's bounded by electric walls on the top and bottom, and it's bounded at the side by magnetic walls. Because of this, the antenna exhibits several orders of resonance and that's why there are different resonant frequencies in a given antenna. The fields traveling on the $\hat{z}$ axis are more easily found by using this method.

2.4 Wave Iterative Method

The purpose of the development of this method was to be a source-free alternative to the expensive 3D electromagnetic solvers in the market. The Wave Iterative Method (WIM) has its fundamental pillars with the reflection, transmission and incident electromagnetic waves calculated by the geometric properties of the patch antenna.

The main difference of this method is that instead of using time and frequency signals, it used pixels signals (as general coordinates) and modal signals. These configuration is analogous to the time and frequency signals used in other methods. With WIM we can calculate the return signal of a patch antenna, it's surface electric and magnetic field. This is a medium based method, meaning that we replicate this method every time there is refraction of the waves induced by a difference in medium.

CHAPTER III

THEORETICAL FRAMEWORK

The key of how to treat the problem of a patch antenna is based on it's geometry and on the signal modeling of your choice. On figure 3.1a we can see depending on which axis (polarization) you place the feed point is going to determine the way to treat the equations to design the patch antenna. As we see on equation 3.1 if we place the feed point only on the y axis which is the length polarization, the resonant frequency is going to have the m mode. If we place the cable in the x axis or the width polarization we are going to get the n mode. These modes are the polarization modes of your antenna which will indicate the operational resonant frequency overall. There are an infinite number of resonant modes which of course is going to change the resonant frequency and the shape of the signal and for the purpose of this investigation we are setting the values of m and n to 1. If you place the feed point on (x,y) coordinates, then the resonant frequency equation is going to include both m and n modes and the return signal is going to have both resonant frequencies [3, p. 830]. Since we have a patch antenna in which sides are of different dimensions we would be getting two different resonant frequencies, but if we were to have a square patch antenna then the resonant frequencies would be the same.

$$(f_r)_{mnp} = \frac{c}{2\sqrt{\varepsilon_{eff}}}\sqrt{\left(\frac{m\pi}{L_p}\right)^2 + \left(\frac{n\pi}{W_p}\right)^2 + \left(\frac{p\pi}{h}\right)^2} \tag{3.1}$$

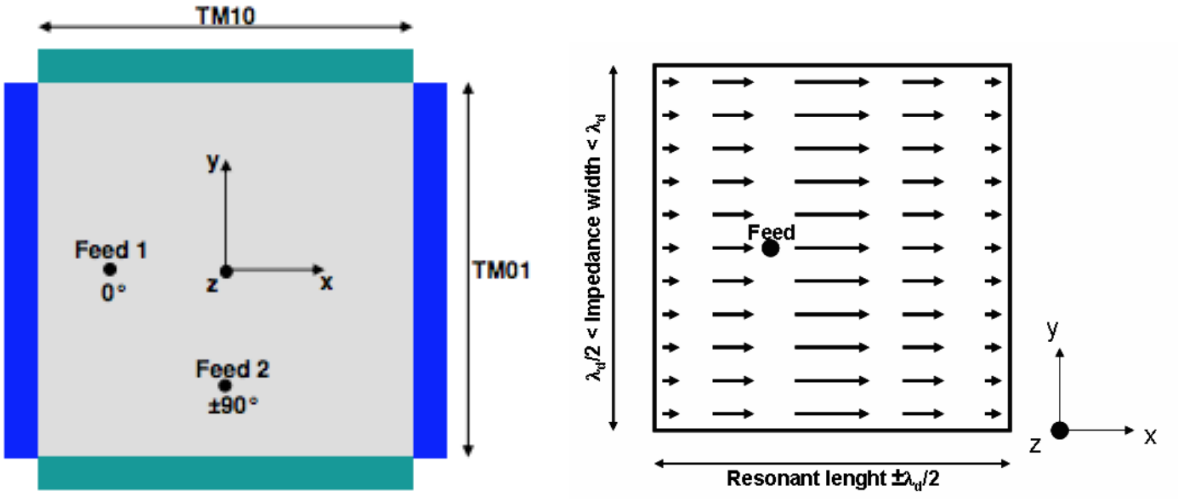

(a) Antenna polarization [16].

(b) Current distribution on the patch surface [16].

Figure 3.1: Antenna fundamentals

For the current distribution, when you are at the center the current distribution is at its maximum, and when you are at the edges the current is at its minimum. Given this information, we can see on figure 3.2c if you place the feed at the center then you will get an impedance of zero, which will generate no radiation. And when you are at the edge of impedance width, you will get maximum impedance, but when you calculate the intersection point, that is dependent on the location in the patch, of the voltage and the current you will achieve maximum output and efficiency [16, p. 4].

On figure 3.2a we can see the cross section of a patch antenna and its individual parts. At the top we see the patch antenna, which is always smaller than the ground plane and with the same material. And at the middle we can see the the dielectric substrate. This configuration produces the fringe fields which are caused by the difference in the dimensions of the patch and the ground plane and they produce the radiation of the antenna. If both the patch and the ground plane were in the same dimensions, then the antenna would behave like a capacitor. We also can see the feed point incision which is inserted at the bottom of the patch, and it goes through the substrate all the way to being connected to the patch.

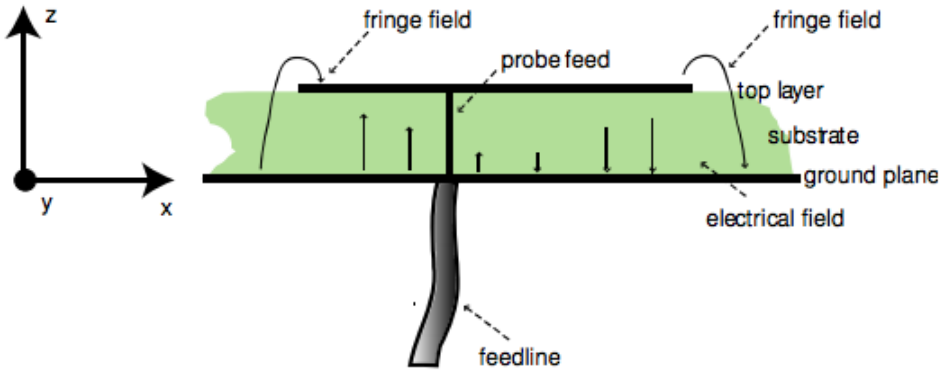

(a) Cross section of a patch antenna [16].

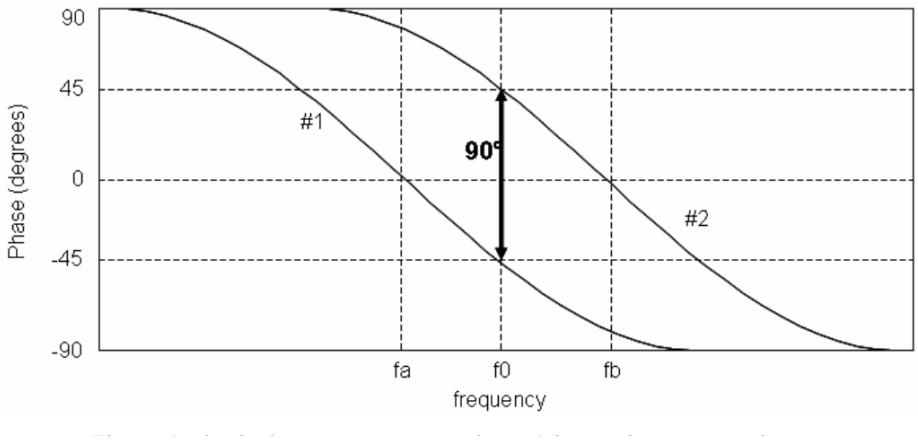

(b) Dual resonant frequency phase diagram [16].

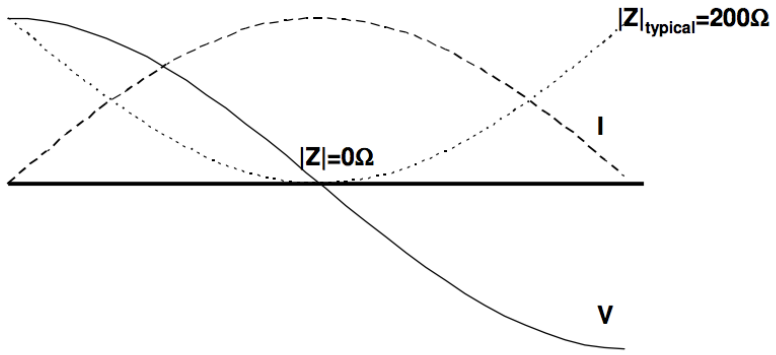

(c) Voltage (V), current (I) and impedance ($|Z|$) distribution along the patch's resonant distance [16].

Figure 3.2: Antenna fundamentals literature.

On figure 3.2b we observe the behaviour of the cable placed at both axis being reflected at the phased diagram as function and the stark difference of both length and width polarizations is about 90°. As we can see on figure 3.1b there are two elements in which high efficiency for a patch antenna can be achieved: resonant width and impedance length. Knowing where to place your feed point will be crucial in order to get high efficiency for your antenna.

3.1 S-Parameters

S-Parameters describe the relationship between the input value and output value in an electrical system, which in this case is dealing with voltage. This is the first result that we are going to deal on this study. As we can see on figure 3.3, we have a magnitude as function of frequency and the minimum value retrieved is called the resonant frequency of the system. On figure 3.3, we see that the y-axis is labeled as S_{11}, this means that in the system, there is only one feed (or for our purposes one cable inserted in the antenna) [5].

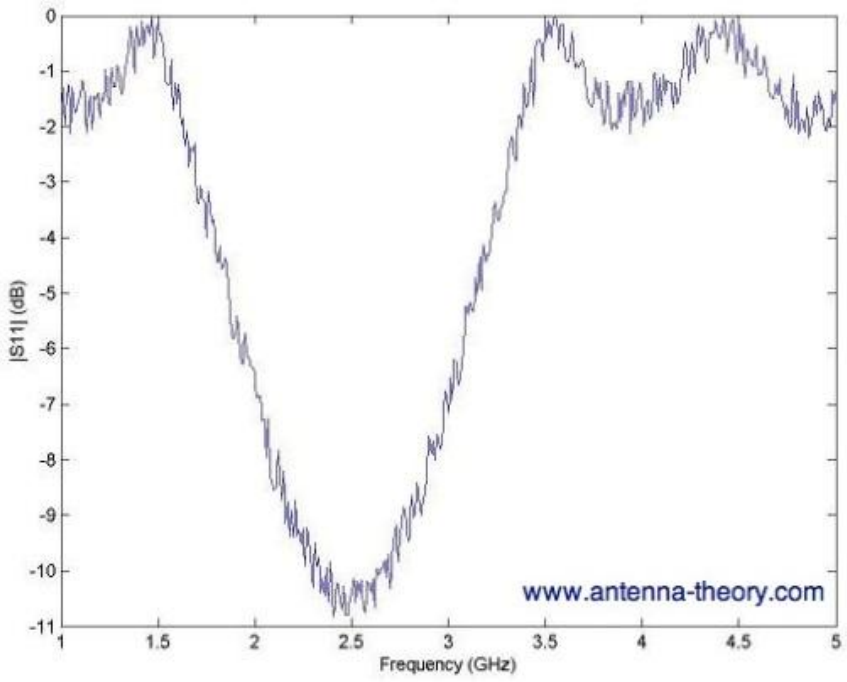

Figure 3.3: S-Parameters as function of frequency (S_{11}) [5].

If we have a system of two ports, then we will have the following:

$$\vec{b}_i = \hat{S}_{ij}\vec{a}_i \tag{3.2}$$

Figure 3.4: Two port black box [19].

This matrix on equation 3.2, which is called a scattering matrix for S-Parameters, will calculate the s-parameters depending on the numbers of feeds in the system. For example, if we have two feeds in the system, then in the S-Parameters matrix there will be only four elements, S_{11}, S_{12}, S_{21}, and S_{22}. The same subscript elements represent the reflection coefficients of the antenna in display, physically, it represents the return loss of antenna n. The physical significance of return loss is the power stored at desired resonant frequency and reflected at the remained frequencies. Different subscript elements represent the transmission coefficients in a system of antennas, basically how much power is being transmitted from antenna n to antenna m. In the previous case, S_{12} is the power transferred from port 2 to port 1, and S_{21} is the power transferred from port 1 to port 2. To analyze the S-Parameters of an antenna, considering the incident and reflected signal, S_{11} will be the reflected signal as is the ratio between the incident and reflected signal [19]. Having said that we conclude that:

$$RL = 10\log_{10}\frac{P_i}{P_r} \tag{3.3}$$

RL: Return Loss.

P_i: Incident Power.

P_r:Reflected Power.

$$\Gamma = \frac{V_r}{V_i} = \frac{Z_L - Z_o}{Z_L + Z_o} \tag{3.4}$$

$$RL = 10\log_{10}\frac{P_i}{P_r} \tag{3.5}$$

Now if we express the power in terms of voltage, we get:

$$RL(dB) = -20\log_{10}|\Gamma| \tag{3.6}$$

This relationship describes that the return loss measures the power as function of frequency that is reflected out of the antenna. For an antenna to be efficient at resonant frequency, the return loss has to be at its minimum. This means that at resonant frequency most of the power is absorbed by the antenna (to later be analyzed) and outside the resonant frequency the power is reflected.

3.2 Impedance

The impedance of an antenna describes the relationship of the ratio of the voltage and the current. Being practical, it's the same as the resistance in electrical circuits, such that the resistance is proportional to the voltage/current ratio. And the impedance, which is proportional to the voltage/current ratio (it changes depending on the circuits and the geometry), can have complex values. The impedance of an antenna can be expressed in real and imaginary forms. For example if we have in impedance in the form $Z = 50 + j0\,\Omega$, then the voltage and current are exactly in time-phase. But if the impedance is in the form $Z = 0 + j50\,\Omega$, the voltage leads the current by 90° in phase. If we take a look at the impedance of the form $Z = 50 + j50\,\Omega$ we can calculate the magnitude and phase of it.

$$|Z| = \sqrt{Re(Z)^2 + Im(Z)^2} \tag{3.7}$$

$$\phi = \arctan\left(\frac{Im(Z)}{Re(Z)}\right) \tag{3.8}$$

The values of magnitude and phase are $70.71\,\Omega$ and 45° respectively. This means that the current lags the voltage by 45°. And if we want to express the voltage and current as function of

time, we have:

$$V(t) = \cos(2\pi ft) \tag{3.9}$$

$$I(t) = \frac{1}{|Z|}\cos(2\pi ft - \phi) \tag{3.10}$$

The real part of the impedance represents the power that is either radiated away or absorbed within the antenna. The imaginary part of the impedance represents the power that is stored in the near field of the antenna (non-radiated power). And for reference, antennas that only have real impedance are considered resonant antennas, and don't have any mismatch loss [5]. There are two fundamental values to be considered in impedance matching if you want a high efficiency patch antenna, the impedance of your cable and the impedance of your antenna.

The cable's impedance is dependent on its dimensions and dielectric constant of its material and we have standard operational values for it and the antenna's impedance depends on the geometry of itself. Achieving a good matching between these two values is going to make your antenna reflect most of the power it receives. Equation 3.11 describes the cable's impedance, equation 3.12 describes the cutoff frequency of the cable, and on figure 3.5 we can see the transectional view of the cable [11].

$$Z_o = \frac{138}{\sqrt{\varepsilon_r}}\log_{10}(\frac{D_i}{D_o}) \tag{3.11}$$

$$f_{cutoff} = \frac{11.8}{\sqrt{\varepsilon_r}\pi(\frac{D_i+D_o}{2})} \tag{3.12}$$

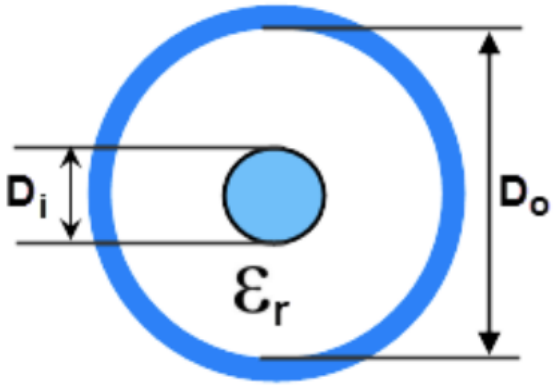

Figure 3.5: Transectional view of a cable [11].

3.3 Smith Chart (Impedance View)

One of the most useful techniques to visualize the impedance of the transmission line (cable's impedance) and the antenna's impedance as function of frequency is the Smith Chart. The Smith Chart is a graphical tool for the determination and efficiency of the return signal and it's an integral part of visualization tools [7].

A huge component of this tool is the reflection coefficient of the antenna (Γ) and antenna's impedance as seen on equation 3.13. The reflection coefficient is the ratio of the complex amplitude of the antenna's reflected and incident signal. Let $Z = R + jX$ be the impedance at some location. The reflection coefficient is:

$$\Gamma = \frac{Z - Z_o}{Z_+ Z_o} = \Gamma_r + j\Gamma_i \tag{3.13}$$

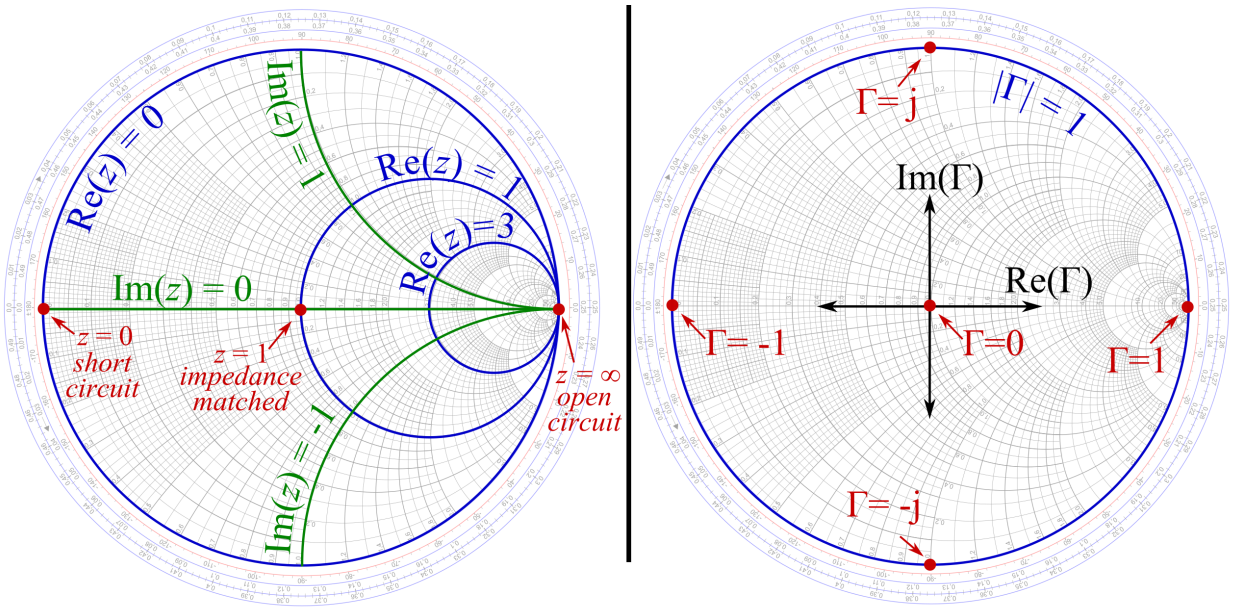

Figure 3.6: Reactance curves and resistance circles [6].

On figure 3.6 we can observe different characteristic of the Smith Chart in which we are going to use for later simulation results. We can see the blue curves representing the real part of the reflection coefficients and the green curves representing the imaginary parts of the reflection coefficients. We see how the real parts of the reflection coefficients are the definition of the resistance circles and how it's radius changes as function of the real part of the normalized impedance line as well as we can see how the reactance curves changes as imaginary part of the normalized impedance line. We also see different coordinates of the plane a circuit can behave. For $z = 0$ the model will be short circuit, when $z = 1$ the model will have its impedance matched with the cable meaning full efficiency of the antenna's output, and when $z = \infty$ the model will have an open circuit, meaning the receiving end of a patch antenna.

3.4 Power Spectrum

The power spectrum is a direct conversion from the s-parameters with more quantities that describes the behavior and health of the signal coming in and out of the antenna.

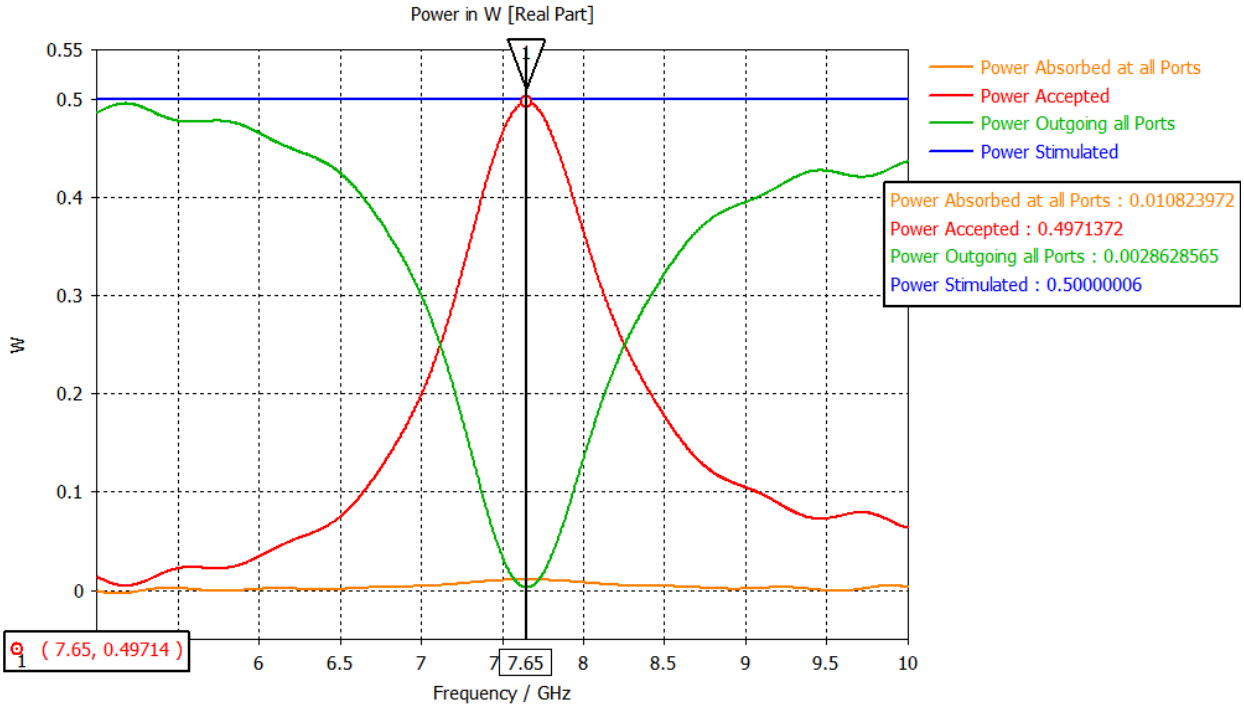

Figure 3.7: Power as function of frequency. Image generated from CST.

As seen on figure 3.7, there are four values to analyze: power absorbed at all ports, power accepted, power outgoing all ports and power stimulated. The power absorbed at all ports describes the power as losses that goes on other ports instead of the port in question. The power accepted is the net energy flow that goes into the ports seen on equation 3.15. Power outgoing all ports is the sum of the power that is reflected from the structure back to the cable or to other ports. And the power stimulated is just simply the input power given to the system (antenna(s)) as calculates on equation 3.14.

$$P_{stim}^{port} = \frac{1}{2}\sum_{n=1}^{N}(Ampl.)_n^2 \tag{3.14}$$

$$P = Re\{\frac{1}{2}\int_A \vec{E}\times\vec{H}^* \cdot dA\} \tag{3.15}$$

3.5 Radiation Pattern

The radiation pattern is the radiation emitted from the antenna as function of space coordinates. There are three types of radiation pattern. The field pattern (in linear scale) describes the electric and magnetic fields as function of angular space. The power pattern (in linear scale) is the same as the field pattern but squared. And the power pattern (in dB) is the magnitude of the electric or magnetic field as function of angular space in decibels [3]. An example can be seen in figure 3.8.

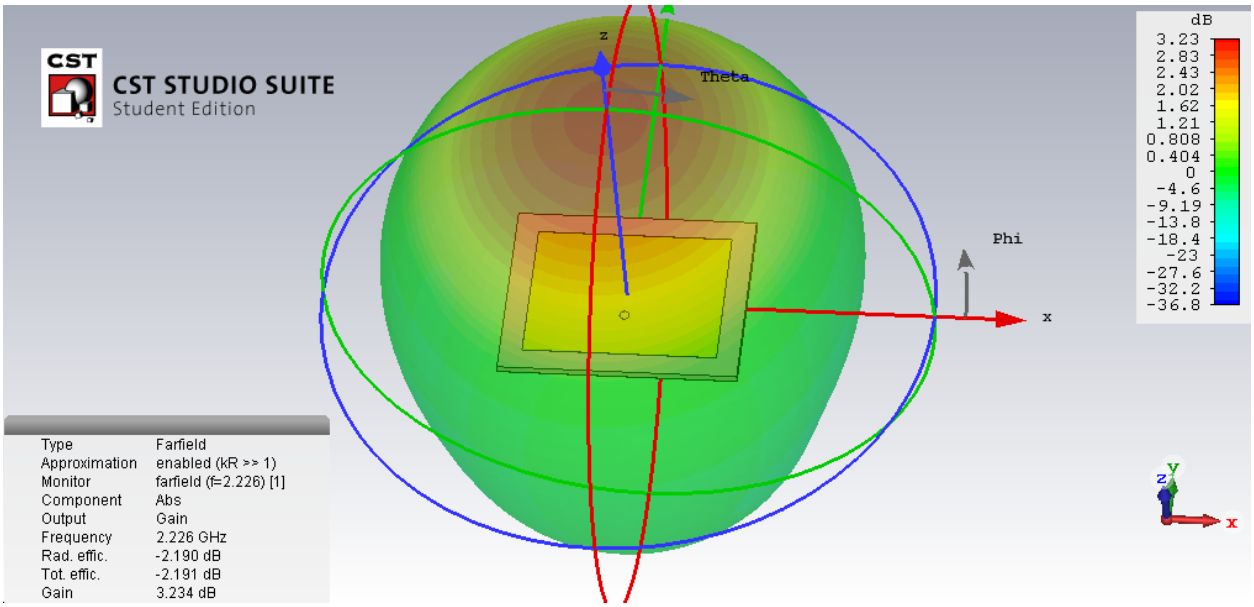

Figure 3.8: Gain as function of space coordinates at a fixed frequency of a patch antenna.

The most important parts of the radiation pattern are the major, side and minor lobes. This lobes are portions of the radiation pattern that is bounded by regions of its respectively radiation intensity. As we can see on figure 3.9a and 3.9b, the major lobe is where most of the radiation intensity is allocated at $\theta = 0$. The side and minor lobes is where the leftover radiation intent is allocated depending on the θ angles respectively. There is also the back lobes which is the lobes in which it has its radiation intensity at $\theta = \pi$.

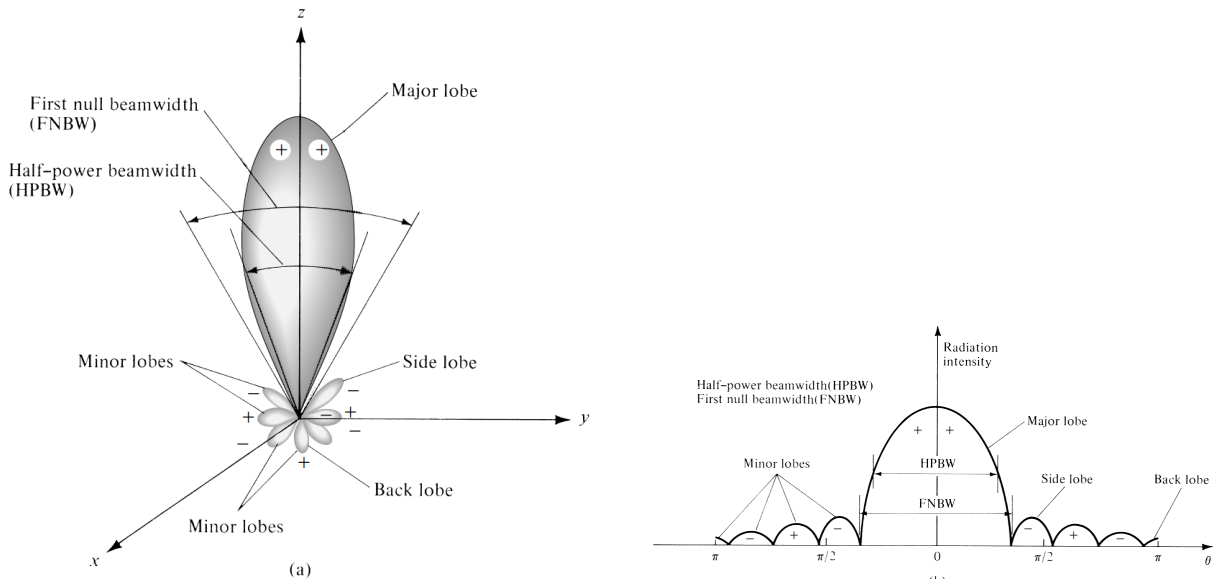

(a) Main and side lobes [3].

(b) Phase diagram of lobes [3].

Figure 3.9: Radiation pattern fundamentals.

In order to analyze several cases of radiation pattern across multiple number of antennas we are going to use several main definitions: gain, realized gain, directivity, electric field pattern and total radiated power (TPR). The gain is defined as the input or accepted power of the antenna.

$$G(\theta,\phi) = 4\pi \cdot \frac{power\,radiated\,per\,unit\,solid\,angle}{input\,(accepted)\,power} \tag{3.16}$$

The realized gain has a similar relationship as the gain but instead of the accepted power is inversely proportional to the stimulated power.

$$G_{realized}(\theta,\phi) = 4\pi \cdot \frac{power\,radiated\,per\,unit\,solid\,angle}{stimulated\,power} \tag{3.17}$$

The directivity of an antenna is defined as the ratio of the radiation intensity in a given direction from the antenna to the radiation intensity averaged over all directions.

$$D(\theta,\phi) = 4\pi \cdot \frac{power\,radiated\,per\,unit\,solid\,angle}{total\,radiated\,power} \tag{3.18}$$

The power radiated per unit angle or radiation intensity can be defined by

$$U(\theta,\phi) = \frac{r^2}{2\eta}\left|\vec{E}(r,\theta,\phi)\right|^2 = \frac{1}{2\eta}\left(|E_\theta(\theta,\phi)|^2 + |E_\phi(\theta,\phi)|^2\right) \tag{3.19}$$

In which the η value is the intrinsic impedance of the medium and $\vec{E}(r,\theta,\phi) = \vec{E}(\theta,\phi)\frac{\exp -jkr}{r}$. Having this information we get that the power radiated is the following

$$P_{rad} = \iint_\Omega U d\Omega \tag{3.20}$$

The electric field pattern provides a distance-independent characterization of the radiation pattern. It is directly related to the electric field evaluated using the farfield approximation:

$$E_{far}(r,\theta,\phi) = E_{pattern}(\theta,\phi)\cdot\frac{exp(-ikr)}{r} \tag{3.21}$$

And if we want to apply this information to a phased array we just multiply it to the array factor,

$$E_{total}(r,\theta,\phi) = E_{far,single}(\theta,\phi)\cdot AF(r,\theta,\phi) \tag{3.22}$$

with,

$$AF(r,\theta,\phi) = \sum_n A_n exp\cdot(ik\vec{x}_n\cdot\hat{e}_r + i\phi_n) \tag{3.23}$$

The total radiated power (TPR) is a measure of how much power is radiated by an antenna when the antenna is connected to an actual radio (or transmitter), because of this condition this is an active measurement. TPR is calculated and summed up over all possible angles. This quantity is also related with the Effective Isotropic Radiated Power (EIRP), in which it describes the power transmitted from the radio (P_t), the cable losses L, and the antenna gain (G),

$$EIRP = P_t - L + G \tag{3.24}$$

And if this quantity and the directivity are known, the TPR can be calculated from this

equation,

$$TPR = EIRP - D \tag{3.25}$$

If we don't have that information TPR can be also be determined by the radiation pattern of the antenna defined by $R(\theta,\phi)$ with units of Watts/Steradians. Since the radiation patter have spherical coordinated, we can integrate over all angles and with units of Watts,

$$TPR = \int_0^{2\pi}\int_0^{\pi} R(\theta,\phi)\sin\theta\, d\theta d\phi \tag{3.26}$$

Now, if we want to measure the antenna in real life in an an-echoic chamber, we can measure EIRP at every angle and then averaging it over the sphere,

$$TPR = \frac{1}{4\pi}\int_0^{2\pi}\int_0^{\pi} EIRP(\theta,\phi)\sin\theta\, d\theta d\phi \tag{3.27}$$

Since every computational calculation is discrete, and we have to take into account the vertical and horizontal (θ and ϕ components) polarization of our antenna we can break it down into the following equation,

$$TPR = \frac{\pi}{2NM}\sum_{n=0}^{N-1}\sum_{m=0}^{M-1}(EIRP_\theta(\theta_n,\phi_m) + EIRP_\phi(\theta_n,\phi_m))\sin\theta_n \tag{3.28}$$

Where N and M are the discretization of θ and ϕ coordinates.

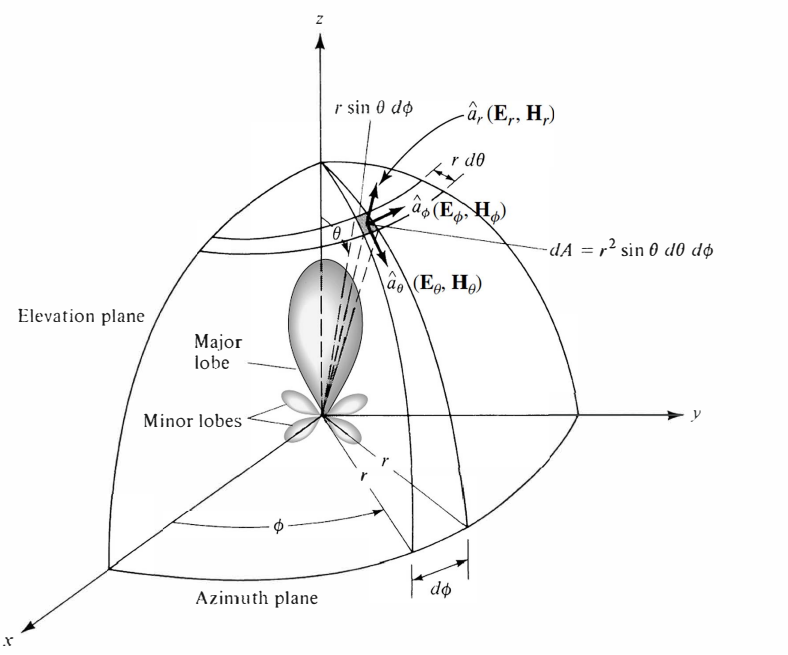

Figure 3.10: Radiation pattern formalism with spherical coordinates [3].

On figure 3.10 we can see the formalism of the radiation pattern in spherical coordinates and from there we can actually calculate the components of the electric field for a patch antenna.

$$E_\theta = \frac{-jV_o k_0 W_p \exp(-jk_0 r)}{\pi r} \operatorname{sinc}\left(\frac{kW_p \sin\theta \sin\phi}{2}\right) \cos\left(\frac{k_0 L_p}{2} \sin\theta \cos\phi\right) \cos\phi \tag{3.29}$$

$$E_\phi = \frac{jV_o k_0 W_p \exp(-jk_0 r)}{\pi r} \operatorname{sinc}\left(\frac{kW_p \sin\theta \sin\phi}{2}\right) \cos\left(\frac{kL_p}{2} \sin\theta \cos\phi\right) \cos\theta \sin\phi \tag{3.30}$$

From here is pretty trivial to get the general form of the electric field vector and we can calculate the radiation pattern as well. The dependence of r radicalizes on the specifications of the antenna, whether is singular or a phased array, and we can see from the formulas that it has an exponential form. What gives the shape of the radiation pattern is the θ and ϕ dependencies. From the formulation we can deduce that it also has a resonant frequency dependency via the dimensions of the length and width. If we simulate the optimal antenna then we get the sharper and more intense radiation pattern.

CHAPTER IV

NUMERICAL MODELS

4.1 Transmission Line Model

The transmission line model is one of the basic and easiest methods to simulate patch antennas, it is the formulaic derivation of the principal dimensions of the structure such as the length, width, thickness and the characteristic impedance. Because of the fact that these dimensions are finite, it produces an effect called fringing.

This effect happens when two slots of the patch antenna undergo radiation. This effect is a function of the substrate thickness and because the length is much higher than the thickness the fringing effect is really small, yet it needs to be considered into the calculations because it has an effect on the resonant frequency. The importance of the effective dielectric constant ε_{reff} relies when the waves travel to the structure of the patch antenna. Depending of the resonant dimension the effective dielectric constant is going to be dependent on that value. We determine a term to include whether we are using length or width dependency.

$$F\left(\frac{a}{h}\right) = \begin{cases} (1+12\frac{h}{a})^{-\frac{1}{2}} + 0.04(1-\frac{a}{h})^2 & \frac{a}{h} \leq 1 \\ \\ (1+12\frac{h}{a})^{-\frac{1}{2}} & \frac{a}{h} \geq 1 \end{cases} \tag{4.1}$$

In this piece-wise function [8, p. 267] a is either length or width. Having this we can compute the effective dielectric constant [8, p. 267] dependent on length and width.

$$\varepsilon_{eff}(W) = \frac{\varepsilon_r + 1}{2} + \frac{\varepsilon_r - 1}{2} F\left(\frac{W}{h}\right) \tag{4.2}$$

$$\varepsilon_{eff}(L) = \frac{\varepsilon_r + 1}{2} + \frac{\varepsilon_r - 1}{2} F\left(\frac{L}{h}\right) \tag{4.3}$$

A very important term that we can derive to take into account the fringing effects is ΔL, this term is useful to us because it can show us the effective length in which we can work out for the resonant frequency.

$$\Delta L = 0.412h \frac{(\varepsilon_{eff}(W) + 0.3)(\frac{W_p}{h} + 0.26h)}{(\varepsilon_{eff}(W) - 0.258)(\frac{W_p}{h} + 0.8)} \tag{4.4}$$

$$L_{eff} = L + 2\Delta L \tag{4.5}$$

Knowing this information we can derive the first mode resonant frequency in terms of the effective length

$$(f_r)_{010} = \frac{c}{2L\sqrt{\varepsilon_{reff}}} \tag{4.6}$$

The following equations are to compute the width, and the ground plate dimensions for the patch antenna [8, p. 266, 267].

$$W_p = \frac{c}{2f_r\sqrt{\frac{\varepsilon_r+1}{2}}} \tag{4.7}$$

$$L_g = 6h + L_p \tag{4.8}$$

$$W_g = 6h + W_p \tag{4.9}$$

As we can observe, the width of the patch antenna is loosely dependent on the resonant frequency, whereas the length of the patch depends more on more dimensions. Therefore the length of the patch plays a bigger role in the resonant frequency. In any design for a patch antenna if $L_p < W_p$, the feed point will be located at $\frac{Wp}{2}$ and the value calculated on equation 4.8. We can see that the feed point location is dependent on the length of the patch, the characteristic impedance (which in most cases is 50 Ohms), and the edge impedance. On equation 4.10 we can see how the

cables insertion location on the y axis is calculated.

$$R_{in}(y = y_0) = R_{in}(y = 0)\cos^2\left(\frac{\pi}{L}y_0\right) \tag{4.10}$$

And from there we can actually solve for y_0. Now that we have this information we can actually move on to the input impedance of the patch antenna in a circuit form. Before we show this formula we must actually describe a few important terms. The quality factor [3, p. 852, 853] is a figure that represents the efficiency of any patch antenna. This figure depends of the radiation, conduction, and dielectric losses. It is represented as the following

$$\frac{1}{Q_t} = \frac{1}{Q_{rad}} + \frac{1}{Q_c} + \frac{1}{Q_d} \tag{4.11}$$

Since we are working with very thin substrates the following terms are

$$Q_c = h\sqrt{\pi f \mu \sigma} \tag{4.12}$$

$$Q_d = \frac{1}{\tan\delta} \tag{4.13}$$

$$Q_{rad} = \frac{2\omega\varepsilon r}{hG_t/l}K \tag{4.14}$$

From these equations δ is the loss tangent of the substrate material, σ is the conductivity of the plates, G_t/l is the total conductance per unit length and K is

$$K = \frac{\int_{area}|E|^2 dA}{\oint_{perimeter}|E|^2 dl} \tag{4.15}$$

After having described these values we can actually move on to the input impedance in circuit form. As we can see in figure 4.1 a patch antenna is considered an RLC resonant circuit device in which we have for the probe part the inductance of the patch and for the cavity part of the antenna we have the rest of the components.

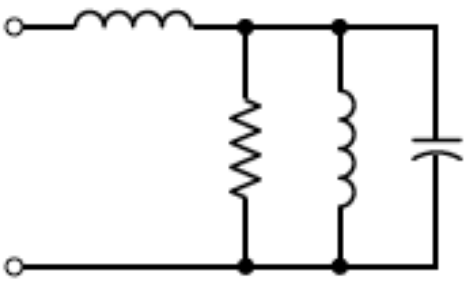

Figure 4.1: Equivalent circuit of a patch antenna [3].

Because of this the input impedance is a real and complex physical property that depends of the resistive and reactive counterparts respectively.

$$Z_{in} = R_{in} + jX_{in} \tag{4.16}$$

And since we know that these terms are frequency dependent, after we expand and use the previous terms we obtain [17, p. 50]

$$Z_{in} = \frac{R_r}{1 + Q_t^2 \left(\frac{f}{f_r} - \frac{f_r}{f}\right)^2} + j \left[X_f - \frac{R_r Q_t \left(\frac{f}{f_r} - \frac{f_r}{f}\right)}{1 + Q_t^2 \left(\frac{f}{f_r} - \frac{f_r}{f}\right)^2} \right] \tag{4.17}$$

We have that R_r is the input resistance at resonance, f_r is the resonant frequency at modes nm and X_f is the feed reactance [3, p. 856] by the probe coaxial feed which is approximately

$$X_f \simeq -\frac{\eta kh}{2\pi} \left[\ln\left(\frac{kd}{4} + 0.577\right) \right] \tag{4.18}$$

Where h is the substrate thickness and d is the diameter of the coaxial feed. If we use this formulation, we can actually plot the return loss of a single antenna via circuit formulation as the following

$$\Gamma = \frac{Z_{in} - Z_o}{Z_{in} + Z_o} \tag{4.19}$$

$$RL(dB) = -20\log_{10}|\Gamma| \tag{4.20}$$

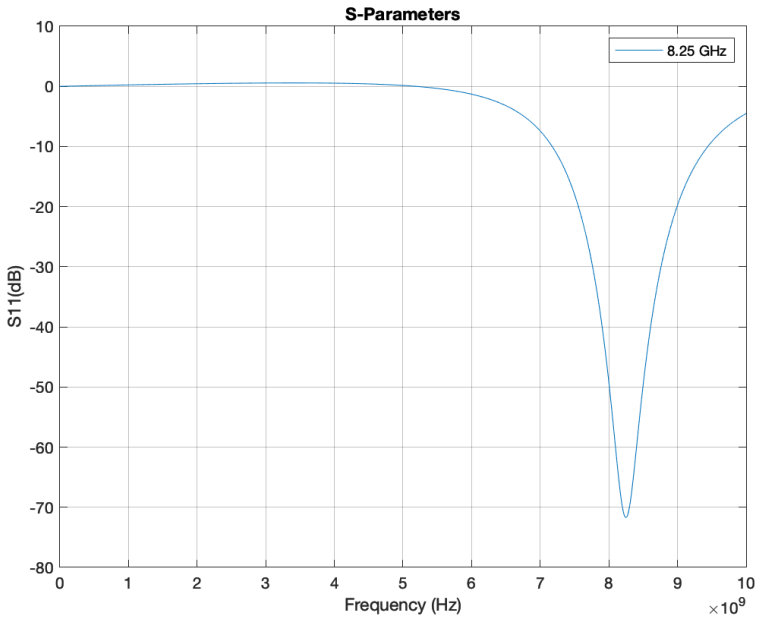

Figure 4.2: Return loss of an 8.25 GHz single patch antenna using circuit model.

4.2 Cavity Model

In order for us to understand the nature of these antennas we need to derive the geometry of the same and to solve the wave equations surrounding the system we want to calculate. In the previous method of transmission line we only take into account the circuit components since the antenna resembles them and from there it is relatively easy to compute important quantities to do antenna analysis. The cavity model, which originated in the late 1970's, takes the approach to treating these antennas as resonant cavities in which we can derive wave equations to solve for important physical properties. It views the rectangular antenna as an electromagnetic cavity with electric and magnetic walls in order to simulate an open circuit.

4.2.1 Field Configurations for Wave Solutions, Approach 1

We can find the solutions of the wave function for the patch antenna using the general geometry and initial conditions of the patch antenna. To achieve this we can use a vector potential

A_z [3, p. 828] and

$$\nabla^2 A_z + k^2 A_z = 0 \tag{4.21}$$

Since we know that this solution is dependent on all axis we know that it takes the solution of $A_z(x,y,z) = f(x)g(y)h(z)$ and from this we can take the following solution

$$A_z = [A_1 \cos(k_x x) + B_1 \sin(k_x x)] \cdot [A_2 \cos(k_y y) + B_2 \sin(k_y y)] \cdot [A_3 \cos(k_z z) + B_3 \sin(k_z z)] \tag{4.22}$$

We know that $k_x = \frac{m\pi}{W}$, $k_y = \frac{n\pi}{L}$ and $k_z = \frac{p\pi}{h}$ are the wave numbers along its axis. Since we have the vector potential we can actually compute the electric and magnetic field across all directions

$$E_x = -j\frac{1}{\omega\mu\varepsilon}\frac{\partial^2 A_z}{\partial x \partial z} \qquad H_x = \frac{1}{\mu}\frac{\partial A_z}{\partial y}$$
$$E_y = -j\frac{1}{\omega\mu\varepsilon}\frac{\partial^2 A_z}{\partial y \partial z} \qquad H_y = \frac{1}{\mu}\frac{\partial A_z}{\partial x}$$

Now we need to apply the boundary conditions [3, p. 829]

$$E_x(0 \le x' \le L, 0 \le y' \le W, z' = 0)$$
$$= E_x(0 \le x' \le L, 0 \le y' \le W, z' = h) = 0$$

$$H_x(0 \le x' \le L, y' = 0, 0 \le z' \le h)$$
$$= H_x(0 \le x' \le L, y' = W, 0 \le z' \le h) = 0$$

$$H_y(x' = 0, 0 \le y' \le W, 0 \le z' \le h)$$
$$= H_x(x' = L, 0 \le y' \le W, 0 \le z' \le h) = 0$$

where x', y', and z' represents the coordinates within the cavity and $B_1 = B_2 = B_3 = 0$, therefore the vector potential takes the following form [3, p. 829]

$$A_z = A_{mnp} \cos(k_x x') \cos(k_y y') \cos(k_z z') \tag{4.23}$$

The value of A_{mnp} represents the amplitude coefficients of each mnp mode. And from the previous wave numbers we can derive the following

$$k_x^2 + k_y^2 + k_z^2 = k_{mn}^2 = \omega^2 \mu \varepsilon \tag{4.24}$$

Since we have the conditions that h is very small we can decide whether or not to use the sinusoidal dependency on $\hat{z}$. Therefore we can write the equations for the electric and magnetic [3, p. 830] field as follows

$$E_x = -j \frac{k_x^2 + k_y^2}{\omega \mu \varepsilon} A_{mn} \sin(k_x x') \cos(k_y y') \sin(k_z z') \tag{4.25}$$

$$E_y = -j \frac{k_y k_x}{\omega \mu \varepsilon} A_{mn} \cos(k_x x') \sin(k_y y') \sin(k_z z') \tag{4.26}$$

$$E_{tot} = \frac{E_x + E_y}{\sqrt{E_x^2 + E_y^2}} \tag{4.27}$$

After computing the electric field we can actually derive the time signals for the patch antenna. We know that for an input general pulse for the patch antenna we can use the general form of a modulated Gaussian pulse [8, p. 215, 216]

$$P_{in}(t) = \exp\left(-\frac{t - t_0}{T}\right)^2 \sin(\omega_0 (t - t_0)) \tag{4.28}$$

Where w_0 is the angular modulation frequency t_0 is the center of the pulse and T is the pulse

spread. For the output pulse of the patch antenna things get more elaborates as follows

$$P_{out}(t) = \exp\left(\left(-\frac{t-t_0}{T}\right)^2 + i\omega_r(t-t_0) + ik_y\frac{(y-y_0)^2}{y_0}\right)\sin\left(\omega_r(t-t_0)\right)E_{tot} \tag{4.29}$$

Where $w_r = w_L + w_h - 18.5w_0$, y_0 is the probe location in the $\hat{y}$ axis and y is iterated at the same number of bins as the time signal at $-L/2 \leq y \leq L/2$. After computing these expressions we can get our return signal by using the following

$$RL = -20\ln\left(\left|\frac{fft(P_{out}(t))}{fft(P_{in}(t))}\right|\right) = -20\ln\left(\left|\frac{Z_L - Z_0}{Z_L + Z_0}\right|\right) \tag{4.30}$$

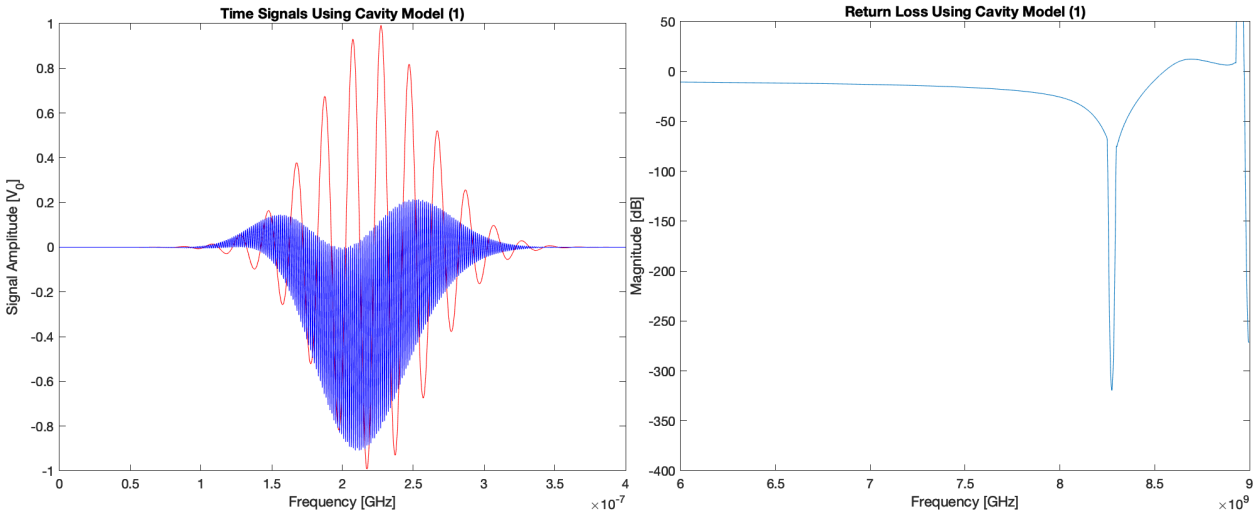

(a) Times signal plot using cavity model approach 1. **(b)** Return loss plot using cavity model approach 1.

Figure 4.3: Time and frequency analysis of cavity model approach 1.

Now we can observe the fundamental differences between the input and output signal. And by doing this work we can see that there is a difference between magnitude between this model and a CST model. Nevertheless, this is a good candidate to use if we want to understand and model a patch antenna in house.

4.2.2 Field Configurations for Wave Solutions, Approach 2

On this subsection we are going to take the approach into calculating the eigenfunctions for the patch antenna. The system of the antenna is going to be divided into two regions: the first region

is going to be the internal fields which are going to determine the input impedance of the antenna and also the currents that produces the radiation, the second region is going to be the exterior fields which are responsible of the radiation characteristics of the patch antennas.

Now, since the substrate of the antenna is too thin we can get that the field distributions for the $\hat{z}$ axis have a $\partial/\partial z = 0$, therefore we are only going to have E_z, H_x and H_y. For the purposes of calculating the return loss we only need the E_z component that satisfy the following wave equation [8, p. 258]

$$\frac{\partial^2 E_z}{\partial x^2} + \frac{\partial^2 E_z}{\partial y^2} + k^2 E_z = j\omega\mu_0 J \tag{4.31}$$

where $k^2 = \omega^2\mu_0\varepsilon_0\varepsilon_r$ and J_z is the excitation electric current density of our probe feed. In most literature the field equations for microstrip antennas and for coaxial probe fed antennas are the same. Now that we have that information we can express the electric field in a modal configuration as the following

$$E_z(x,y) = \sum_{m,n} A_{mn}\psi_{mn}(x,y) \tag{4.32}$$

where A_{mn} are the amplitude coefficients corresponding to the eigenfunctions of ψ_{mn}. The boundary conditions of the eigenfunction are the following

$$\left.\frac{\partial\psi_{mn}}{\partial x}\right|_{x=0} = \left.\frac{\partial\psi_{mn}}{\partial x}\right|_{x=W} = 0 \tag{4.33}$$

$$\left.\frac{\partial\psi_{mn}}{\partial y}\right|_{y=0} = \left.\frac{\partial\psi_{mn}}{\partial y}\right|_{y=L} = 0 \tag{4.34}$$

$$\left(\frac{\partial^2}{\partial x^2} + \frac{\partial^2}{\partial y^2} + k_{mn}^2\right)\psi_{mn} = 0 \tag{4.35}$$

$$\int_x\int_y \psi_{mn}\psi_{mn}^* dxdy = 1 \tag{4.36}$$

The solutions to these orthonormalized eigenfunctions are the following

$$\psi_{mn}(x,y) = \sqrt{\frac{\varepsilon_m\varepsilon_n}{LW}}\cos(k_m x)\sin(k_n y) \tag{4.37}$$

We know that $k_m = m\pi/W$, $k_n = n\pi/L$ and that $k_{mn}^2 = k_m^2 + k_n^2$. The coefficients of A_{mn} are determined by the excitation current, for this we solve for that term to get [8, p. 259]

$$A_{mn} = \frac{j\omega\mu_0}{k^2 - k_{mn}^2} \int_{feed} \int \psi_{mn}^* J_z dxdy \tag{4.38}$$

The excitation current is determined by the parameters of the coaxial fed probe of its cross-sectional area D_x and D_y centered at (x_0,y_0) which follows that

$$J_z = \begin{cases} \frac{I_0}{D_x D_y} & x_0 - \frac{D_x}{2} \leq x \leq x_0 + \frac{D_x}{2}; y_0 - \frac{D_y}{2} \leq y \leq y_0 + \frac{D_y}{2} \\ \\ 0 & elsewhere \end{cases} \tag{4.39}$$

Using 4.39 in 4.38 gives us the following

$$\begin{aligned} A_{mn} &= \frac{1}{D_x D_y} \frac{j\omega\mu_0}{k^2 - k_{mn}^2} \int_{feed} \int I_0 \psi_{mn}^* dxdy \\ &= \frac{j\omega\mu_0 I_0}{k^2 - k_{mn}^2} \sqrt{\frac{\varepsilon_m \varepsilon_n}{LW}} \cos(k_m x_0) \sin(k_n y_0) G_{mn} \end{aligned} \tag{4.40}$$

where

$$G_{mn} = \text{sinc}\left(\frac{n\pi D_x}{2W}\right) \text{sinc}\left(\frac{m\pi D_y}{2L}\right) \tag{4.41}$$

Now that we have the definitions derived we can compute the electric field

$$E_z(x,y) = j\omega\mu_0 I_0 \sum_{m,n=0}^{\infty} \frac{\psi_{mn}(x,y)\psi_{mn}(x_0,y_0)}{k^2 - k_{mn}^2} G_{mn} \tag{4.42}$$

If we think in a case where we have an RF circuit for a patch antenna, we can develop the following quantities

$$\begin{aligned} V_{in} &= -hE_z(x_0, y_0) \\ &= -j\omega\mu_0 hI_0 \sum_{m,n=0}^{\infty} \frac{\psi_{mn}(x_0, y_0)^2}{k^2 - k_{mn}^2} G_{mn} \end{aligned} \tag{4.43}$$

$$Z_{in} = -j\omega\mu_0 h \sum_{m,n=0}^{\infty} \frac{\psi_{mn}(x_0, y_0)^2}{k^2 - k_{mn}^2} G_{mn} \tag{4.44}$$

Now, if we use the value of loss tangent $\delta_{eff} = \tan\delta + \frac{\Delta}{h} + \frac{P_r}{\omega W_T}$, where $\tan\delta$ is the loss tangent of the substrate, Δ is the skin depth for the patch conductor, p_r is the power radiated by the patch antenna and W_T is the time-averaged total energy stored in the patch. If we include this information with the value of $k^2 = k_0^2(1 - j\delta_{eff})$, we can derive the final form of the impedance of a coaxial fed patch antenna [8, p. 230]

$$Z_{in} = -j\omega\mu_0 h \sum_{m,n=0}^{\infty} \frac{\psi_{mn}(x_0, y_0)^2}{k_0^2(1 - j\delta_{eff}) - k_{mn}^2} G_{mn} \tag{4.45}$$

After all of this we can compute the time signals and the return loss following the previous approaches. We are using the same input signal but in this time we are going to try to achieve a dual resonant approach by using the following output signal

$$\begin{aligned} P_{out}(t) = \exp\left(-\left(\frac{t - t_0}{T}\right)^2 + i\omega_r(t - t_0) + i\omega_\omega t + ik_y \frac{(y - y_0)^2}{y_0} + ik_x \frac{(x - x_0)^2}{x_0} \right) \\ \sin\left(\omega_r(t - t_0)\right) \sin\left(\omega_\omega t\right) E_z \end{aligned} \tag{4.46}$$

In this approach we iterate as well x and y by the same number of bins as the time signals and with intervals of $-W/2 \leq x \leq W/2$ and $-L/2 \leq y \leq L/2$ respectively. The important features for the output equation are the following: the sinusoidal expression as function of resonant mode frequency, the exponential term as function of resonant mode frequencies, and the exponential terms describing the spatial information.

The term of $\exp\left(-\left(\frac{t-t_0}{T}\right)^2\right)$ describes the properties of the Gaussian modulated pulse in which the value of T describes the spread of the pulse. The term of $\sin\left(\omega_r(t-t_0)\right))$ describes the resonant mode frequency of the system, if it only depends of one mode it would only behave like a single resonant frequency, and if its dependent on two modes it will behave like a dual resonant frequency as shown in 4.3b and that when the term of $\sin\left(\omega_\omega t\right)$ is needed. The purpose of the term of $i\omega_r(t-t_0)$ and $i\omega_\omega t$ is two attenuate the lower residual harmonic resonant frequency of our computation in which we had previously at 3-4 GHz, which it would basically work as a LPF.

The term of E_z describes the behaviour of the geometry of the patch antenna via the electric field information. And the purpose of the term for $ik_y\frac{(y-y_0)^2}{y_0}$ and $ik_x\frac{(x-x_0)^2}{x_0}$ is to attenuate any residual resonant frequencies attributed to E_z and to handle the physical behaviour of the feed point location.

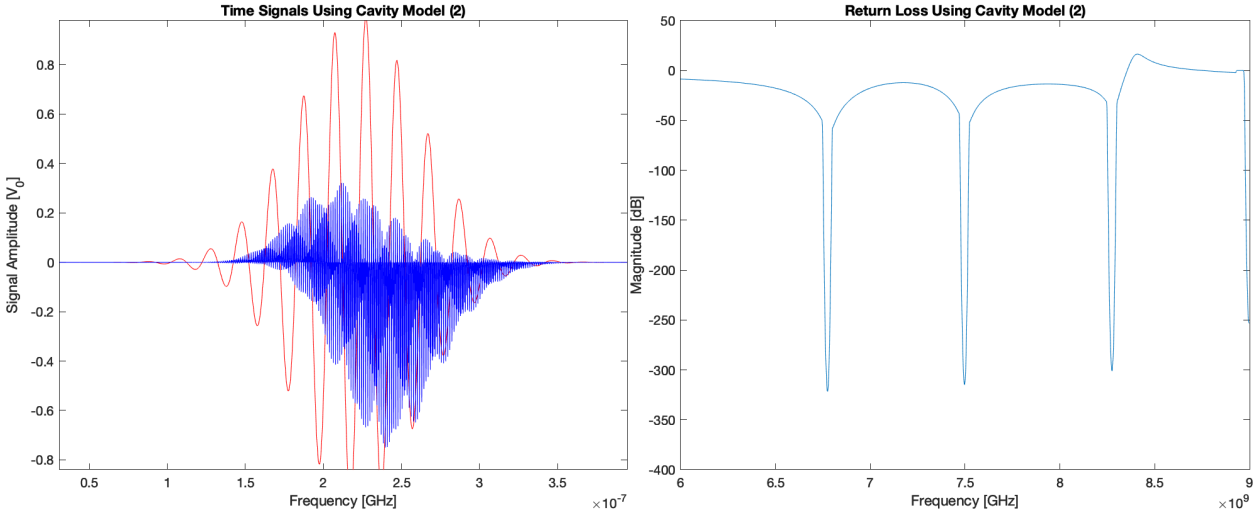

(a) Times signal plot using cavity model approach 2. **(b)** Return loss plot using cavity model approach 2.

Figure 4.4: Time and frequency analysis of cavity model approach 2.

4.3 Wave Iterative Method

The Wave Iterative Method is a numerical model for patch antenna electromagnetic fields. This method is a full wave analysis that was developed in 2001 and can be a great cost effective and low computer power electromagnetic simulator. It calculates the return loss signals for a patch antenna and can compute electric and current distribution of structures. WIM is an interesting method because of the fact that most methods uses time signals in their calculations, whereas this method uses modal and pixel calculations which is going to be discussed later.

In this method we have two fundamental operators on which an initial set of equations is going to interact in order to calculate final results, the diffraction or scattering operator and the reflection coefficient operator. The diffraction operator is dependent on the metallic structure material properties and the reflection coefficient operator is dependent on the dielectric material information. This method used the relationship information of different mediums and for the purpose of this thesis we are going to use a two medium problem, medium one will be the air and medium two will be the dielectric material.

This method is different from previous ones because instead of using time and frequency signals it uses pixels and modes signals. The pixel signals are the sources equations in which they are dependent on the coordinate system of choice. This signals represent the spatial domain part from the wave equations. The mode signals represent the mode number of the grid and they are the spectral or modal domain part of the wave equations. Later on we are going to expand on the process of the relationship between this set of wave equations [4].

After this, it's necessary to set up the boundary conditions for this procedure that involves the diffraction operator and the dimensions of the structure [12], [21].

$$\vec{E}_i = \vec{E}_{i+1} = \begin{cases} 0, & \text{on dielectric} \\ \vec{E}, & \text{on metal,} \end{cases} \tag{4.47}$$

$$\vec{J}_i + \vec{J}_{i+1} = \begin{cases} 0, & \text{on metal} \\ \vec{J}, & \text{on dielectric,} \end{cases} \tag{4.48}$$

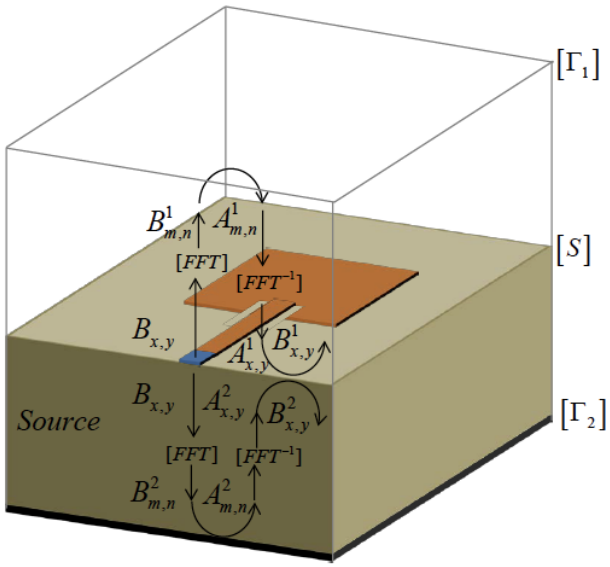

Figure 4.5: Wave propagation using WIM [15].

On figure 4.5 we can observe the pathway of the wave propagation for the method of WIM. We can see the relationship between parameters A and B with its respective x-y and m-n counterparts. These features will be discussed briefly as it accounts for the real and spectrum domain of the process.

4.3.1 WIM Pipeline Development

First Step: Source Equations To begin with WIM we have to define excitation source waves A^i_{xo} and A^i_{yo} which is going to be in the real domain (pixels (x,y)), each medium i is going to have a set of these wave. We also have to define on [1, 15] the spatial waves for each medium of A^i_x and A^i_y:

$$A^i_{xo} = \frac{k^2 - k_x^2}{\omega\mu_0\varepsilon_0\sqrt{Z_{oi}}}(\cos(k_x x)\sin(k_y y)) \tag{4.49}$$

$$A^i_{yo} = \frac{k_y k_x}{\omega\mu_0\varepsilon_0\sqrt{Z_{oi}}}(\sin(k_x x)\cos(k_y)) \tag{4.50}$$

$$A_x^i = \frac{k^2 - k_x^2}{\omega\mu_0\varepsilon_0^2 Z_{oi}^2 \varepsilon_i}(\cos(k_x x)\sin(k_y(y-y_0))) \tag{4.51}$$

$$A_y^i = \frac{k_y k_x}{\omega\mu_0\varepsilon_0^2 Z_{oi} \varepsilon_i}(\sin(k_x x)\cos(k_y(y-y_0))) \tag{4.52}$$

Second Step: Reflection Waves Then we convert the wave of the incident medium which is directly proportional to the product of the S-Parameters and the excitation wave

$$\begin{bmatrix} B_x^i \\ B_y^i \end{bmatrix} = \hat{S}_\Omega \begin{bmatrix} A_x^i \\ A_y^i \end{bmatrix} + \begin{bmatrix} A_{xo}^i H_S(x) \\ A_{yo}^i H_S(y) \end{bmatrix} \tag{4.53}$$

Since the diffraction operator depends on $x-y$ coordinates we can separate them into the following matrix [13],[22]:

$$\begin{bmatrix} B_x^i \\ B_y^i \end{bmatrix} = \begin{bmatrix} S_{11}^x & 0 & S_{12}^x & 0 \\ 0 & S_{11}^y & 0 & S_{12}^y \\ S_{21}^x & 0 & S_{22}^x & 0 \\ 0 & S_{21}^y & 0 & S_{22}^y \end{bmatrix} \begin{bmatrix} A_1^x \\ A_1^y \\ A_2^x \\ A_2^y \end{bmatrix} + \begin{bmatrix} A_{xo}^1 H_S(x) \\ A_{yo}^1 H_S(y) \\ A_{xo}^2 H_S(x) \\ A_{yo}^2 H_S(y) \end{bmatrix} \tag{4.54}$$

We define the diffraction operator $\hat{S}_\Omega$ as the following [10]:

$$\hat{S}_\Omega = \begin{vmatrix} -H_M + \frac{1-N^2}{1+N^2}H_I + \frac{-Z_{01}Z_{02}-Z_{01}Z_s+Z_{02}Z_s}{Z_{01}Z_{02}+Z_{01}Z_s+Z_{02}Z_s}H_Z & \frac{2N}{1+N^2}H_I + \frac{2Z_S\sqrt{Z_{01}Z_{02}}}{Z_{01}Z_{02}+Z_{01}Z_s+Z_{02}Z_s}H_Z \\ \frac{2N}{1+N^2}H_I + \frac{2Z_S\sqrt{Z_{01}Z_{02}}}{Z_{01}Z_{02}+Z_{01}Z_s+Z_{02}Z_s}H_Z & -H_M(x,y) - \frac{1-N^2}{1+N^2}H_I + \frac{-Z_{01}Z_{02}+Z_{01}Z_s-Z_{02}Z_s}{Z_{01}Z_{02}+Z_{01}Z_s+Z_{02}Z_s}H_Z \end{vmatrix} \tag{4.55}$$

We define the following values as:

$$Z_{0i} = \sqrt{\frac{\mu_0}{\varepsilon_0\varepsilon_i}} \qquad N = \sqrt{\frac{Z_{01}}{Z_{02}}} \qquad Z_S = \frac{W}{L}Z_L \tag{4.56}$$

$$H_I(x,y) = \begin{cases} 1, & \text{on the dielectric surface} \\ 0, & \text{elsewhere,} \end{cases} \tag{4.57}$$

$$H_M(x,y) = \begin{cases} 1, & \text{on the metal surface} \\ 0, & \text{elsewhere,} \end{cases} \tag{4.58}$$

$$H_Z(x,y) = \begin{cases} 1, & \text{on the lumped element surface} \\ 0, & \text{elsewhere,} \end{cases} \tag{4.59}$$

$$H_S(x,y) = \begin{cases} 1, & \text{on the source (cable) surface} \\ 0, & \text{elsewhere,} \end{cases} \tag{4.60}$$

These piece wise functions will allow us to construct the geometry of the patch antenna and implement it into the simulation. The more complicated is the design, the more lengthy would be these particular functions. These functions are essential for the final product of electric and current field plots.

Third Step: Fast Modal Transform Later this wave is going to be converted into the spectral domain (modes, (*m*,*n*)) by implementing FMT's (fast modal transforms [18], [9]):

$$\begin{bmatrix} B^i_{x(m,n)} \\ B^i_{y(m,n)} \end{bmatrix} = Q_{m,n} \begin{bmatrix} \frac{n}{L} & \frac{-m}{W} \\ \frac{m}{W} & \frac{n}{L} \end{bmatrix} FFT \begin{bmatrix} B^i_x \\ B^i_y \end{bmatrix} \tag{4.61}$$

where $Q_{m,n} = \sqrt{\frac{ab}{2\Phi_{m,n}}} \frac{1}{\sqrt{(m/a)^2+(n/b)^2}}$, and $\Phi_{m,n} = 2$ if m and n aren't zero and 1 if they are.

Fourth Step: Reflection Coefficients After this we apply the reflection coefficients to calculate the incident waves [20]:

$$\begin{bmatrix} A^{TE,i}_{(m,n)} \\ A^{TM,i}_{(m,n)} \end{bmatrix} = \begin{bmatrix} \Gamma^i_{TE} & 0 \\ 0 & \Gamma^i_{TM} \end{bmatrix} \begin{bmatrix} B^i_{x(m,n)} \\ B^i_{y(m,n)} \end{bmatrix} \tag{4.62}$$

where

$$Y_{TE} = \frac{\gamma}{j\omega\mu_0} \tag{4.63}$$

$$Y_{TM} = \frac{j\omega\mu_0\varepsilon_r}{\gamma} \tag{4.64}$$

$$\gamma = \sqrt{\left(\frac{m\pi}{W}\right)^2 + \left(\frac{n\pi}{L}\right)^2 - k_0^2\varepsilon_r} \tag{4.65}$$

$$\Gamma_\alpha^i = \begin{cases} \frac{1-Z_{0i}Y_\alpha^i \coth(\gamma h)}{1+Z_{0i}Y_\alpha^i \coth(\gamma h)}, & \text{short circuited} \\ \\ \frac{1-Z_{0i}Y_\alpha^i}{1+Z_{0i}Y_\alpha^i}, & \text{open circuit} \end{cases} \tag{4.66}$$

Where $\alpha = TE, TM$.

Fifth Step: Inverse Fast Modal Transform Now, we can transform the reflected modal waves into the real domain using the IFMT's (inverse fast modal transform):

$$\begin{bmatrix} A_x^i \\ A_y^i \end{bmatrix} = FFT^{-1}\left(\frac{1}{Q_{m,n}}\begin{bmatrix} \frac{n}{b} & \frac{-m}{a} \\ \frac{m}{a} & \frac{n}{b} \end{bmatrix}^{-1}\begin{bmatrix} A_{(m,n)}^{TE,i} \\ A_{(m,n)}^{TM,i} \end{bmatrix}\right) \tag{4.67}$$

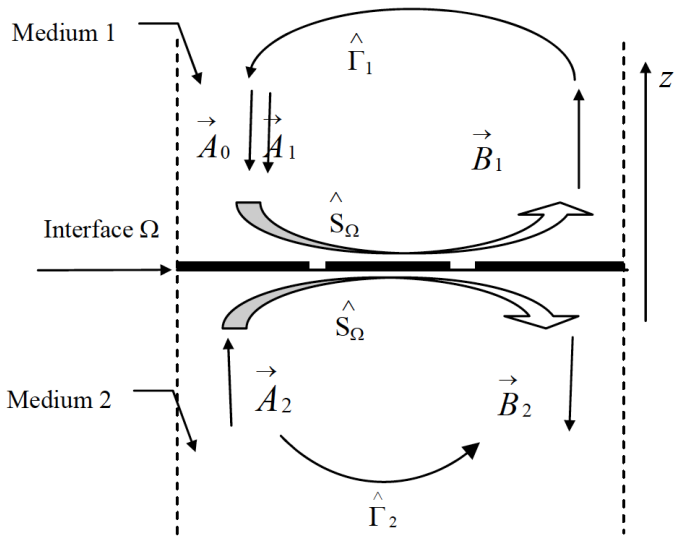

Figure 4.6: Two medium problem for WIM [4].

Summary and Results We can have a more general perspective of this method if we look at figure 4.6, since we are going to implement a two medium problem for our general case of the patch antenna we are replicating this pipeline for each medium, afterwards we sum the results.

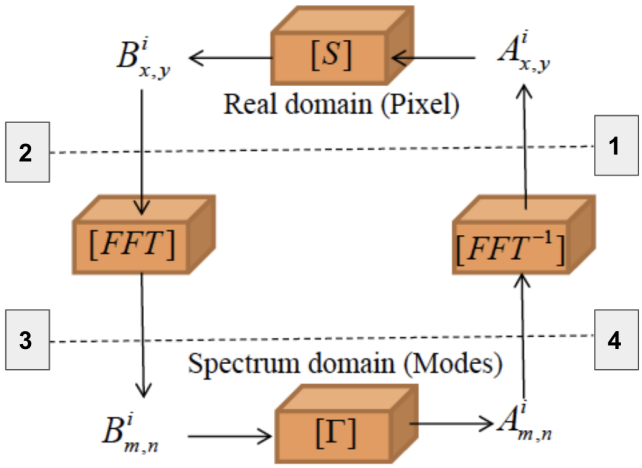

Figure 4.7: WIM pipeline [15].

On figure 4.7 we see the procedure being summarized in a useful pipeline. Now that we have the real domain components for both the incident and reflective waves we can calculate important

values like the following:

$$E^i_{(x,y)} = \sqrt{Z_{0i}}(A^i_{(x,y)} + B^i_{(x,y)}) \tag{4.68}$$

$$J^i_{(x,y)} = \frac{(A^i_{(x,y)} - B^i_{(x,y)})}{\sqrt{Z_{0i}}} \tag{4.69}$$

$$Z^i_{(x,y)} = \frac{E^i_{(x,y)}}{J^i_{(x,y)}} \tag{4.70}$$

$$\Gamma = \frac{Z^i_{(x,y)} - Z_0}{Z^i_{(x,y)} - Z_0} \tag{4.71}$$

$$RL(f) = -20\log|\Gamma| \tag{4.72}$$

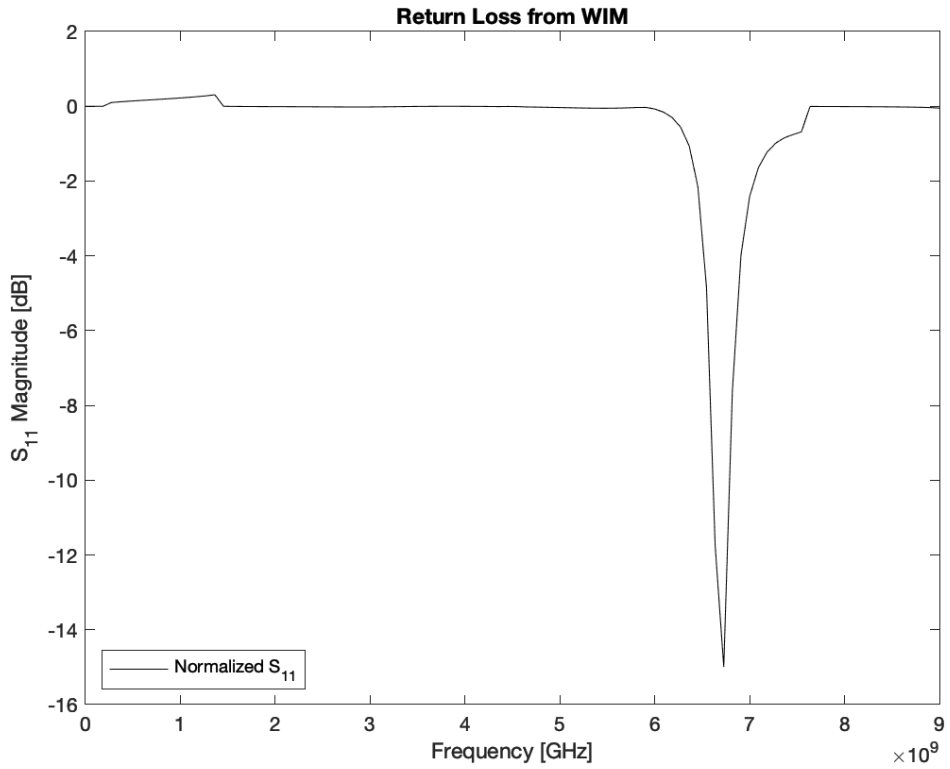

Figure 4.8: S-Parameters retrieved from WIM.

On figure 4.8 we have the return loss signals of a patch antenna. We gladly observe correct behaviour for return loss on non-resonant frequencies and at resonant frequency we achieved a healthy magnitude of -15 dB. This is the most simple version of the model because coordinates are

not mesh-grid, therefore we can only retrieve return loss plots.

Iterated and E/J Results On figure 4.9 we have the return loss plot of a single antenna when we meshgrid the $x-y$ coordinates as well as it's follow up results.

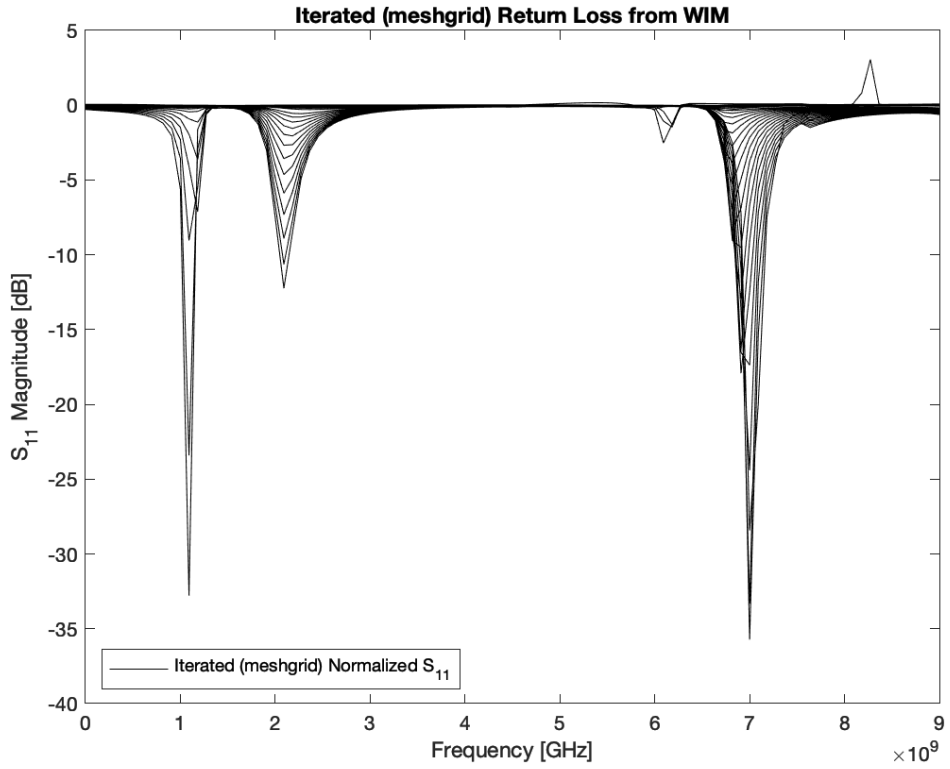

Figure 4.9: Iterated S-Parameters retrieved from WIM.

We can interpret this data as all of the possible combinations of dimension parametrization of length and width. We still observe a general dominant resonant frequency with lower mode resonant frequencies. In general, this is a good approximation for later simulations dealing with the idea of dimension parametrization.

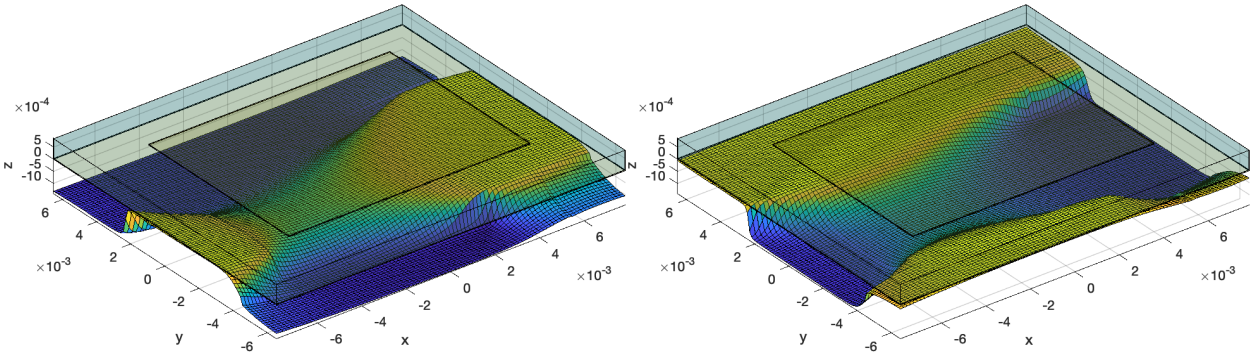

(a) Electric field distribution with patch antenna. **(b)** Current distribution with patch antenna.

Figure 4.10: E/J distributions using WIM. All axis on mm.

On figure 4.10a and 4.10b we accomplished the electric and current distributions for a patch antenna by meshing the coordinates systems and the $A's$ and $B's$ results. By perfecting the diffraction and reflection coefficient operators of the metal in question we would achieve that. Having said that, we can observer general traits of the electric and current distribution across a patch antenna, with the electric field having most of its influence on the patch and the current distribution having its influence on the dielectric material. This method show great potential for us to do more complex simulations.

4.3.2 Implementation of New Diffraction Operator

Since all of the components of the diffraction operator on the past WIM simulations didn't depend on all geometrical step functions, we decided to base now a new type of diffraction operator that does using [2]:

$$S_{11}^{x,y} = -\kappa_1 H_I(x,y) - H_M(x,y) + \xi_{11}^{x,y} H_S(x,y) + v_{11} H_Z(x,y) \tag{4.73}$$

$$S_{12}^{x,y} = \kappa_2 H_I(x,y) + \xi_{12}^{x,y} H_S(x,y) + v_{12} H_Z(x,y) \tag{4.74}$$

$$S_{21}^{x,y} = \kappa_2 H_I(x,y) + \xi_{21}^{x,y} H_S(x,y) + v_{21} H_Z(x,y) \tag{4.75}$$

$$S_{22}^{x,y} = -\kappa_1 H_I(x,y) - H_M(x,y) + \xi_{22}^{x,y} H_S(x,y) + v_{22} H_Z(x,y) \tag{4.76}$$

where the following values are:

$$\kappa_1 = (\rho^2 - 1)(\rho^2 + 1)^{-1} \tag{4.77}$$

$$\kappa_2 = 2\rho(\rho^2 + 1)^{-1} \tag{4.78}$$

$$v_{11} = (Z_s(1 - \rho^2) + Z_{01})(Z_s(1 + \rho^2) + Z_{01})^{-1} \tag{4.79}$$

$$v_{12} = v_{21} = 2\rho Z_s(Z_s(1 + \rho^2) + Z_{01})^{-1} \tag{4.80}$$

$$v_{22} = (Z_s(\rho^2 - 1) + Z_{01})(Z_s(1 + \rho^2) + Z_{01})^{-1} \tag{4.81}$$

For this type of diffraction operators we are going to use two modalities of sources excitation: unilateral and bilateral.

Unilateral Excitation Results For unilateral circuits the direction of the voltage or energy goes only in one way. For this mode we are going to use two values of u: $u = 1$ when the unilateral excitation sources is towards medium 1, and $u = 2$ when the unilateral excitation goes towards medium 2 [2]. The value of τ will represent the x polarization ($\tau = 1$) and y polarization ($\tau = -1$). $\rho = \sqrt{\frac{Z_{01}}{Z_{02}}}$, $\rho_{i=1,2} = \frac{Z_{||}}{Z_{0i}}$, and $Z_{||} = \frac{Z_{01}Z_{02}}{Z_{01}+Z_{02}}$. The parameters for ξ are the following:

$$\xi^x_{11} = \frac{1+\tau}{2}(1-u) + \frac{\tau-1}{2} \qquad \xi^x_{12} = (1+\tau)\rho(2-u)$$
$$\xi^x_{21} = (1+\tau)\rho^{-1}(u-1) \qquad \xi^x_{22} = \frac{1+\tau}{2}(u-2) + \frac{\tau-1}{2}$$

$$\xi^y_{11} = \frac{1-\tau}{2}(1-u) - \frac{\tau+1}{2} \qquad \xi^y_{12} = \frac{1-\tau}{2}\rho(2-u)$$
$$\xi^y_{21} = \frac{1-\tau}{2}\rho^{-1}(u-1) \qquad \xi^y_{22} = \frac{1-\tau}{2}(u-2) - \frac{\tau+1}{2}$$

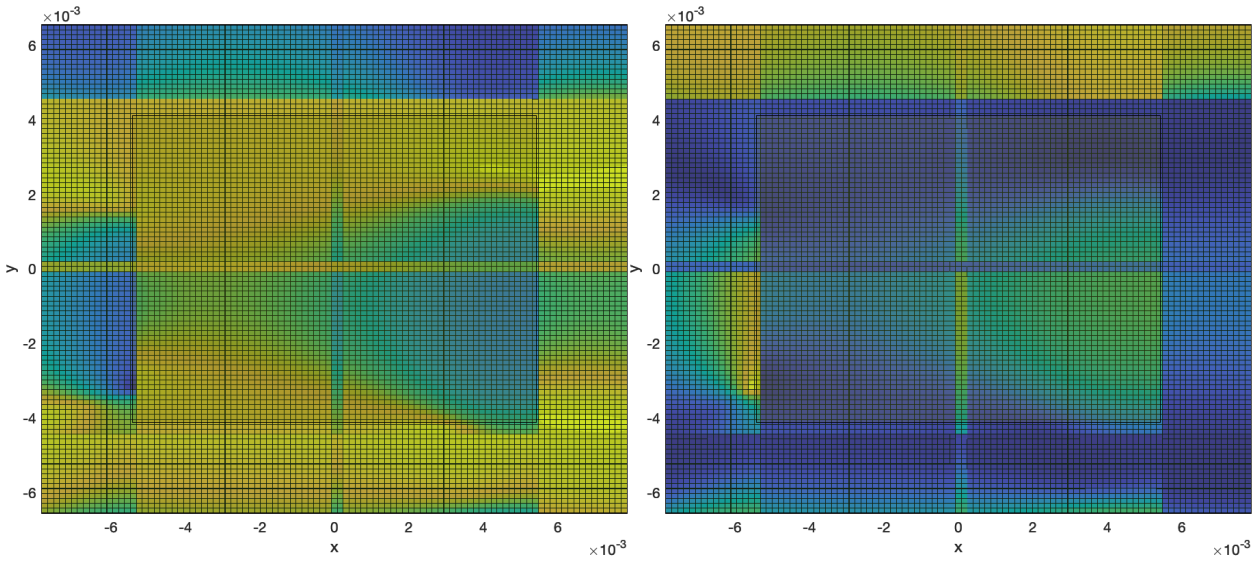

(a) Electric field distribution for patch antenna with unilateral excitation towards medium 1 and x polarization.

(b) [Current distribution for patch antenna with unilateral excitation towards medium 1 and x polarization.

Figure 4.11: E/J distributions with $u = 1 \;\; \tau = 1$. All axis on mm.

We can observe on figures 4.11a and 4.11b how the electric field and the current distribution behaves when we choose the configurations of unilateral excitation going for medium 1 and for x polarization. We achieve some general features of polarization axis given the fact that our feed-point is located at $y_0 = 2.1\,\text{mm}$ and at $x_0 = 0\,\text{mm}$, and we can conclude because we have the x polarization the y axis has low amplitude values and the x axis has the highest amplitude values, this also means that the x polarization is best suited for patch antennas with feed-points only at the x axis. On the x-polarized electric field plot we can see that the fourth quadrant is the one with less amplitude while quadrants 2 and 3 have the highest amplitude and the first quadrant has a mixed amplitude behaviour. We also observe some general limitations to the dielectric area mainly at the top side. For the x-polarized current distribution we expected that its influence would not be at the patch area but rather to the dielectric area and its observed at the top side of the dielectric area. We can also identify the polarization axis. We can also observe that the highest values are located at the y axis and the x axis has the lowest values.

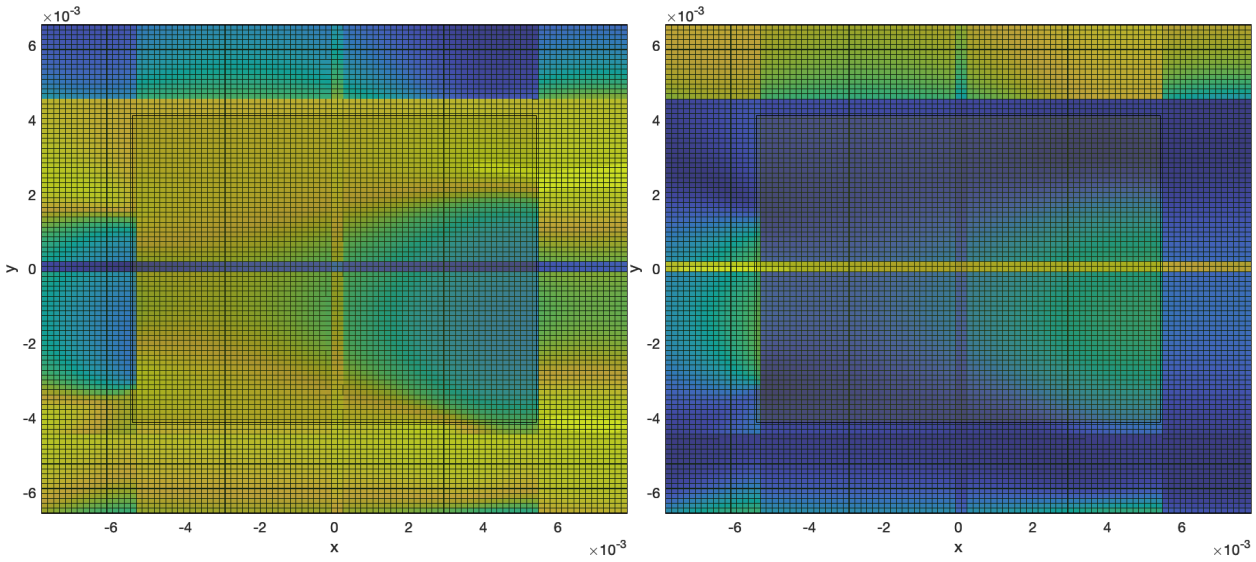

(a) Electric field distribution for patch antenna with unilateral excitation towards medium 1 and y polarization.

(b) [Current distribution for patch antenna with unilateral excitation towards medium 1 and y polarization.

Figure 4.12: E/J distributions with $u = 1 \quad \tau = -1$. All axis on mm.

For figures 4.12a and 4.12b we can identify the difference of the same medium excitation but this time with the y polarization and is reflected in the enhancement of the y axis amplitude for the y-polarized electric field and the diminishing of the x axis diminished amplitude. Se observe similar amplitude behaviour from the last x polarized electric field. For the y-polarized current distribution we see that the x axis is the one who has the highest values and overall it has similar behavior than the x-polarized current distribution plot.

Bilateral Excitation Results In bilateral circuits the bilateral circuit allows the current flow in both directions. The transmission line is the main example of the bilateral circuit because if you give power supply from any direction, the circuit properties remain constant. For the bilateral excitation source we don't need the use of the parameter u but only the polarization values. The values of ξ are the following:

$$\xi^x_{11} = \frac{1+\tau}{4}(-1+\rho_1-\rho_2)+\frac{\tau-1}{2} \qquad \xi^x_{12} = \frac{(1+\tau)}{2}\sqrt{\rho_1\rho_2}$$

$$\xi^x_{21} = \frac{(1+\tau)}{2}\sqrt{\rho_1\rho_2} \qquad \xi^x_{22} = \frac{1+\tau}{4}(-1-\rho_1+\rho_2)+\frac{\tau-1}{2}$$

$$\xi_{11}^{y} = \frac{1-\tau}{4}(-1+\rho_1-\rho_2) - \frac{\tau+1}{2} \qquad \xi_{12}^{y} = \frac{1-\tau}{2}\sqrt{\rho_1\rho_2}$$

$$\xi_{21}^{y} = \frac{1-\tau}{2}\sqrt{\rho_1\rho_2} \qquad \xi_{22}^{y} = \frac{1-\tau}{4}(-1-\rho_1+\rho_2) - \frac{\tau+1}{2}$$

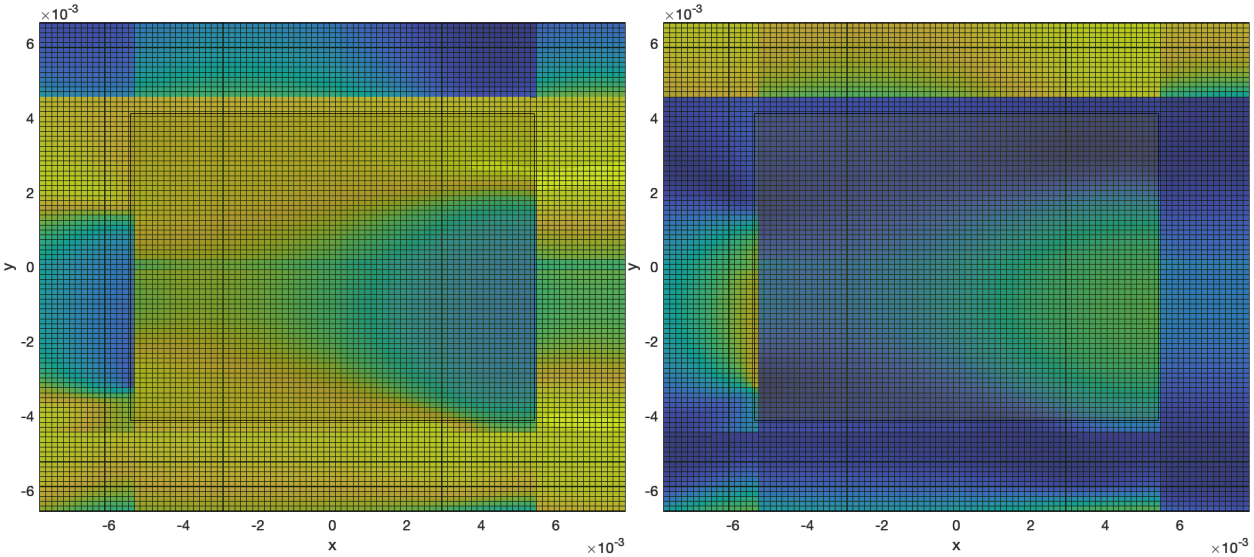

(a) Electric field distribution for patch antenna with bilateral excitation and x polarization.

(b) Current distribution for patch antenna with with bilateral excitation and x polarization.

Figure 4.13: Bilateral E/J distributions with $\tau = 1$. All axis on mm.

For figures 4.13a and 4.13b we can observe that with x-polarized bilateral excitation we achieve smother patterns of the electric field and current distributions. For the x-polarized electric field we see that the fourth quadrant is at the lowest amplitude and everywhere else looks of high amplitude. We can distinguish some general patterns at the dielectric area mainly at the top side being the lowest amplitude. For the x-polarized current distribution we see an inverse pattern in which the fourth quadrant is the highest amplitude.

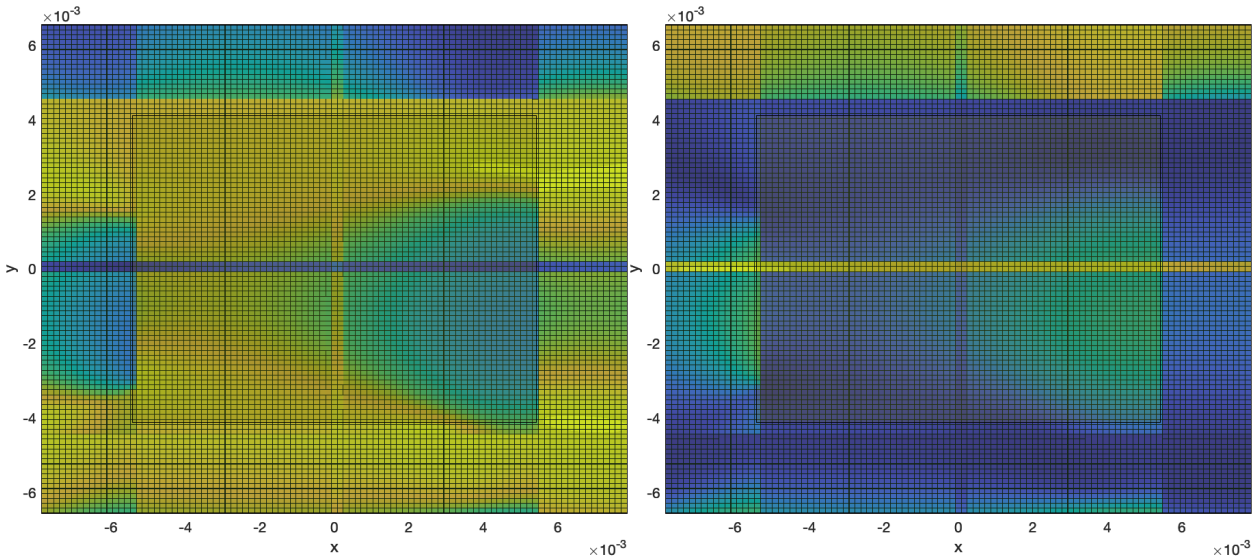

(a) Electric field distribution for patch antenna with bilateral excitation and *y* polarization.

(b) Current distribution for patch antenna with with bilateral excitation and *y* polarization.

Figure 4.14: Bilateral E/J distributions with $\tau = -1$. All axis on mm.

For figures 4.14a and 4.14b with *y*-polarized bilateral excitation we achieve better results for the *y* axis and the lowest of amplitudes are located at the *x* axis and the fourth quadrant at the *y*-polarized electric field. For the *y*-polarized current distribution we get an inverse reaction in which the *y* axis has the lowest amplitude and the *x* axis has the highest amplitude.

CHAPTER V

PATCH ANTENNA SIMULATION CASES

Using equations 4.4- 4.9, we are going to calculate the dimensions and simulation results of a 2.25 GHz, and a 8.25 patch antenna. After that we are going to present a 2x2, 3x3, 4x4, 5x5, 6x6, 7x7, and 8x8 element phased array respectively for the 8.25 GHz antenna.

5.1 A 2.25 GHz Patch Antenna

5.1.1 Single Element Patch Antenna

In the following case for a single element patch antenna, the dimensions and materials are table 5.1:

Parameter	Value
Substrate Type	FR-4
Dielectric Constant	4.6
Substrate Height (h)	1.5 mm
Resonant Frequency	2.25 GHz
Patch Thickness (t)	0.035mm
L_p	30.79 mm
W_p	39.84 mm
Feed point (y_o)	7.96 mm

Table 5.1: Parameters for a 2.25 GHz patch antenna.

Analyzing the return loss (s-parameters) on figure 5.1a for this patch antenna it is observed that it has a narrow shape that is centered at around a resonant frequency of 2.26 GHz with a magnitude of -28.54. It is important to consider that the most influential parameters for this behavior are the length of the patch and the substrate thickness. On figure 5.1b we have the results for the impedance view in which we can observe that around the resonant frequency in the

S-Parameters, the impedance of the antenna is $52.49\,\Omega$, which is important because it needs to be as close as possible from the cable's impedance which is $50\,\Omega$ as it has a $4\,\%$ error. For the power spectrum on figure 5.2a we can see that when the default energy into the system is $0.5\,W$, we get a return power at resonant frequency of $0.49\,W$. Which makes our antenna efficient. And to finalize the single element $2.25\,GHz$ single element patch antenna we can observe on figure 5.2b that the radiation pattern on resonant frequency has a good general shape for this type of antennas. We can see that there is more radiation focused at the top of the shape and its peak is of $0.888\,dB$.

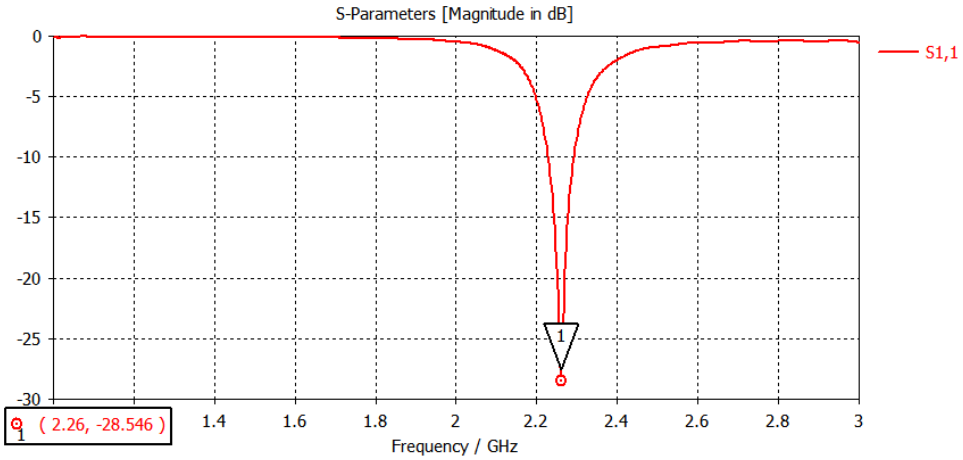

(a) S-parameters of the antenna . Image generated from CST.

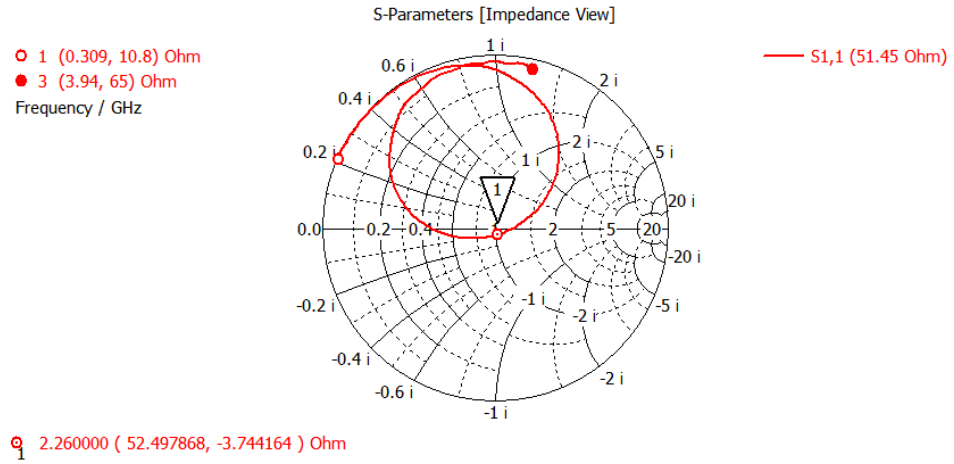

(b) Impedance view of the antenna. Image generated from CST.

Figure 5.1: S-Parameters and Smith Chart of 2.25 GHz patch antenna.

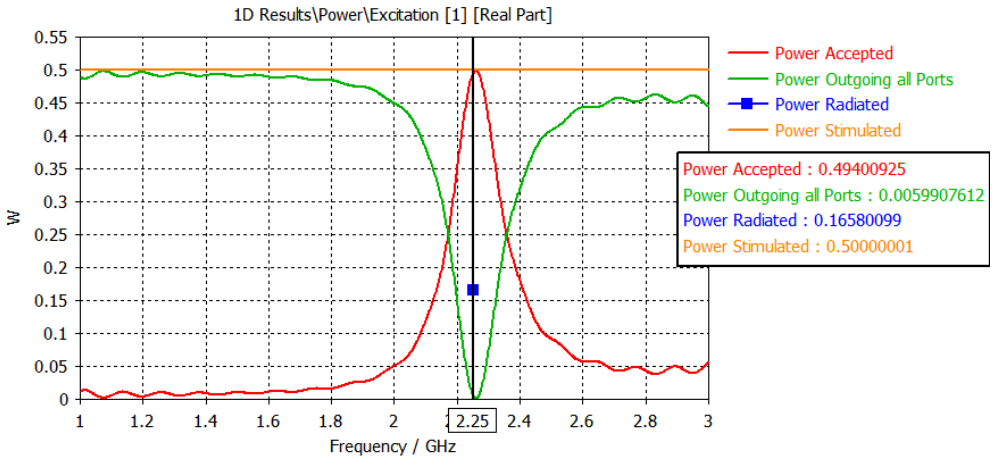

(a) Power spectrum of the antenna. Image generated from CST.

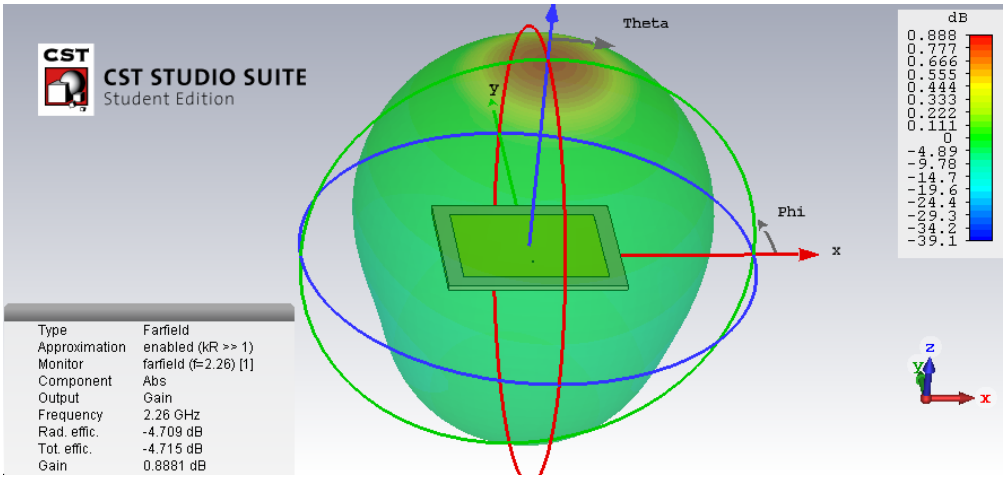

(b) Gain pattern of the antenna. Image generated form CST.

Figure 5.2: Power spectrum and radiation pattern of 2.25 GHz patch antenna.

5.1.2 2x2 Element Phased Array

On this sub-case of the 2.25 GHz patch antenna, we are going to extend the number of antennas to 4 in order to make a 2x2 element phased array as seen on figure 5.3. The horizontal and vertical spacing is $\lambda/2 = 66.66\,mm$.

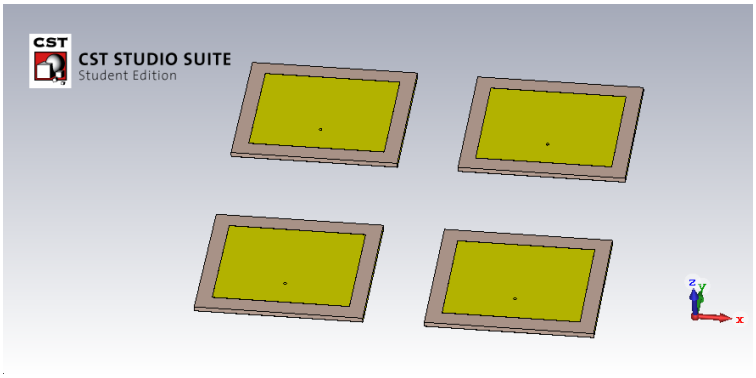

Figure 5.3: 2.25 GHz 2x2 element phased array. Image generated form CST.

Analyzing the s-parameters results from this scenario it is observed that the antenna's individual return (or reflective coefficients S_{nn}) the resonant frequency is shifted to the left to 2.042 GHz with a magnitude of -8.5 dB as seen on figure 5.4a. The other curves that we can observe are the transmission coefficients (S_{nm}) and typically those are symmetric between crossed located antennas (i.e 1 4, 2 3). Generally, the output for this phased array can be improved by changing the substrate thickness or the feed point location, but we want to see the behavior of this phased array with the same dimensions as of the single element antenna. The considerable reduction of magnitude from the single element case to the 2x2 element phased array is reflected on the impedance of each antenna as seen on the Smith Chart on figure 5.4b. We can see an average impedance of 59 Ω, which is not the best case but we are going to stick with these values in this scenario.

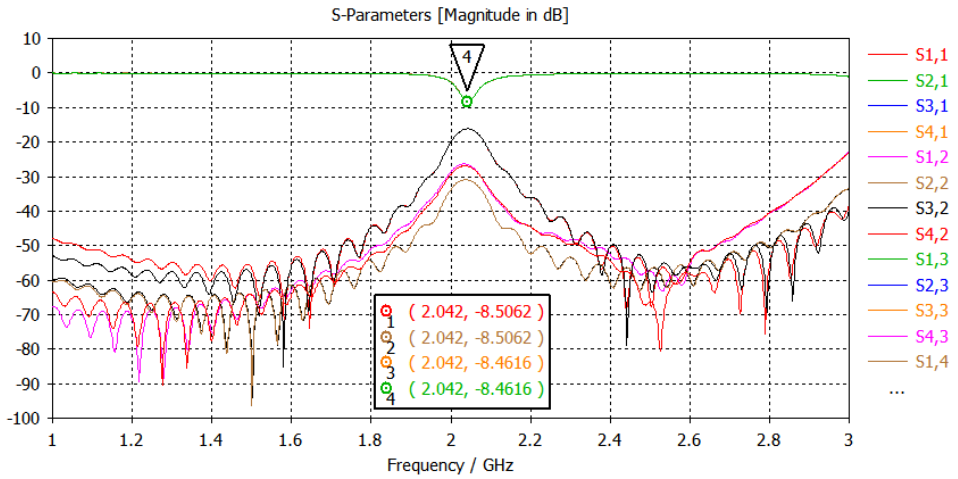

(a) S-Parameters for the 2.25 GHz 2x2 element phased array. Image generated form CST.

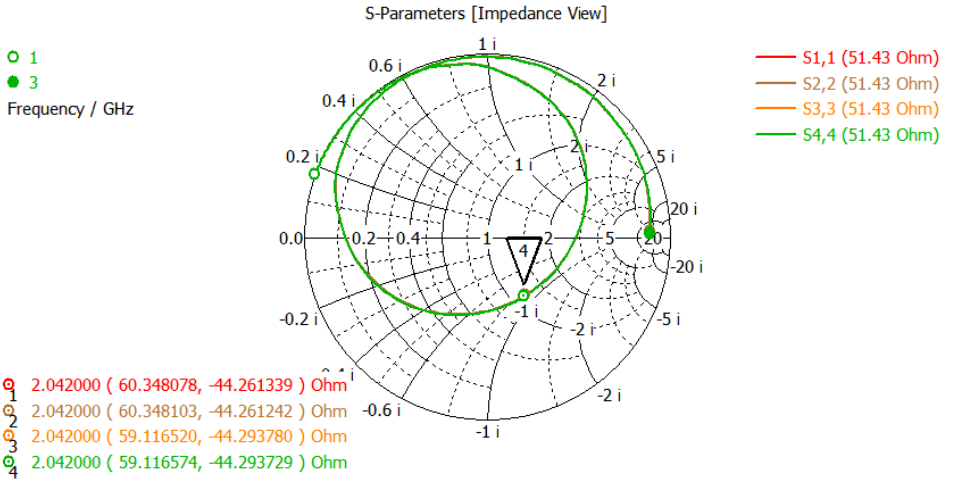

(b) Impedance view of the 2.25 GHz 2x2 element phased array. Image generated form CST.

Figure 5.4: S-Parameters and Smith chart of 2x2 element 2.25 GHz patch antenna.

For the power spectrum it is necessary to combine the results from all of the antennas in order to acquire a general perspective of the behaviour of the phased array. This is achieved by combining every antenna in amplitude and phase. On figure 5.5a we can see a reduction on efficiency almost by 12%. Even though we've seen a reduction in efficiency in this case, we can observe on figure 5.5a that the radiation pattern has a healthy shape and efficiency. At resonant frequency for most antennas (2.046 GHz) we can see a peak magnitude of 10.1 dB, on figure 5.5a all antennas results are combined.

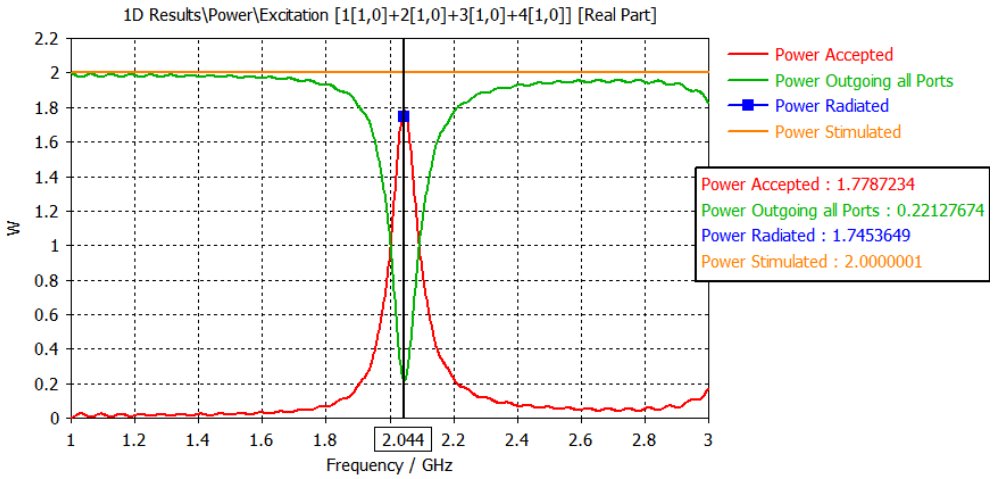

(a) Power spectrum of the 2.25 GHz 2x2 element phased array. Image generated form CST.

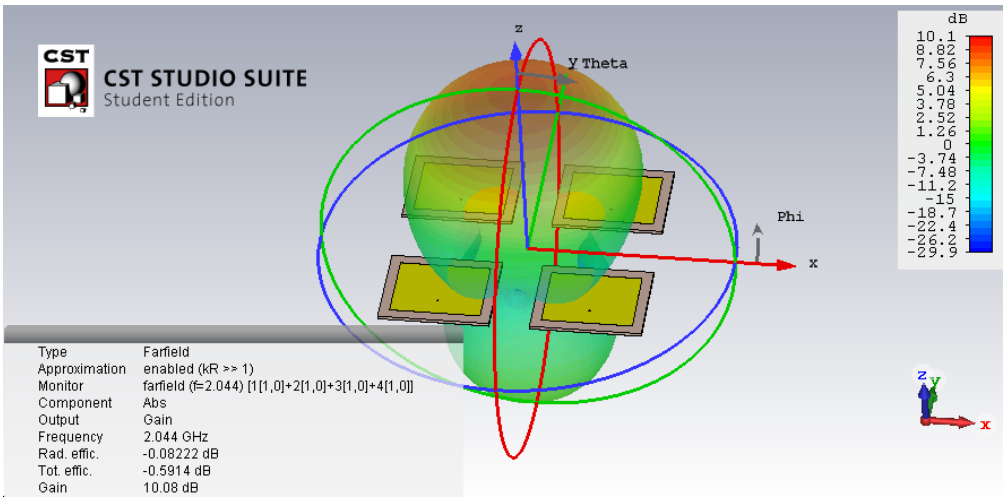

(b) Gain pattern of the 2.25 GHz 2x2 element phased array. Image generated form CST.

Figure 5.5: Power spectrum and radiation pattern of 2x2 element 2.25 GHz patch antenna.

5.1.3 Antenna Testing

To have some reference on how to interpret these results, testing to physical antennas needs to be done. The tested antenna is seen on figure 5.6. We can observe that a resonant frequency is met at exactly 2.25 GHz with a magnitude of -18.59 dB and an impedance magnitude of 53.8 Ω. This makes us confident in our simulations. The general setup for this testing is the following: FSH3 Spectrum Analyzer 100kHz-3GHz, 2.25 GHz patch antenna.

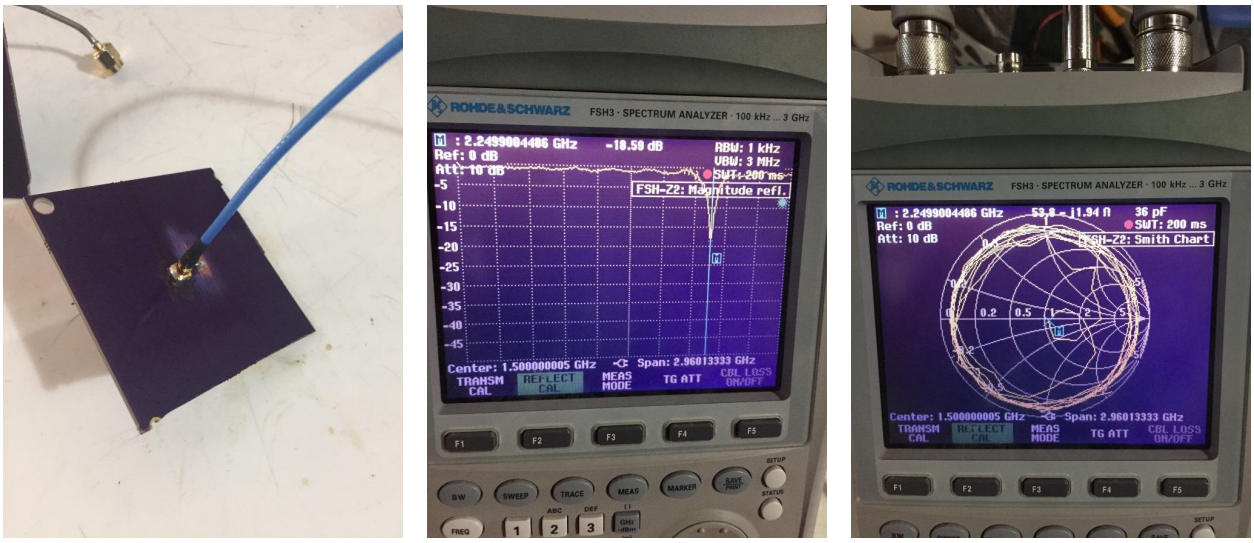

Figure 5.6: Photo of a patch antenna. S-Parameters and Smith Chart.

5.2 A 8.25 GHz Patch Antenna

On the second case for this thesis we are going to analyze the behaviour of an 8.25 GHz patch antenna as in a single element, a 2x2, 3x3, 4x4, 5x5, 6x6, 7x7, and 8x8 element phased array. On this configuration instead of using a coaxial cable simulated on the previous case, we are going to use a function on CST called discrete port. This function offers a simpler and more computational power friendly alternative for the calculation of the antenna properties results. The discrete port is defined by a start point and endpoint, these two connected by a perfectly conducting wire and the respective source (red cone) is in the center of the wire.

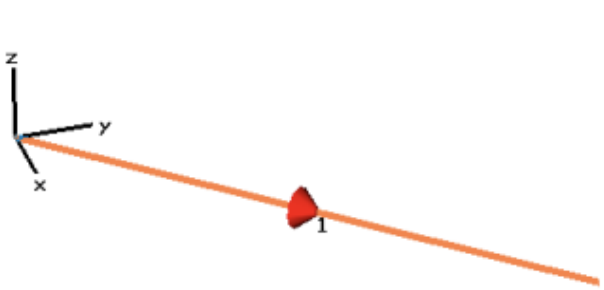

(a) Visualization of the discrete port in CST.

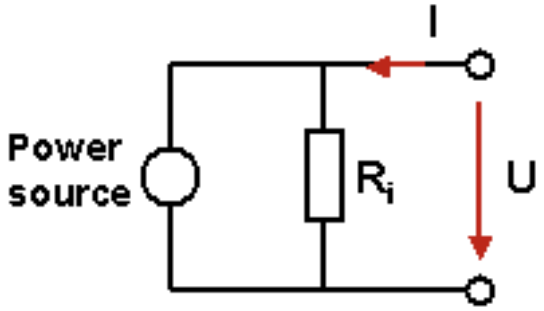

(b) Equivalent circuit diagram for a discrete port S-Parameter calculation.

Figure 5.7: Discrete port CST visualization and equivalent circuit.

5.2.1 Single Element 8.25 GHz Patch Antenna

In the following case for a single element patch antenna, the dimensions and materials are in table 5.2:

Parameter	Value
Substrate Type	FR-4
Dielectric Constant	4.6
Substrate Height (h)	0.7 mm
Resonant Frequency	8.25 GHz
Patch Thickness (t)	0.035mm
L_p	8.28 mm
W_p	10.86 mm
Feed point (y_o)	2.1 mm

Table 5.2: Parameters for a 8.25 GHz patch antenna.

To increase the resonant frequency to higher orders of magnitude, the dimensions of the patch antenna needs to be smaller, following all of the formulae presenter earlier we got the dimensions as seen on table 5.2 and in this case for a single element patch antenna the resonant frequency was achieved at a value of 8.216 GHz with a magnitude of -41.45 dB as seen on figure 5.8a. This great result was reflected on the impedance view with a value of 49.76 Ω at resonant frequency as seen on figure 5.8b.

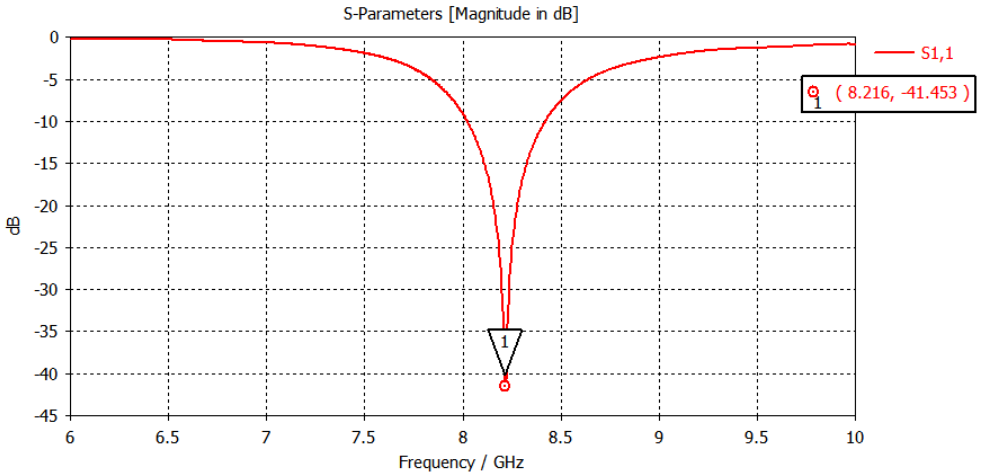

(a) S-Parameters of the 8.25 GHz single element patch antenna. Image generated form CST.

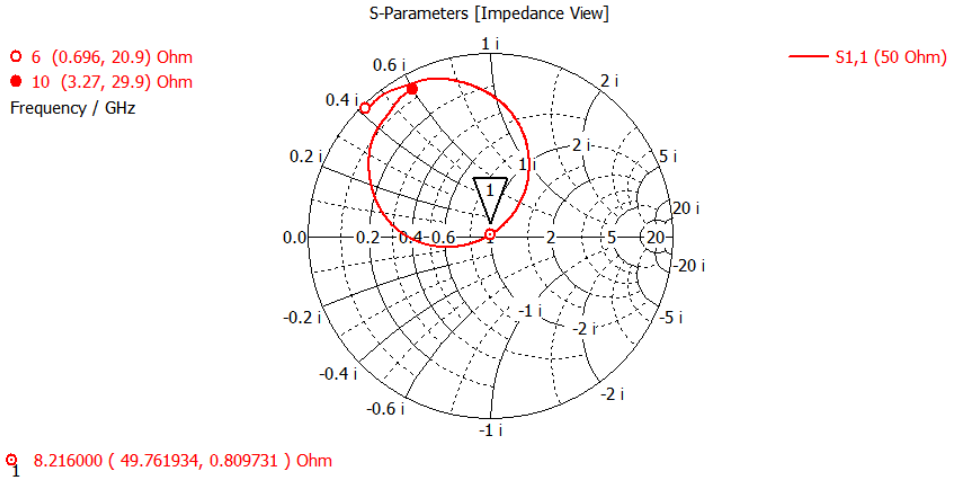

(b) Impedance view of the 8.25 GHz single element patch antenna. Image generated form CST.

Figure 5.8: S-Parameters and Smith chart of single element 8.25 GHz patch antenna.

On figure 5.9a we can observe that at resonant frequency we have a high power efficiency, with an initial $0.5\,W$ fixed power given into the system we get an output of $0.499\,W$. On figure 5.9b we can analyze that the radiation pattern of the antenna is in good shape with a peak gain of 8.798 dB, realized gain of 8.797 dB and directivity of 11.12 dB.

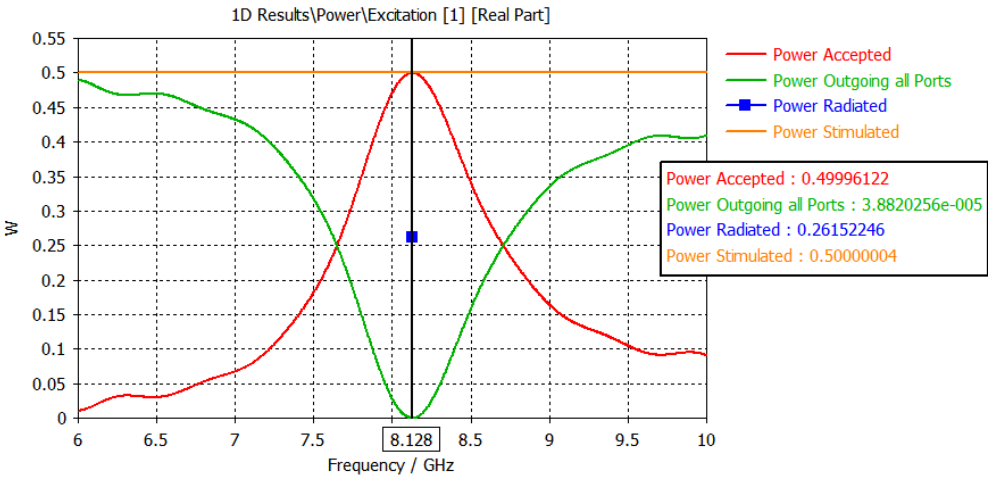

(a) Power spectrum of the 8.25 GHz single element. Image generated form CST.

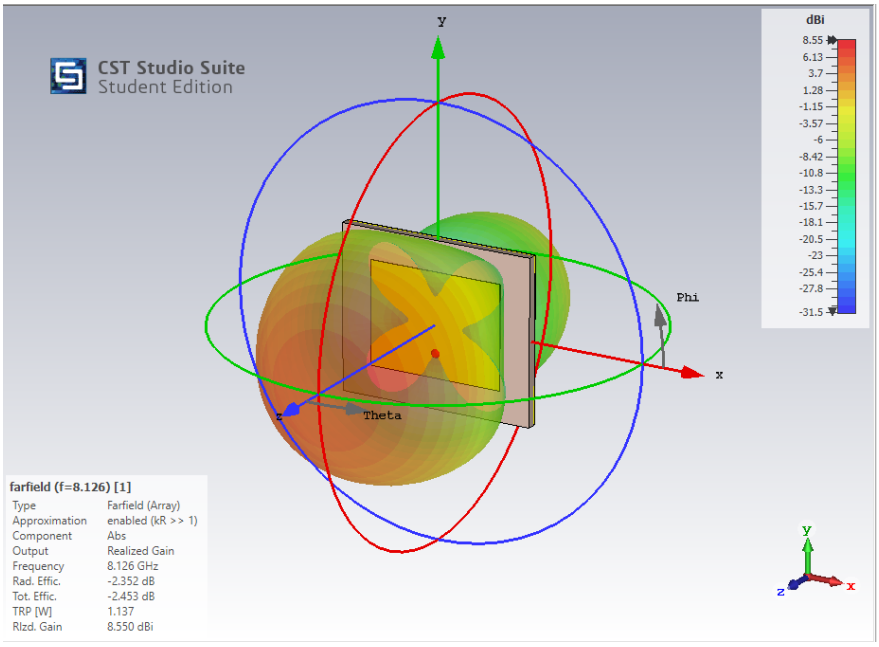

(b) Radiation Pattern of the 8.25 GHz single element. Image generated form CST.

Figure 5.9: Power spectrum and radiation gain of single element 8.25 GHz patch antenna.

5.2.2 2x2 Element 8.25 GHz Phased Array

On this sub-case of the 8.25 GHz patch antenna, we are going to extend the number of antennas to 4 to make a 2x2 element phased array. The horizontal and vertical spacing is $\frac{\lambda}{2} = 18.18\,mm$. Some features of this 2x2 phased array are that all patched are on top of a single ground/substrate plate and it is using FR-4 as substrate material with the following property values ($\varepsilon = 4.6$, loss tangent $\delta = 0.018$ at $0.016\,\text{GHz}$)

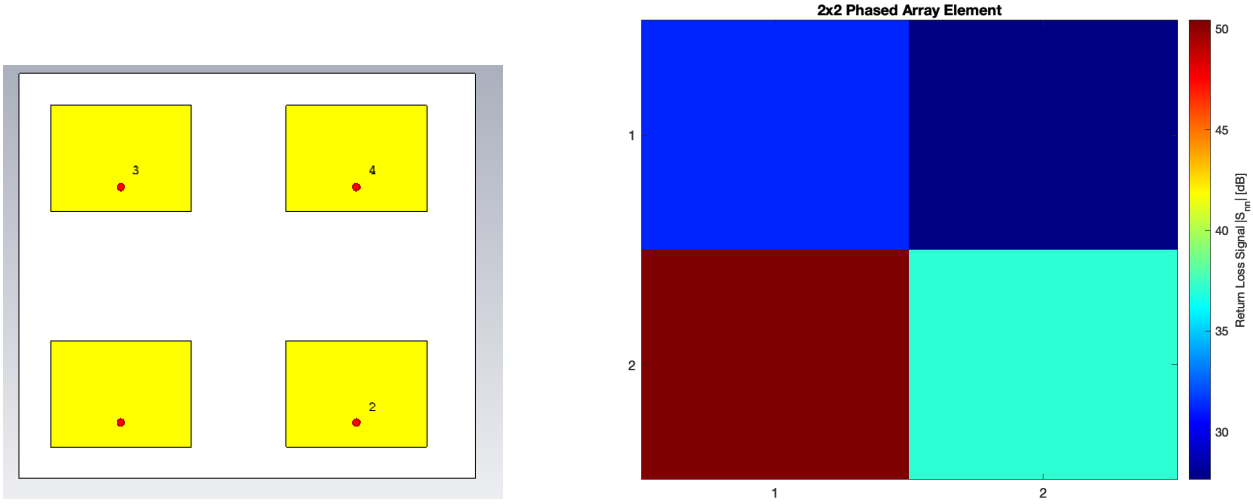

(a) Visualization and antenna positioning of the 8.25 GHz 2x2 element phased array. Image generated form CST.

(b) Color map for 2x2 return loss signal.

Figure 5.10: Visualization and color mapping for return loss signal for 2x2 phased array element.

In this scenario we can observe that by adding 3 antennas the resonant frequency has shifted to the left at 7.972 GHz, on antennas 1, 2, 3, 4 it is observed that the magnitude has values of $-50.75\,\text{dB}$ and $-37.66\,\text{dB}$, $-31.21\,\text{dB}$ and $-27.61\,\text{dB}$, there is some symmetry with these results as the effect of the location of the antennas mainly on the transmission coefficients. The values for the impedance for antennas 1,2,3,4 are ($49.94\,\Omega$, $49.15\,\Omega$, $48.28\,\Omega$, $47.03\,\Omega$,) respectively, we can observe that these values are around the $50\,\Omega$ mark.

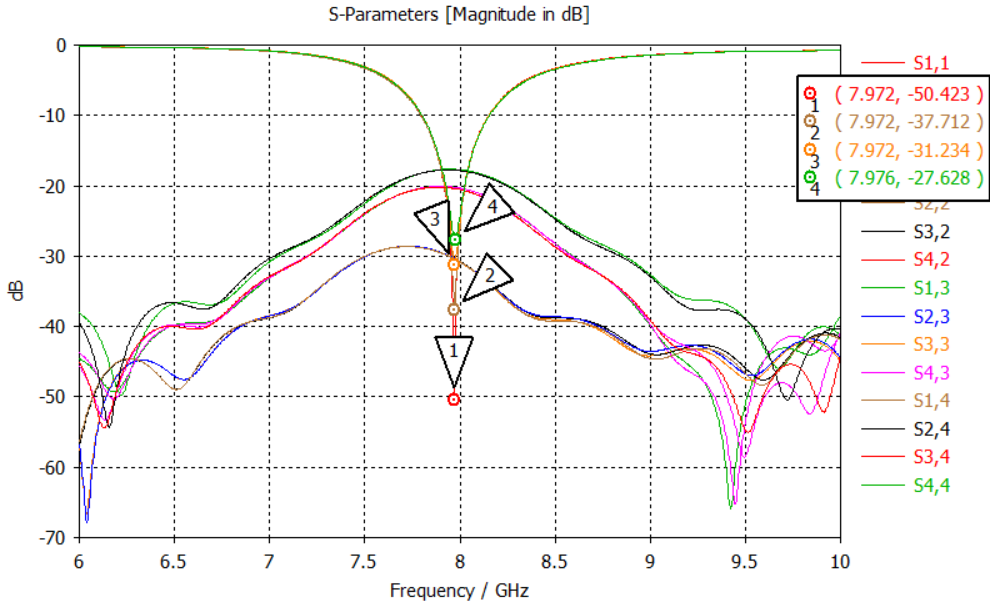

(a) S-parameters of the 8.25 GHz 2x2 element phased array. Image generated form CST.

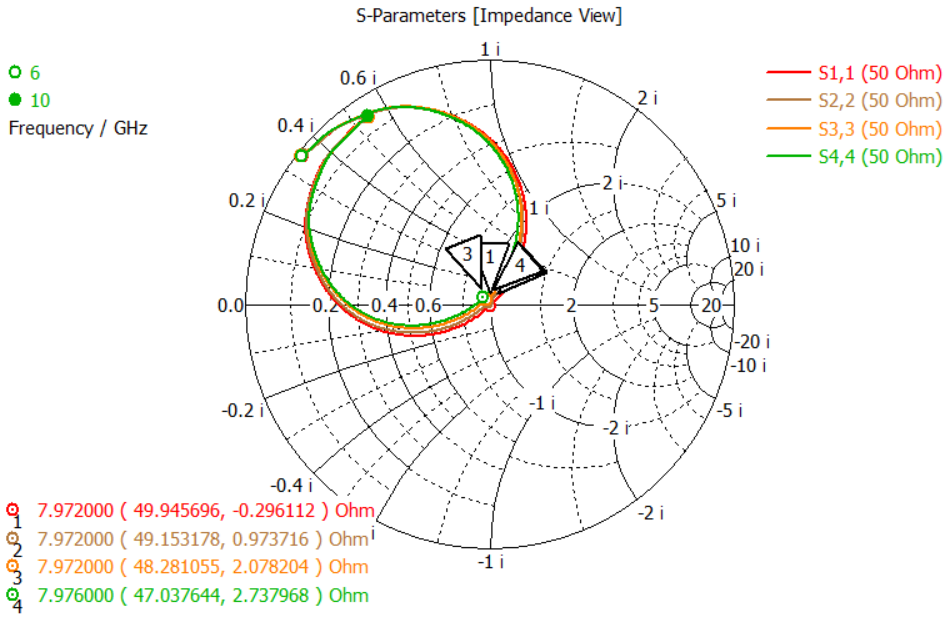

(b) Impedance view of the 8.25 GHz 2x2 element phased array. Image generated form CST.

Figure 5.11: S-Parameters and Smith chart of 2x2 element 8.25 GHz patch antenna.

In the power spectrum results at resonant frequency it is observed that the power accepted is of 1.92 W, great efficiency, and the power outgoing all ports has a value of 0.076 W. And lastly for the radiation pattern for the phased array, we can see that at resonant frequency the peak of the gain is about 10.79 dB, for realized gain it's 10.61 dB and for directivity is 13.17 dB. It is also observed that the shape of the radiation pattern as its centered between the four antennas, and, at some extend, the feed point location has a factor on the orientation of the radiation pattern.

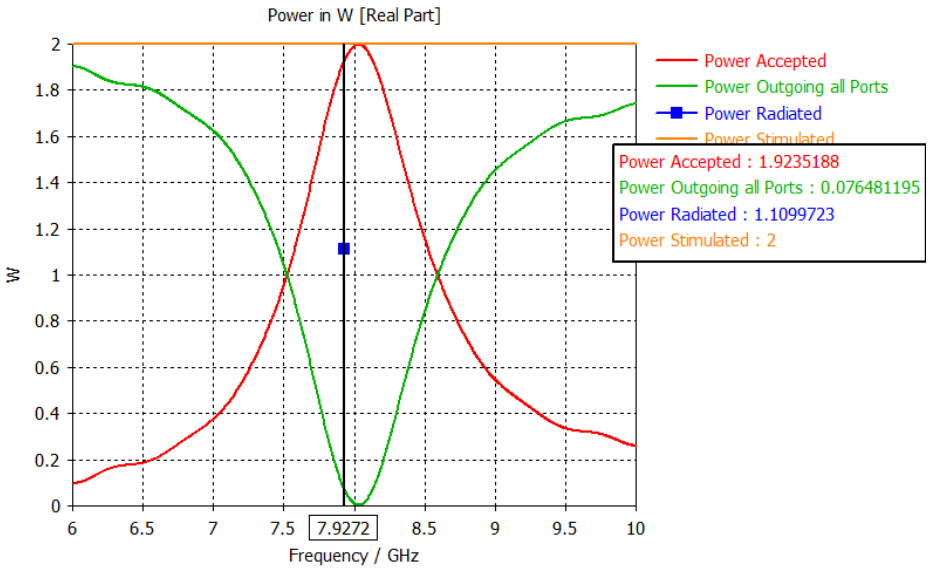

(a) Power spectrum of the 8.25 GHz 2x2 element phased array. Image generated form CST.

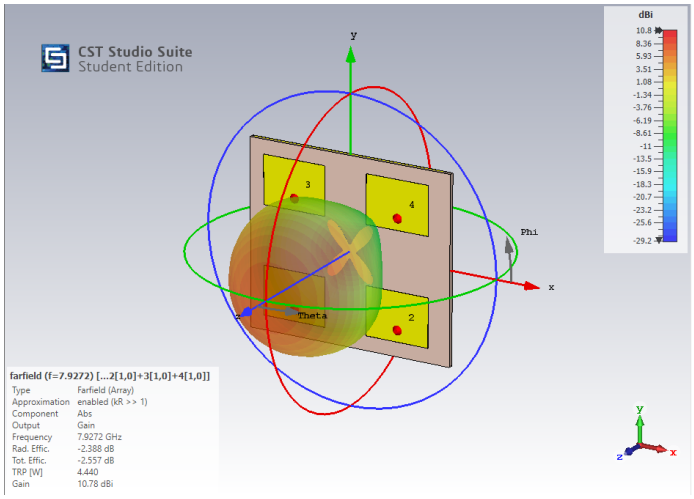

(b) Radiation pattern of the 8.25 GHz 2x2 element phased array. Image generated form CST.

Figure 5.12: Power results and radiation pattern of 2x2 element 8.25 GHz patch antenna.

5.2.3 3x3 Element 8.25 GHz Phased Array

On these batch of results we are going to analyze the physical properties of a 3x3 phased array element with the same specifications as before. In this scenario we can observe that the resonant frequency have remained relatively the same between 7.98 GHz and 7.94 GHz.

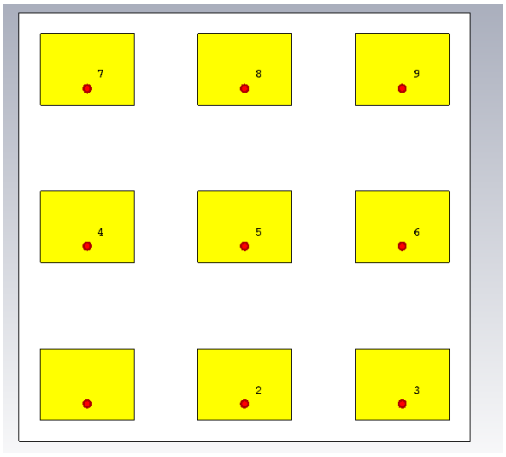

(a) Visualization and antenna positioning of the 8.25 GHz 3x3 element phased array. Image generated form CST.

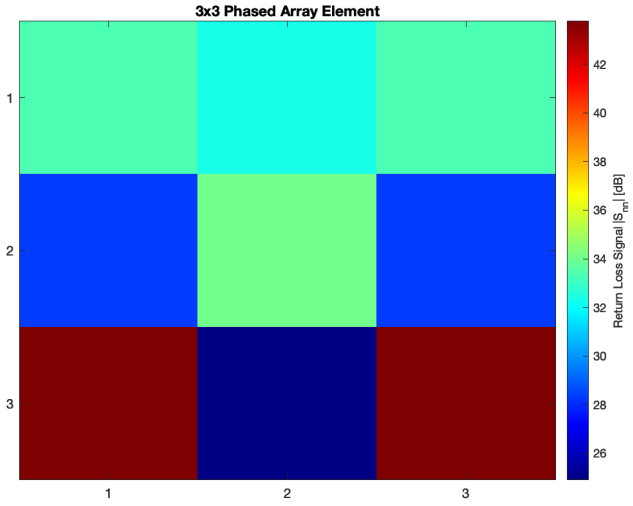

(b) Color map for 3x3 return loss signal.

Figure 5.13: Visualization and color mapping for return loss signal for 3x3 phased array element.

The elements with the highest return signal values are antennas 1 and 3 with -43.811 dB, and the element with the lowest values is antenna 2 with -24.81 dB. The highest magnitude of return loss signal is been concentrated on the bottom corners of the phased array and the center. The values for the impedance for antennas are around the 50 Ω mark.

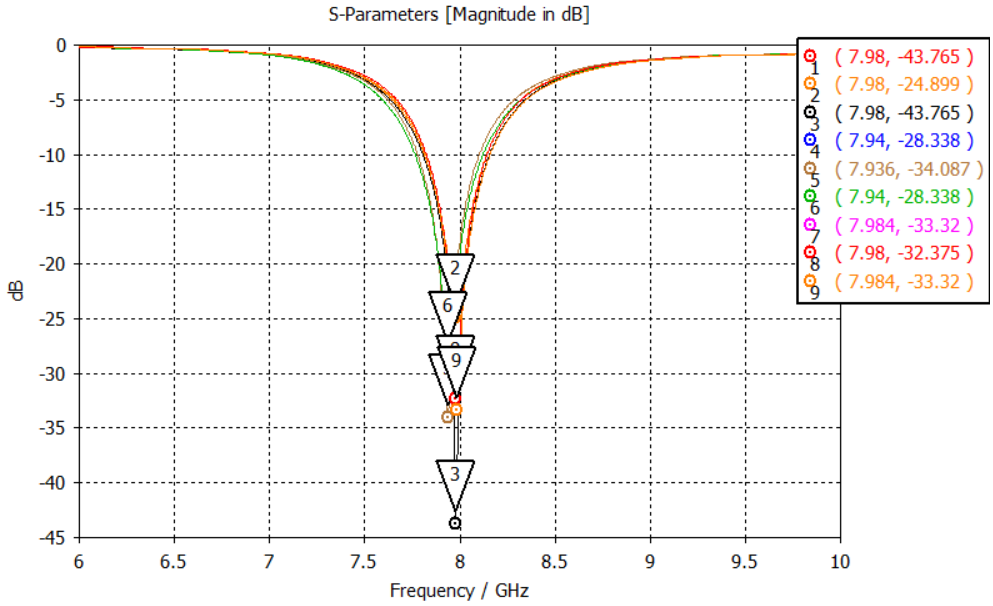

(a) S-parameters of the 8.25 GHz 3x3 element phased array. Image generated form CST.

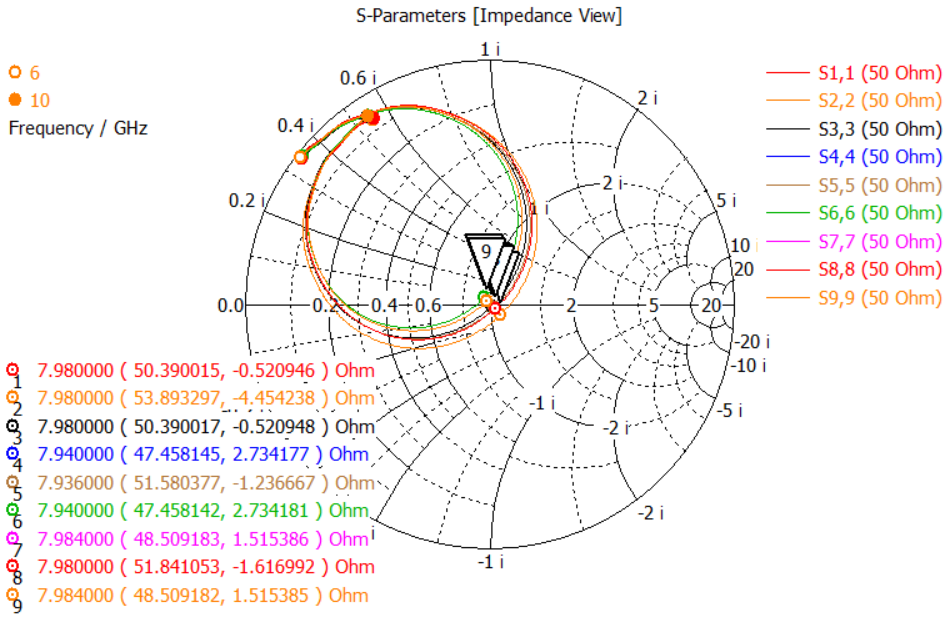

(b) Smith Chart of the 8.25 GHz 3x3 element phased array. Image generated form CST

Figure 5.14: S-Parameters and Smith chart of 3x3 element 8.25 GHz patch antenna.

In the power spectrum results at resonant frequency it is observed that the power accepted is of 4.44 W out of 4.5 W for stimulated power, the power outgoing all ports has a value of 0.058 W, and the power radiated has a value of 2.619 W. And lastly for the radiation pattern for the phased array, we can see that at resonant frequency the peak of the gain is about 13.59 dB, for realized gain it's 13.53 dB and for directivity is 15.88 dB. It is also observed that the shape of the radiation pattern as its centered between the 9 antennas and we see that the major lobe has a higher degree of influence between the radiation shape and there are several minor lobes surrounding the major lobe.

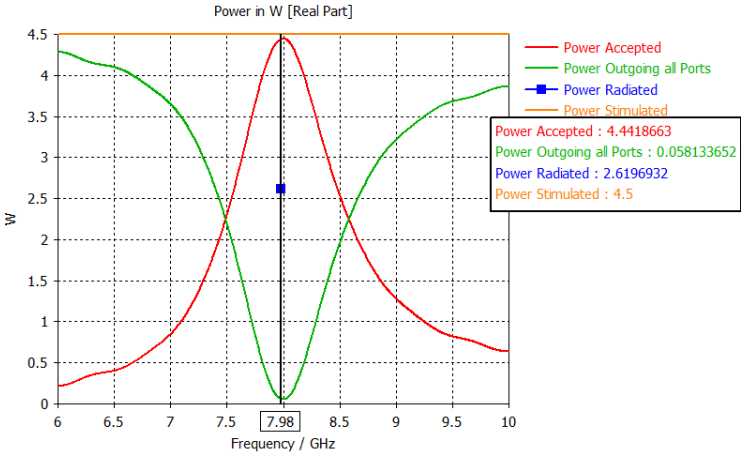

(a) Power results of the 8.25 GHz 3x3 element phased array. Image generated form CST.

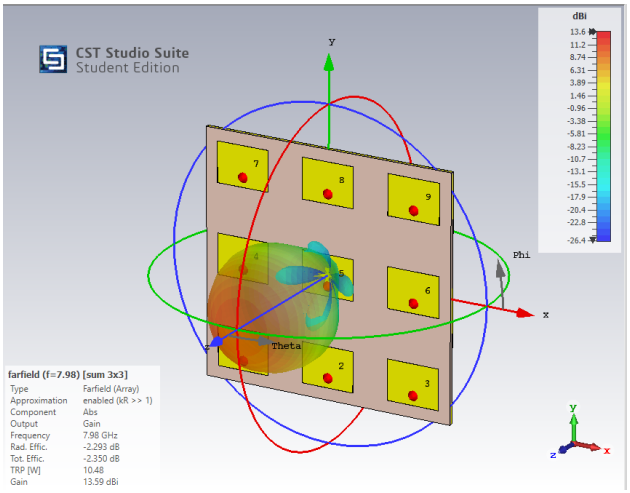

(b) Radiation pattern of the 8.25 GHz 3x3 element phased array. Image generated form CST.

Figure 5.15: Power results and radiation pattern of 3x3 element 8.25 GHz patch antenna.

5.2.4 4x4 Element 8.25 GHz Phased Array

On these batch of results we are going to analyze the physical properties of a 4x4 phased array element with the same specifications as before.

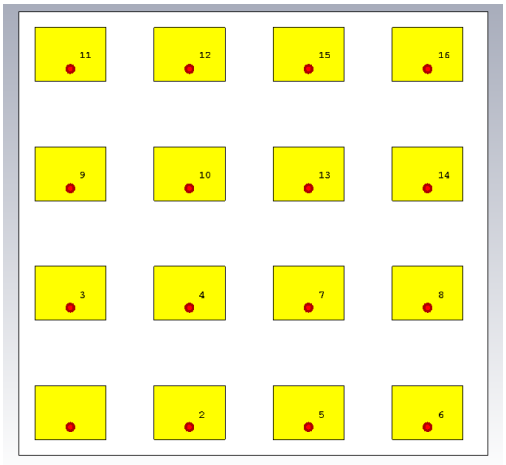

(a) Visualization and antenna positioning of the 8.25 GHz 4x4 element phased array. Image generated form CST.

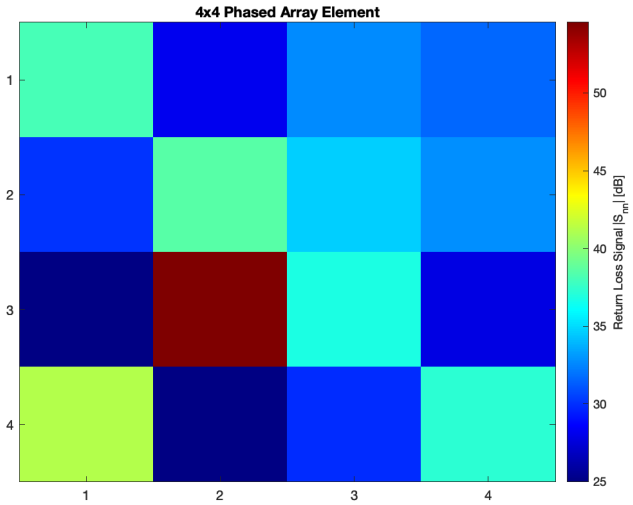

(b) Color map for 4x4 return loss signal.

Figure 5.16: Visualization and color mapping for return loss signal for 4x4 phased array element.

In this scenario we can observe that the resonant frequency have remained relatively the same between 7.98 GHz and 7.94 GHz. The elements with the highest return signal values are antenna 6 -54.53 dB, and the element with the lowest values is antenna 2 with -24.97 dB. We can observe that the highest value is located at the center of the phased array and it kind of has some diagonal influence on the corners to have more magnitude. The values for the impedance for antennas are around the 50 Ω mark.

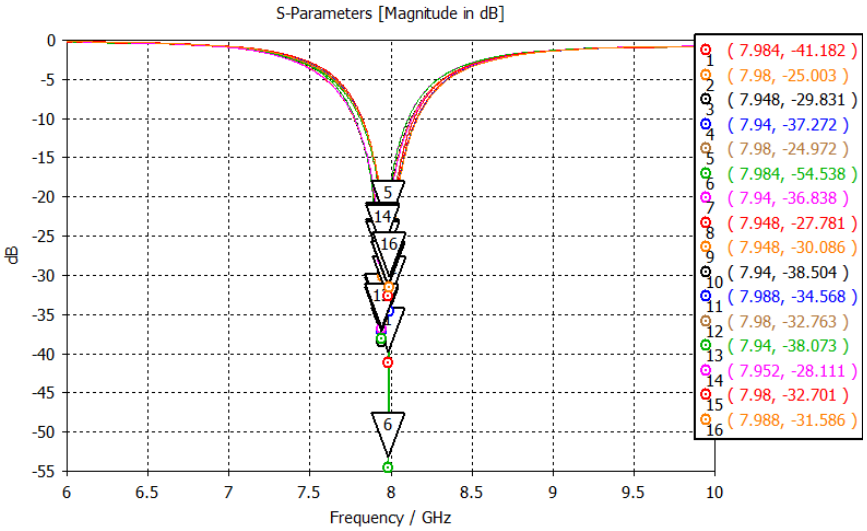

(a) S-Parameters of the 8.25 GHz 4x4 element phased array. Image generated form CST.

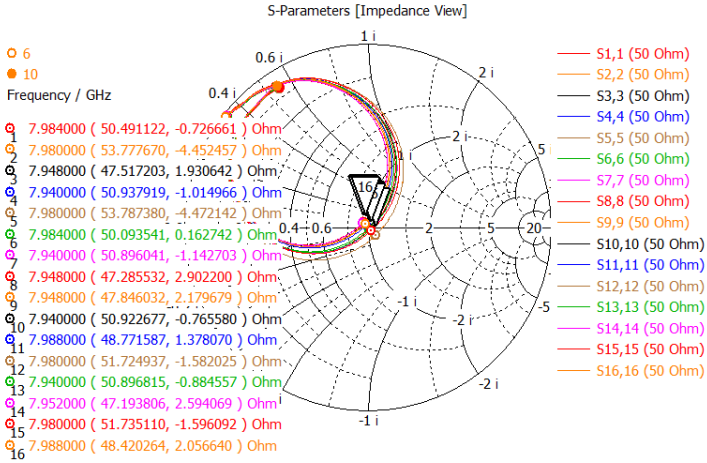

(b) Smith Chart of the 8.25 GHz 4x4 element phased array. Image generated form CST.

Figure 5.17: S-Parameters and Smith Chart of 4x4 element 8.25 GHz patch antenna.

In the power spectrum results at resonant frequency it is observed that the power accepted is of 7.93 W out of 8 W for stimulated power, the power radiated has a value of 4.73 W. And lastly for the radiation pattern for the phased array, we can see that at resonant frequency the peak of the gain is about 15.62 dB, for realized gain it's 15.59 dB and for directivity is 17.87 dB. The major lobe is still at the center of the phased array but now there are four minor lobes with considerable influence in the radiation.

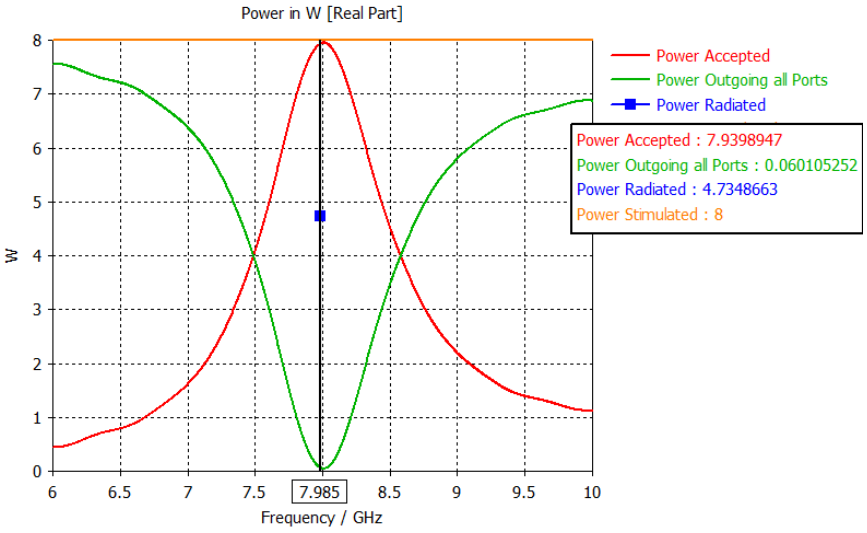

(a) [Power results of the 8.25 GHz 4x4 element phased array. Image generated form CST.

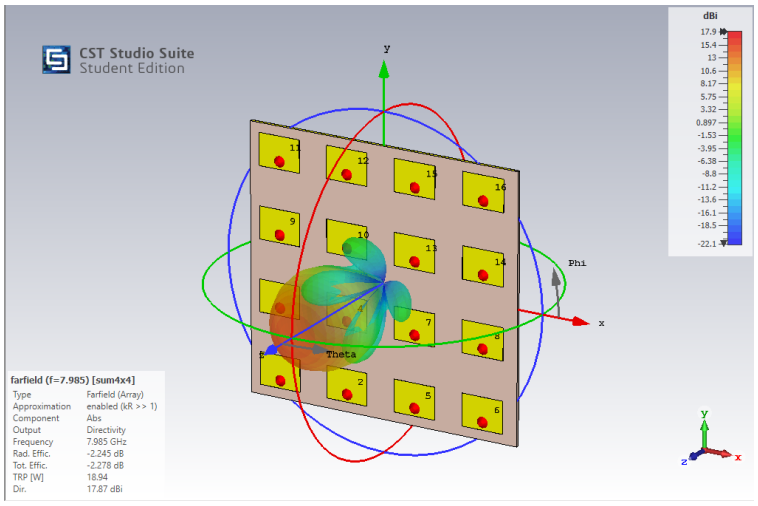

(b) Aerial view radiation pattern of the 8.25 GHz 4x4 element phased array. Image generated form CST.

Figure 5.18: Power results and radiation pattern of 8.25 GHz 4x4 element phased array.

5.2.5 5x5 Element 8.25 GHz Phased Array

On these batch of results we are going to analyze the physical properties of a 5x5 phased array element with the same specifications as before. We can now observe that on figure 5.19b that the distribution of return loss signals from each individual antenna is being centered and we even have some high intensity cross-polarized amplitudes. With the highest amplitude going into the absolute center of the phased array. This may be explained because of the geometry of the structure. We can also observe some relatively low amplitude measurements at the sides of the phased array.

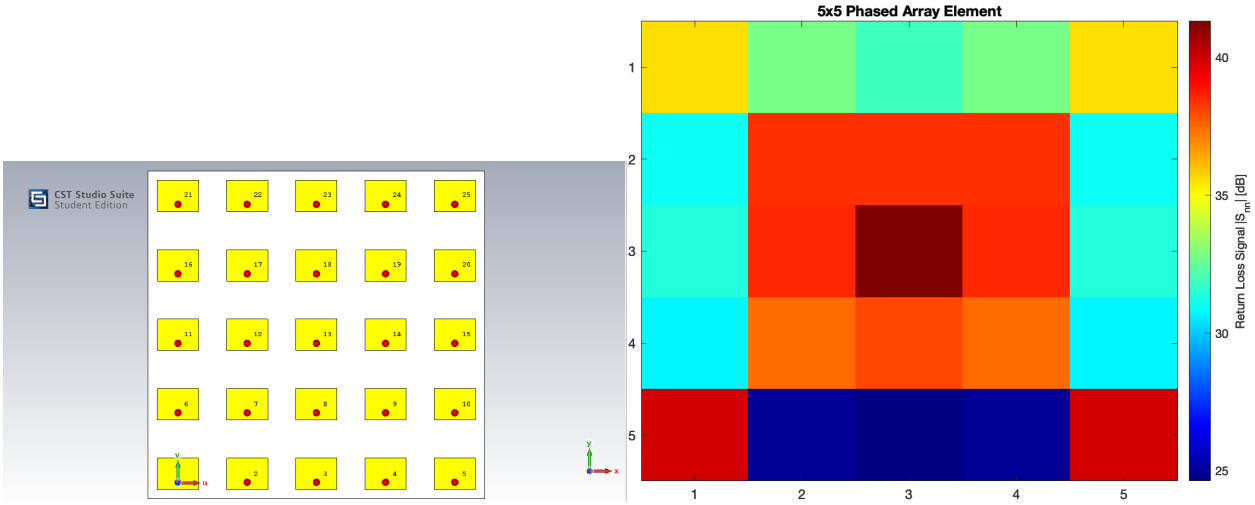

(a) Visualization and antenna positioning of the 8.25 GHz 5x5 element phased array. Image generated form CST.

(b) Color map for 5x5 return loss signal.

Figure 5.19: Visualization and color mapping for return loss signal for 5x5 phased array element.

In this scenario we can observe that the resonant frequency have remained relatively the same between 7.98 GHz and 7.94 GHz. The values for the impedance for antennas are around the 50 Ω mark.

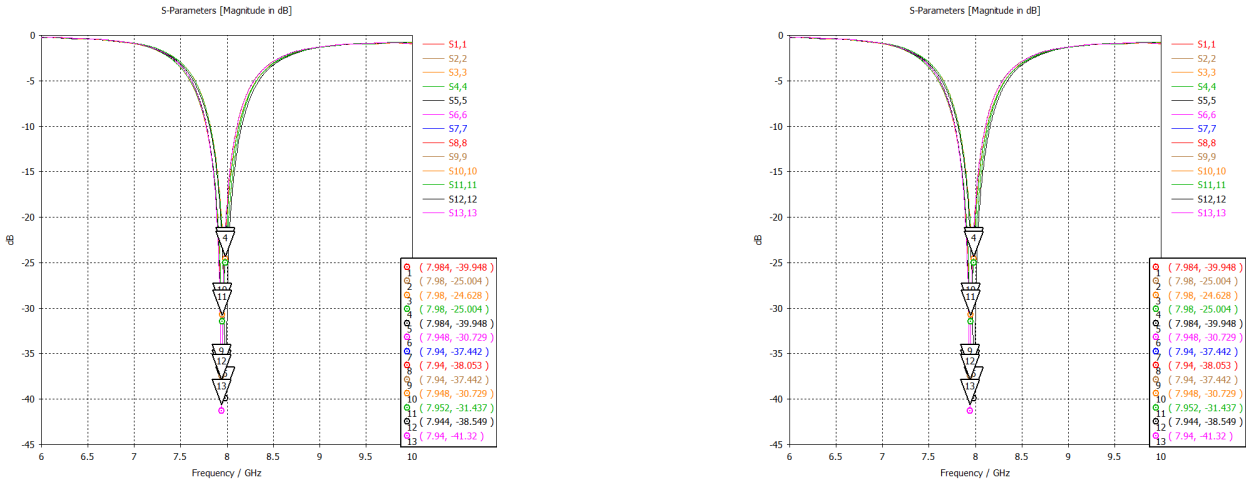

(a) a) S-Parameter return loss signals of antennas 1-13.

(b) b) S-Parameter return loss signals of antennas 14-25.

Figure 5.20: Return loss signals for 5x5 phased array element.

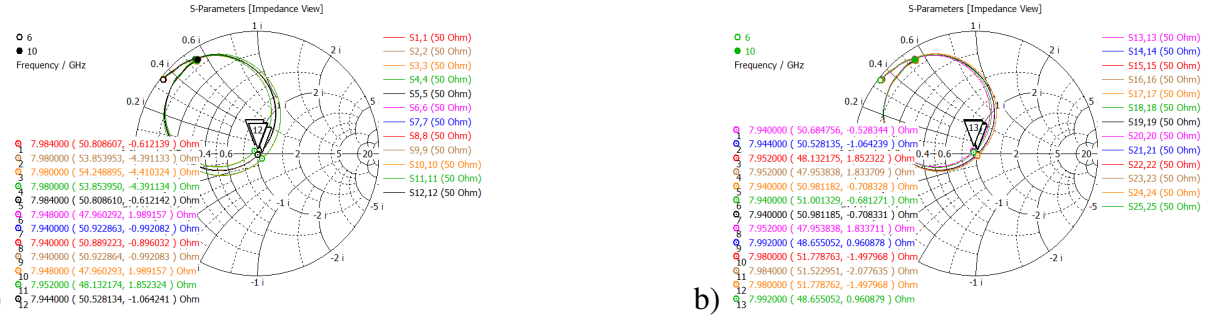

a) b)

Figure 5.21: a) Smith Chart return loss signals of antennas 1-13. b) Smith Chart return loss signals of antennas 14-25.

In the power spectrum results at resonant frequency it is observed that the power accepted is of 12.3 W out of 12.5 W for stimulated power, the power outgoing all ports has a value of 0.19 W, and the power radiated has a value of 7.37 W. And lastly for the radiation pattern for the phased array, we can see that at resonant frequency the peak of the gain is about 17.34 dB, for realized gain it's 17.27 dB and for directivity is 19.56 dB. The major lobe has now a more sharp shape and its

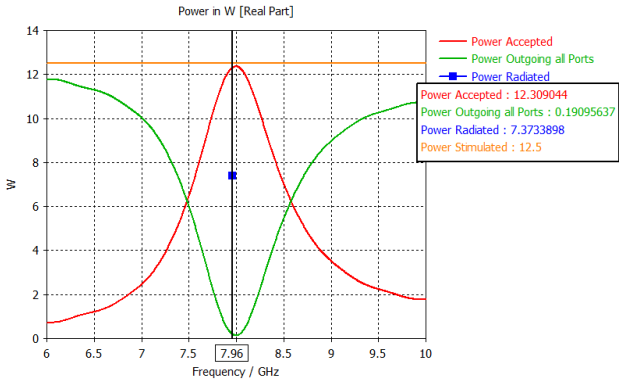

(a) Power results of the 8.25 GHz 5x5 element phased array. Image generated form CST.

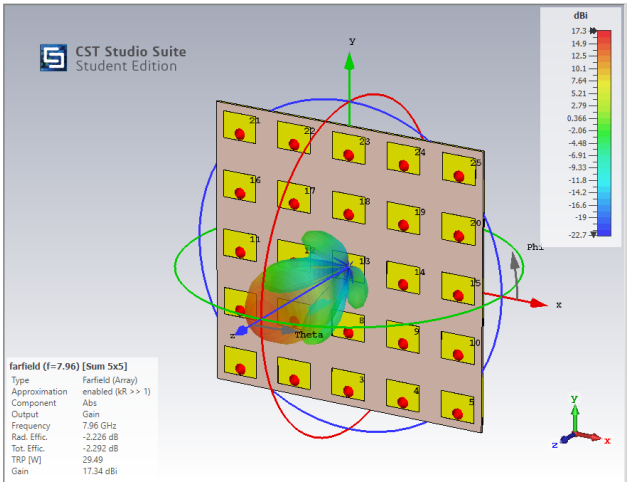

(b) Aerial view radiation pattern of the 8.25 GHz 5x5 element phased array. Image generated form CST.

Figure 5.22: Power results and radiation pattern of 8.25 GHz 5x5 element phased array.

still at the center of the phased array, there are still four minor lobes with considerable influence in the radiation and sharp shape.

5.2.6 6x6 Element 8.25 GHz Phased Array

On these batch of results we are going to analyze the physical properties of a 6x6 phased array element with the same specifications as before. We can observe that the highest return loss values are concentrated again at the center of the phased array and also diagonal antennas benefits with extra magnitude for their signals.

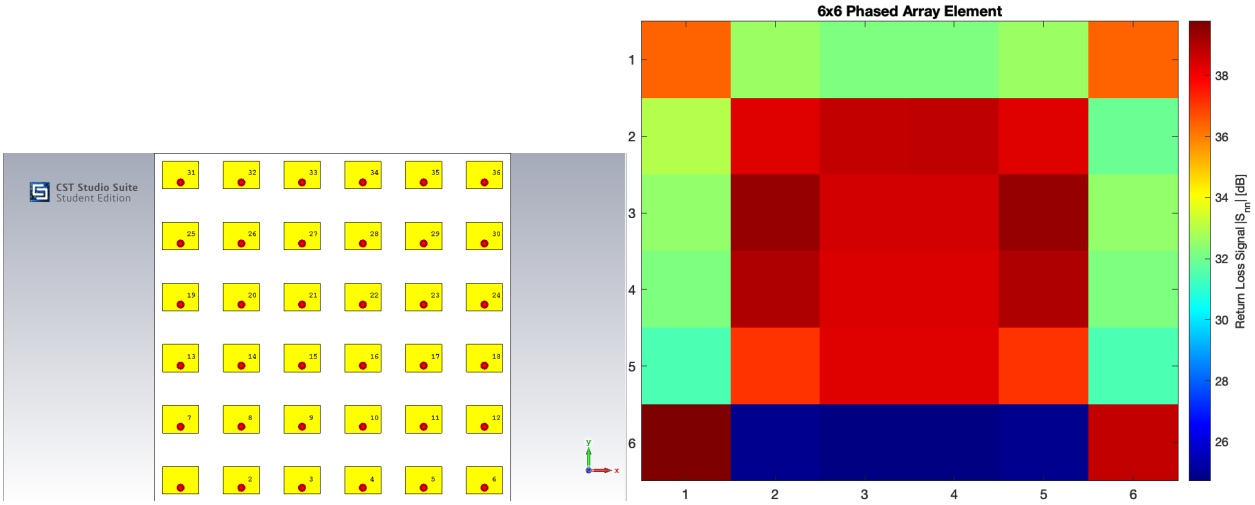

(a) Visualization and antenna positioning of the 8.25 GHz 6x6 element phased array. Image generated form CST.

(b) Color map for 6x6 return loss signal.

Figure 5.23: Visualization and color mapping for return loss signal for 6x6 phased array element.

In this scenario we can observe that the resonant frequency have remained relatively the same between 7.98 GHz and 7.94 GHz. The values for the impedance for antennas are around the 50 Ω mark. In the power spectrum results at resonant frequency it is observed that the power accepted is of 17.86 W out of 18 W for stimulated power, the power outgoing all ports has a value of 0.13 W, and the power radiated has a value of 10.79 W.

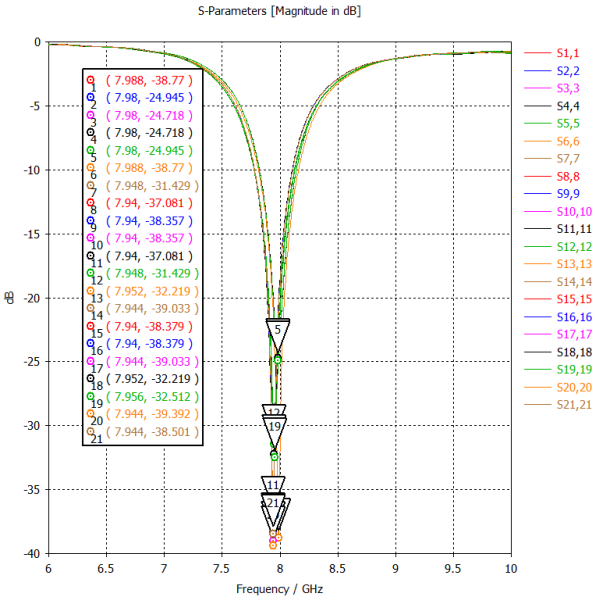

(a) S-Parameter return loss signals of antennas 1-21.

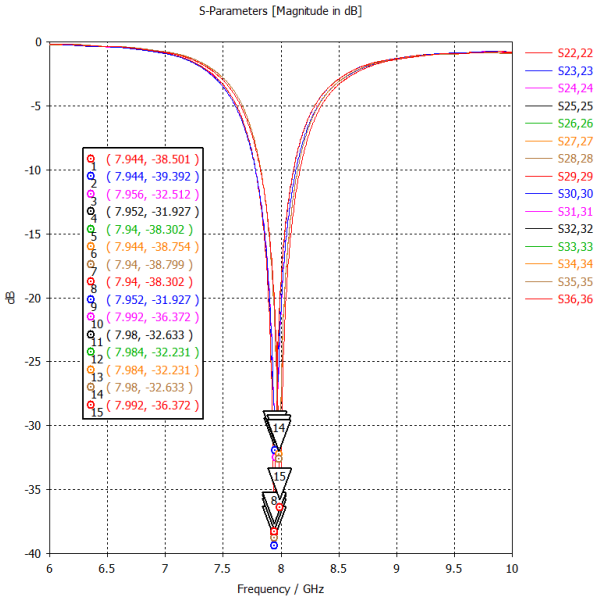

(b) S-Parameter return loss signals of antennas 22-36.

Figure 5.24: Reflection coefficients of all elements of 8.25 GHz 6x6 phased array.

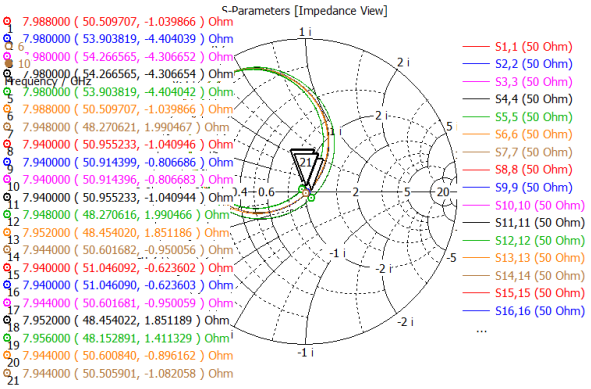

(a) Smith Chart return loss signals of antennas 1-21.

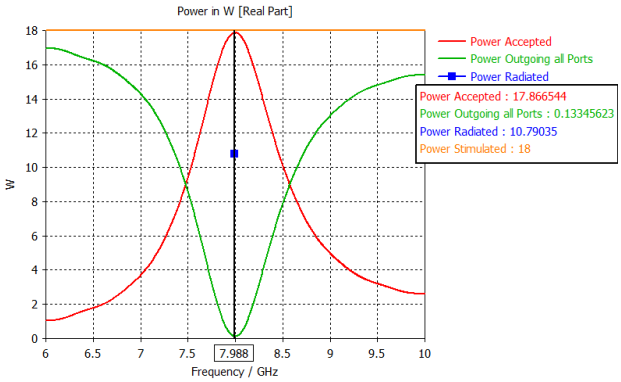

(b) Power results of the 8.25 GHz 6x6 element phased array. Image generated form CST.

Figure 5.25: Smith Chart and power results of of 8.25 GHz 6x6 phased array.

And lastly for the radiation pattern for the phased array, we can see that at resonant frequency the peak of the gain is about 18.81 dB, for realized gain it's 18.77 dB and for directivity is 21 dB. The major lobe has now a more sharp shape and its still at the center of the phased array, there are still four minor lobes with considerable influence in the radiation and sharp shape and now we can see that it has been developed a subset of another four minor lobes which are at least a third of size from the previous minor lobes.

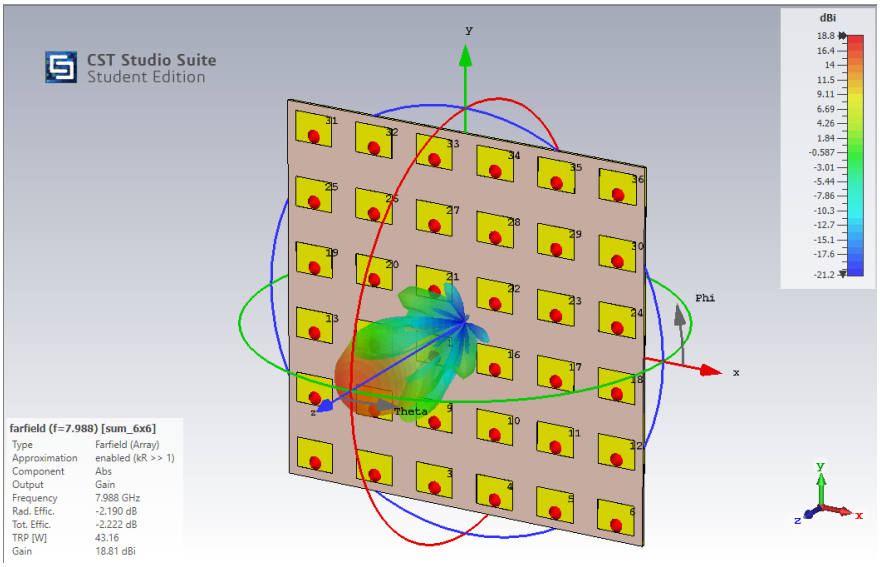

Figure 5.26: Radiation pattern of the 8.25 GHz 6x6 element phased array. Image generated form CST.

5.2.7 7x7 Element 8.25 GHz Phased Array

On these batch of results we are going to analyze the physical properties of a 7x7 phased array element with the same specifications as before. This is the first case that the corners of the phased array doesn't have one of the highest values of them all, yet they still benefit for that diagonal influence from the center. In this scenario we can observe that the resonant frequency have remained relatively the same between 7.76 GHz and 7.88 GHz. The values for the impedance for antennas are around the 50 Ω mark.

In the power spectrum results at resonant frequency it is observed that the power accepted is of 23.78 W out of 24.5 W for stimulated power, the power outgoing all ports has a value of 0.71 W, and the power radiated has a value of 14.46 W. And lastly for the radiation pattern for the phased

array, we can see that at resonant frequency the peak of the gain is about 19.79 dB, for realized gain it's 19.66 dB and for directivity is 21.95 dB. The major lobe has now a more sharp shape and its still at the center of the phased array, now the sub-minor lobes have been sequentially merges with the minor lobes.

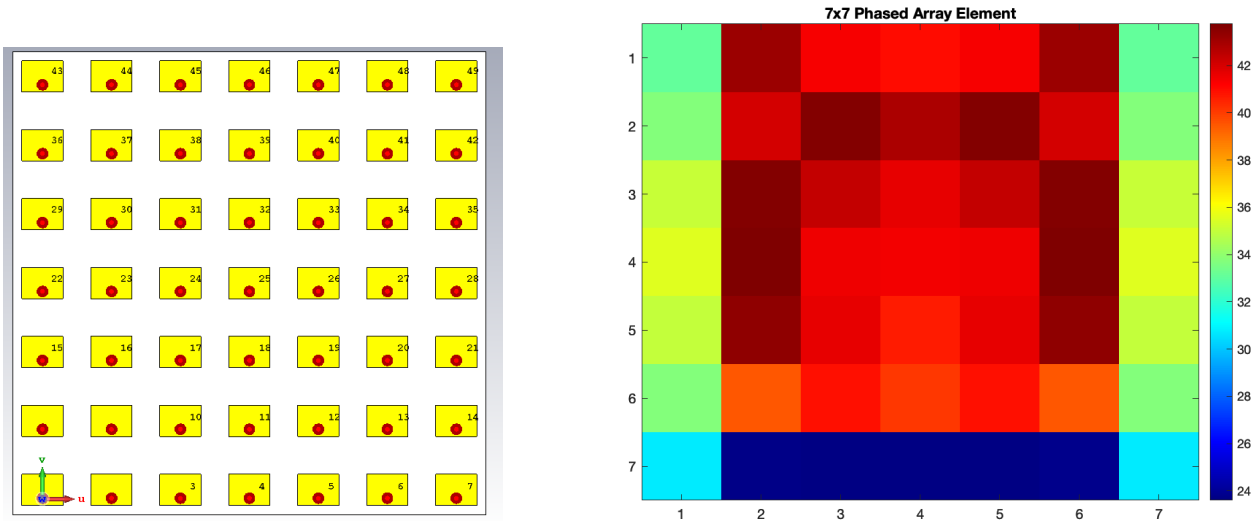

(a) Visualization and antenna positioning of the 8.25 GHz 7x7 element phased array. Image generated form CST.

(b) Color map for 7x7 return loss signal.

Figure 5.27: Visualization and color mapping for return loss signal for 7x7 phased array element.

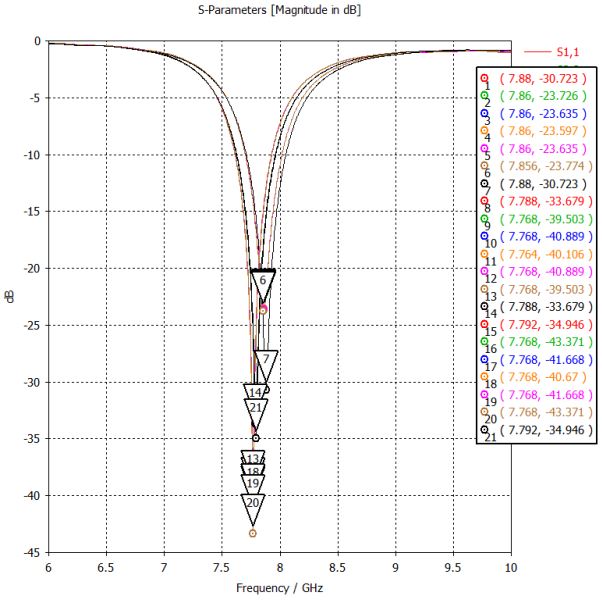

(a) S-Parameter return loss signals of antennas 1-21.

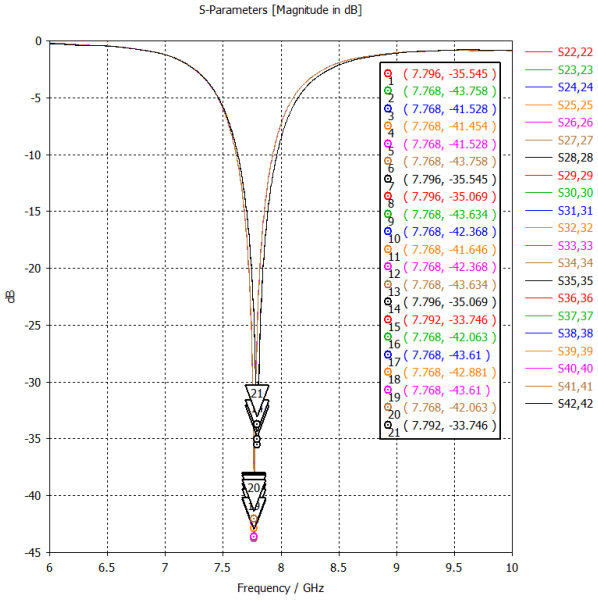

(b) S-Parameter return loss signals of antennas 22-42.

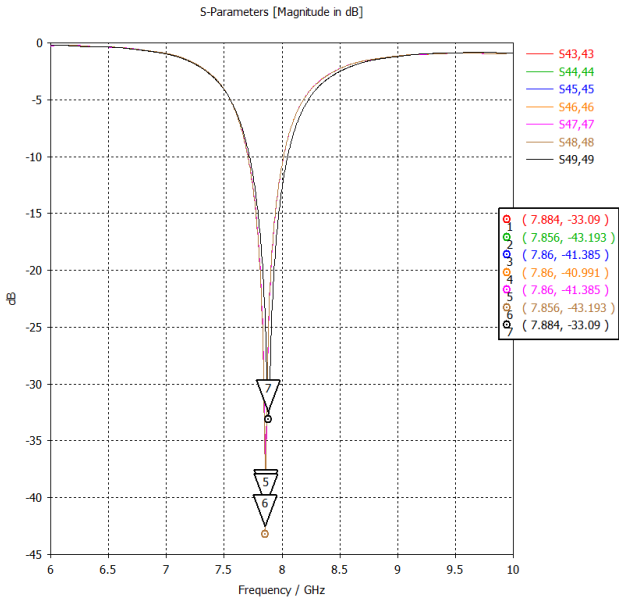

(c) S-Parameter return loss signals of antennas 43-49.

Figure 5.28: Power results and radiation pattern of 8.25 GHx 7x7 element phased array.

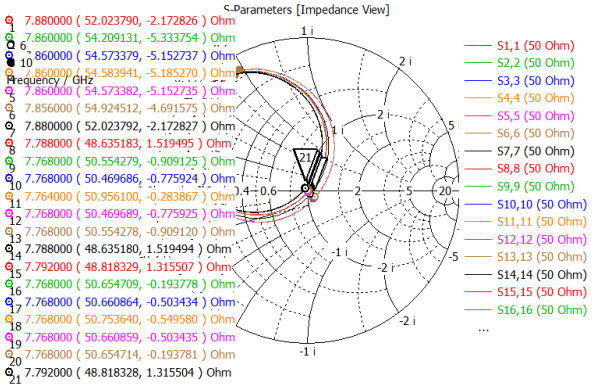

(a) Smith Chart of the 8.25 GHz 7x7 element phased array Image generated form CST.

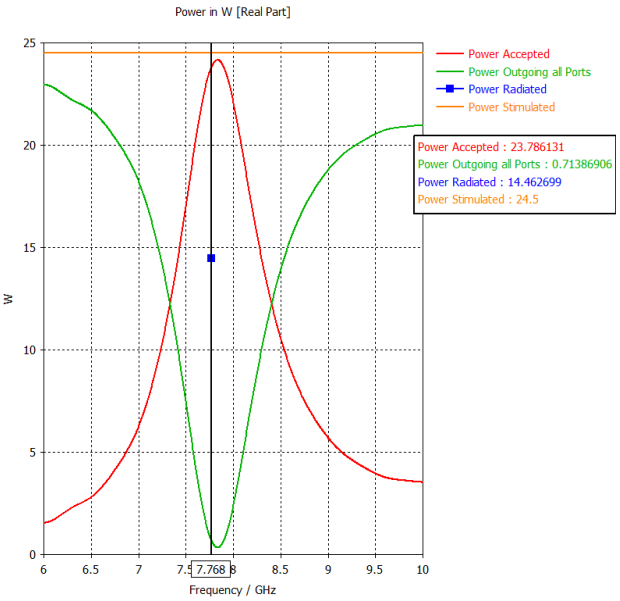

(b) Power results of the 8.25 GHz 7x7 element phased array. Image generated form CST.

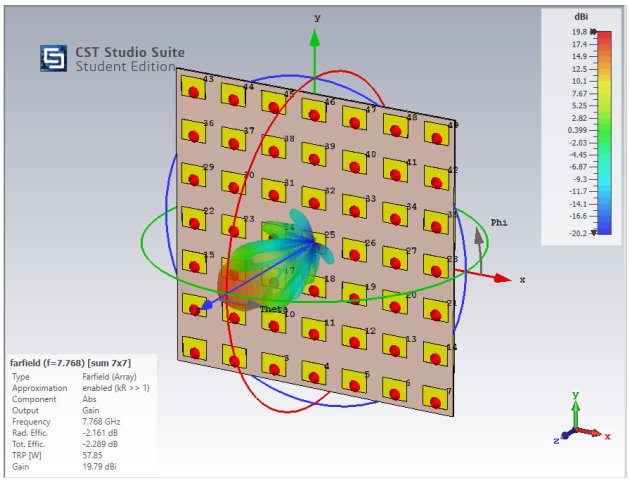

(c) Radiation pattern of the 8.25 GHz 7x7 element phased array. Image generated form CST.

Figure 5.29: Power results and radiation pattern of 8.25 GHx 7x7 element phased array.

5.2.8 8x8 Element 8.25 GHz Phased Array

On these batch of results we are going to analyze the physical properties of a 8x8 phased array element with the same specifications as before. In this scenario we can observe that the resonant frequency have remained relatively the same between 7.76 GHz and 7.88 GHz. This time we can observe that the a rows at the top and the sides of the phased array has the highest values, but the general shape for return signals are such that the center gets most of the signal. The values for the impedance for antennas are around the 50 Ω mark.

In the power spectrum results at resonant frequency it is observed that the power accepted is of 31.3 W out of 32 W for stimulated power, the power outgoing all ports has a value of 0.69 W, and the power radiated has a value of 19.29 W. And lastly for the radiation pattern for the phased array, we can see that at resonant frequency the peak of the gain is about 20.82 dB, for realized gain it's 20.71 dB and for directivity is 22.92 dB. The major lobe has now a more sharp shape and its still at the center of the phased array, there are now several sharp minor lobes and at the base of the radiation we can see some small sub-minor lobes.

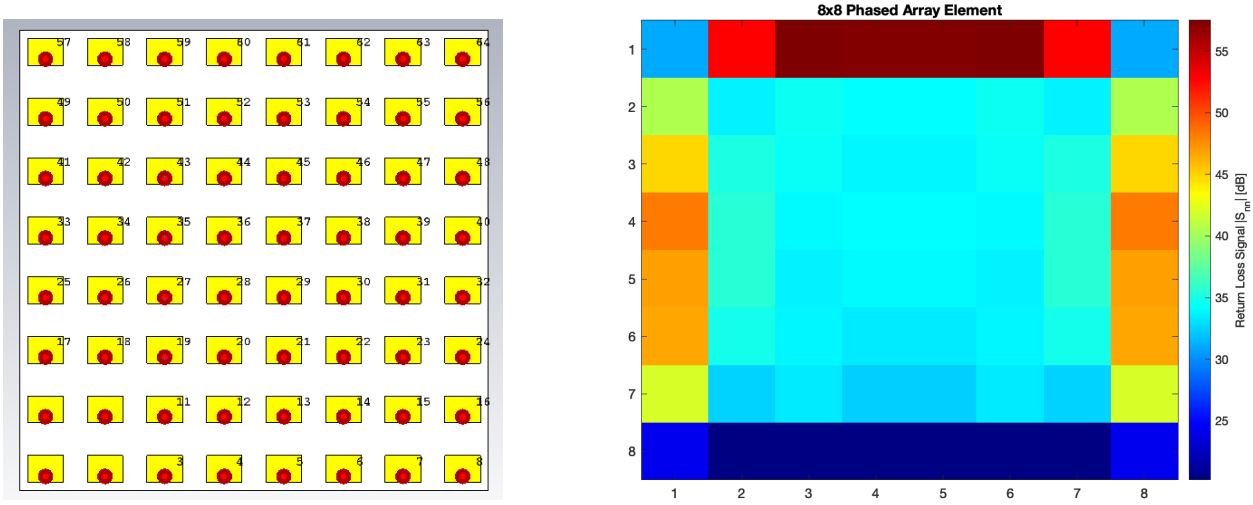

(a) Visualization and antenna positioning of the 8.25 GHz 8x8 element phased array. Image generated form CST.

(b) Color map for 8x8 return loss signal.

Figure 5.30: Visualization and color mapping for return loss signal for 8x8 phased array element.

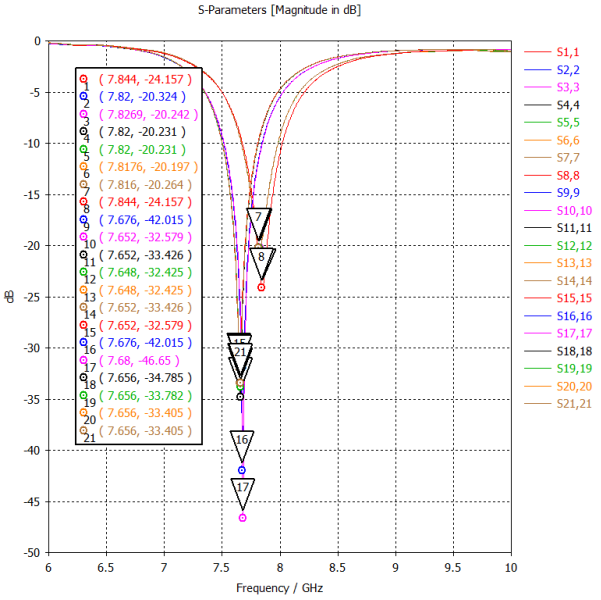

(a) S-Parameter return loss signals of antennas 1-21.

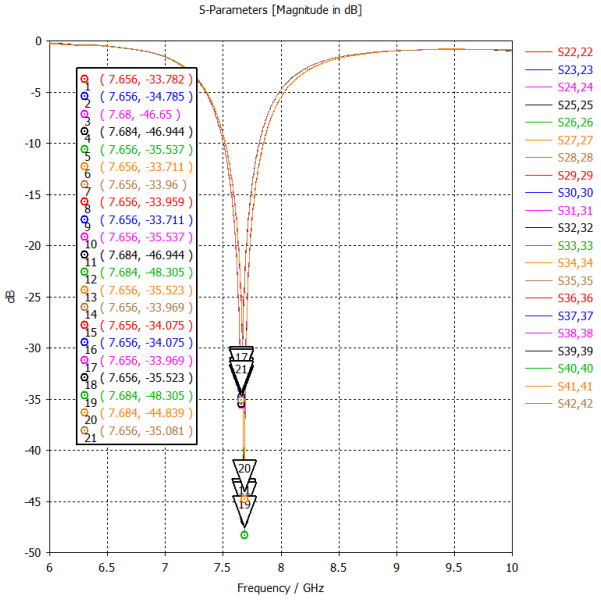

(b) S-Parameter return loss signals of antennas 22-42.

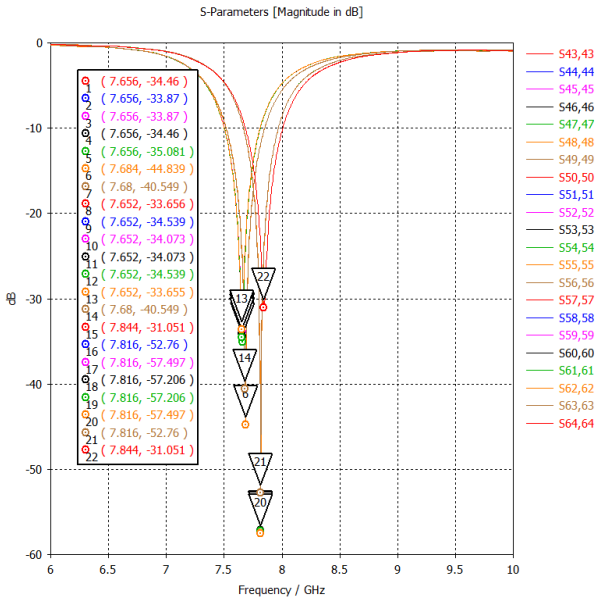

(c) S-Parameter return loss signals of antennas 43-64.

Figure 5.31: Power results and radiation pattern of 8.25 GHx 8x8 element phased array.

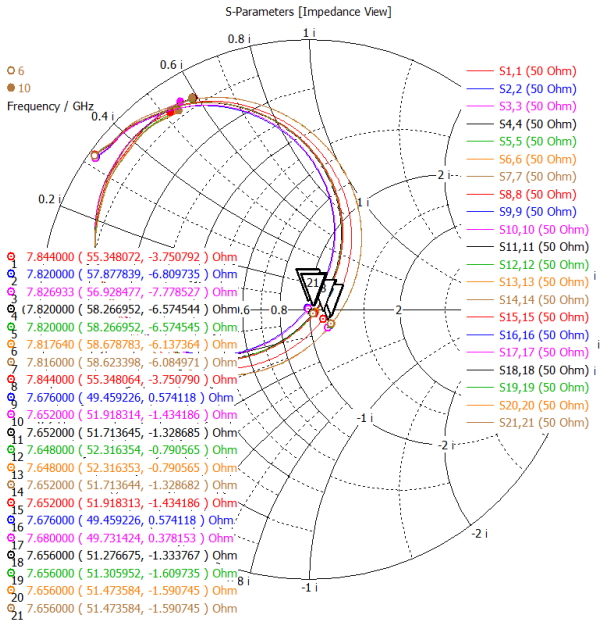

(a) Smith Chart of the 8.25 GHz 8x8 element phased array. Image generated form CST.

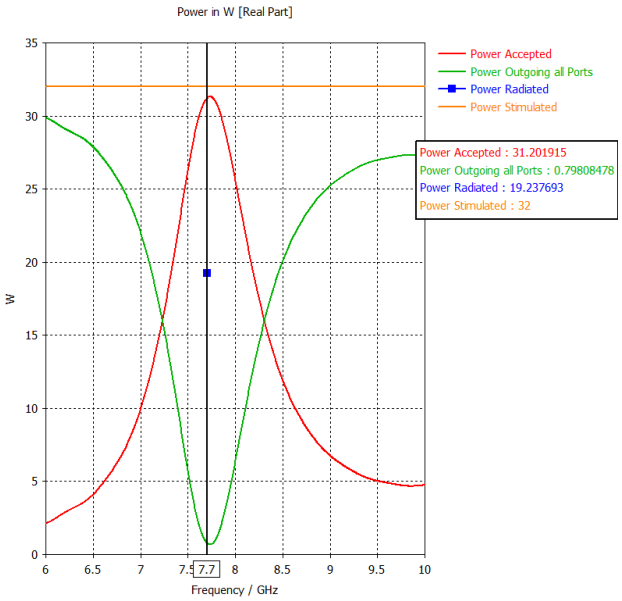

(b) Power results of the 8.25 GHz 8x8 element phased array. Image generated form CST.

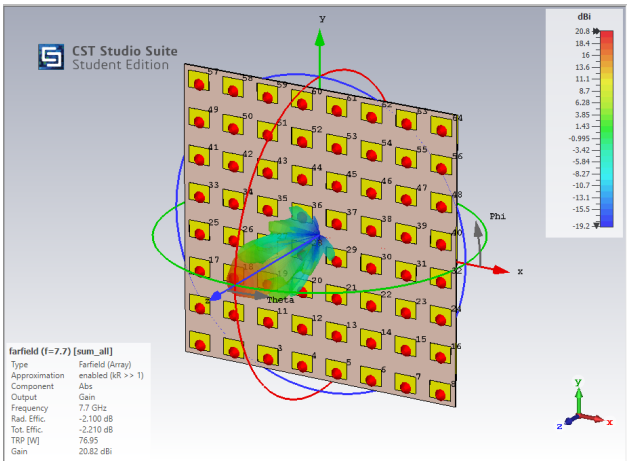

(c) Radiation pattern of the 8.25 GHz 7x7 element phased array. Image generated form CST.

Figure 5.32: Power results and radiation pattern of 8.25 GHx 8x8 element phased array.

5.2.9 Comparison of Gain Values Across Number of Elements for Phased Array

Now that have a lot of data concerning phased array elements from a single patch antenna all the way to an 8x8 element, we can compare and see the behaviour of how the radiation pattern would affect the maximum gain and the frequency allocation. One could infer that since you are adding more and more antennas then the gain should increase linearly, but the following plots proves that's not necessarily the case.

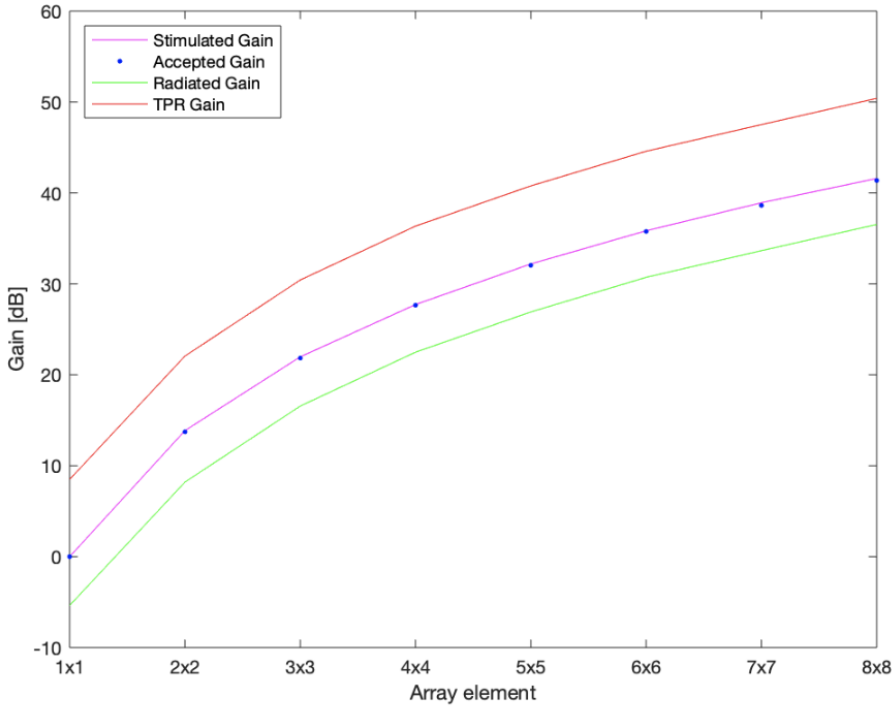

Figure 5.33: Comparison of gain values across number of elements for phased array

First, lets discuss the frequency allocation, from a single element to an 8x8 element the frequency allocation goes to the following values (8.216, 7.972, 7.98, 7.9884,7.94, 7.988, 7.768, 7.328) [GHz]. From this data set we can conclude that the more elements you add to your phased array the resonant frequency shifts towards the left by a considerable amount of 0.244 GHz from single element to 2x2 element and from 2x2 to 7x7 it stays in a relatively similar resonant frequency

up until we reach the 8x8 phased array element. A possible reason for this behaviour is that until that number of elements the phase configuration of the system is such that the resonant frequency gets affected to reach that value.

On figure 5.33 we are analyzing the gain behavior across several data points from the power spectrum results. The stimulated power, accepted power, radiated power and TPR are results that CST gives us and we are going to convert these values into units of dB across all element configurations. Since all measurements are dependent on each other they would show similar behaviour and the only difference would be on their scale. We can see that the lowest in magnitude quantity is the radiated gain. In the middle range of values we have at the same magnitude the accepted gain and the stimulated gain, since in most power spectrum results the accepted gain had high efficiency in comparison to the stimulated gain we can see that they are basically in the same magnitude in the gain conversion. And to finalize we can see that the highest in magnitude quantity would be the TPR gain.

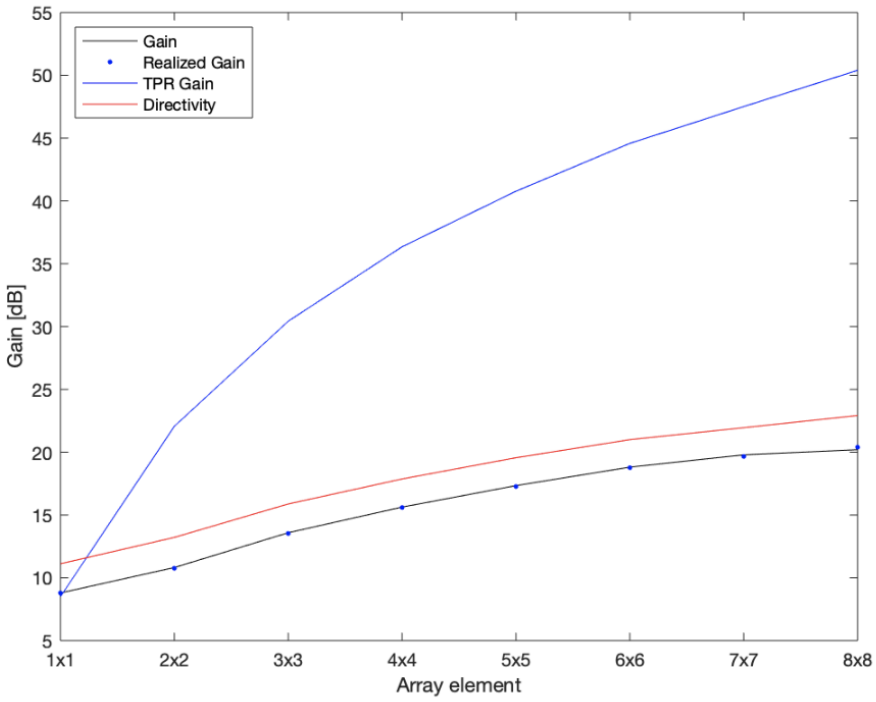

Figure 5.34: Comparison of gain values across number of elements for phased array

On figure 5.34 we are comparing the behaviour of the TPR gain against the measurements of Gain, Realized Gain and Directivity retrieved from the radiation pattern results across all element phased arrays. We can see that there is a huge difference between TPR gain against all the other three measurements and that these measurements don't have a linear growth across number of elements and that the highest value that in gain results go is to 20.82 dB, for realized gain is to 20.71 dB, and of directivity is to 22.92 dB. Whereas TPR gain almost reaches 50 dB. An easy explanation of this phenomenon is because since gain, realized gain and directivity are normalized by the accepted power, stimulated power, and total radiated power respectively, they are not going to follow the common conception of linear growth in power whereas TPR does follow that conception to a certain degree (we should note that radiated power and TPR are not the same quantities and it's visible on figure 5.33). And because we had this problem for a little bit of time it was rewarding to discover the reason of this problem after taking a dive in the nomenclature of CST literature.

CHAPTER VI

PARAMETRIC STUDY OF A SINGLE ELEMENT PATCH ANTENNA

It is important to understand the relevancy of several dimensions across any structure of an antenna. The main values that we have come across as important are the length, width, thickness of substrate, feed point location, thickness of metal plates, dielectric constant, amongst other things. Knowing this would help us to optimize any future design of a patch antenna and gives us a greater understanding of both the theory and the testing.

6.1 Length's Effect on Return Signal

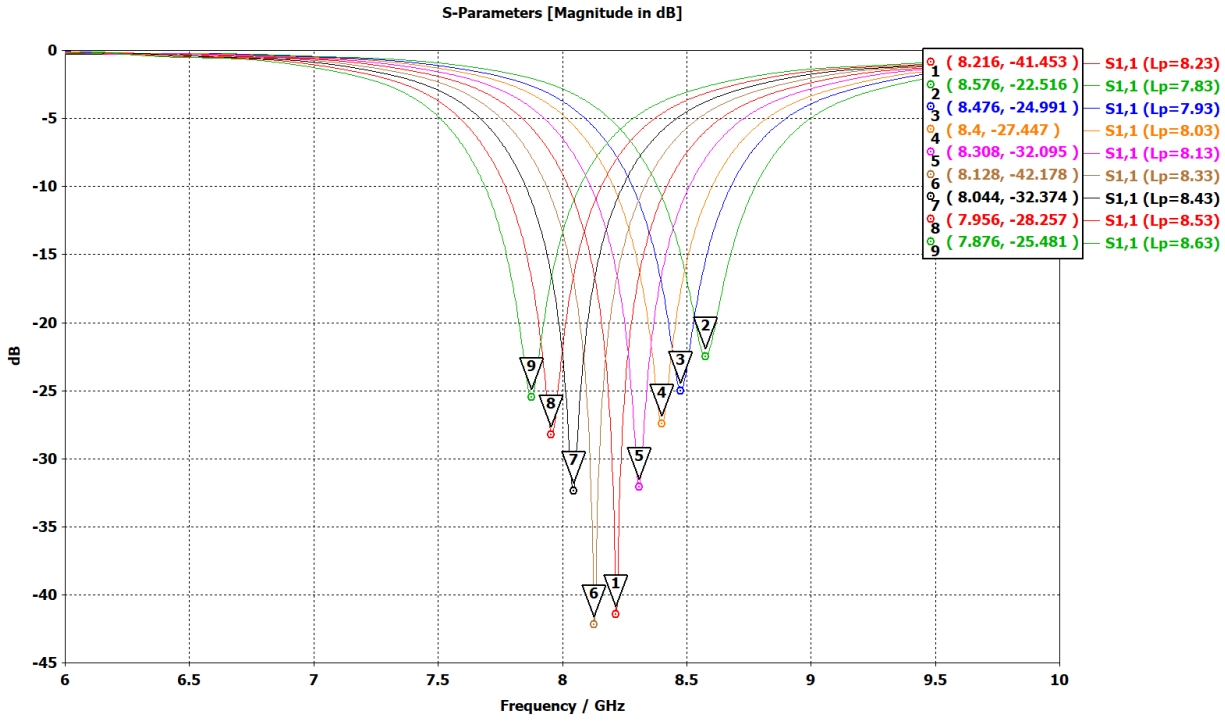

Figure 6.1: Length parametric study of a single element patch antenna.

On figure 6.1 we can observe that the length has a greater effect on the resonant frequency. The greater the length it is the smaller the resonant frequency (8.63 mm, 7.87 GHz) and the smaller the length the greater the resonant frequency (7.83 mm, 8.58 GHz). Length has also an influence on the magnitude of the return loss by having our extreme frequency data points in the lower end of it's magnitude (7.83 mm, -22.47 dB and 8.63 mm, -25.481 dB) and the center frequency data point been the highest (8.23 mm, 8.216 GHz, -41.45 dB and 8.33 mm, 8.128 GHz, -42.178 dB).

6.2 Width's Effect on Return Signal

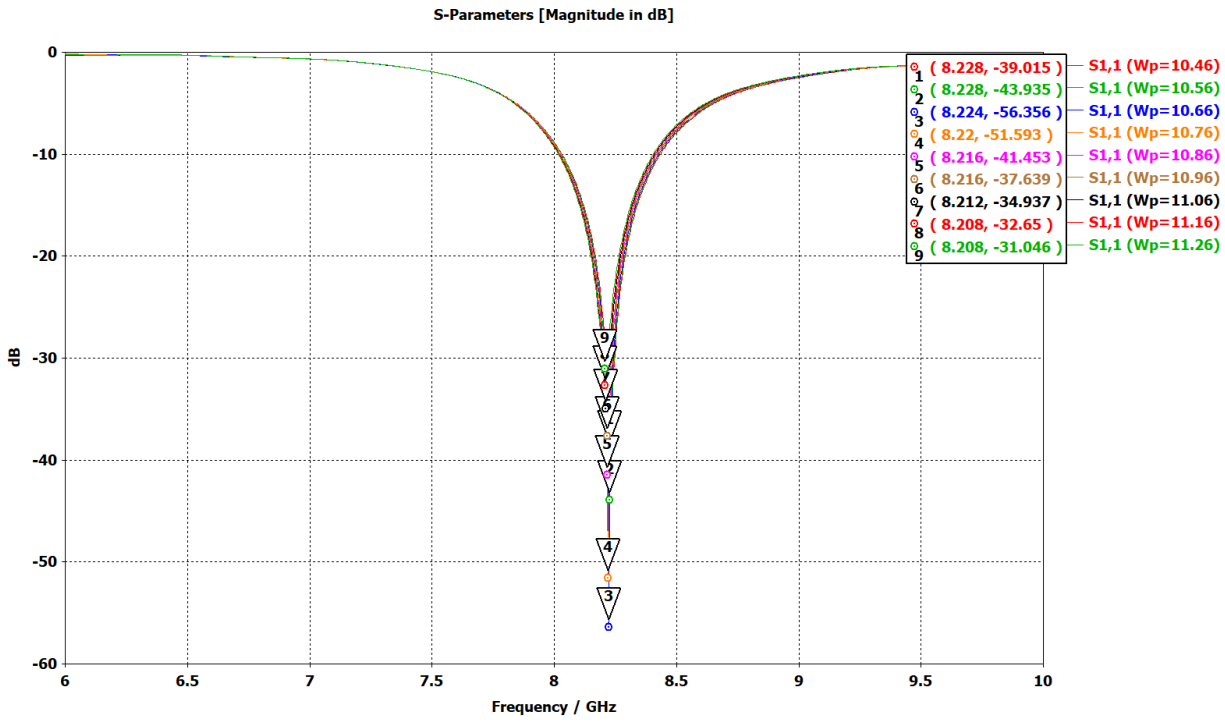

Figure 6.2: Width parametric study of a single element patch antenna.

The width's effect on the resonant frequency has a lower amount of influence in our parametric study as we can see on figure 6.2, this is due to the fact that the feed point location is located across the $\hat{y}$ axis, giving the central mode to the length instead of the width. Nevertheless, it has an effect on the magnitude of the return signal with the highest width having values of (10.66 mm, 8.224 GHz, -56.356 dB) and the lowest width value of (11.26 mm, 8.208 GHz, -31.04 dB).

6.3 Substrate thickness' Effect on Return Signal

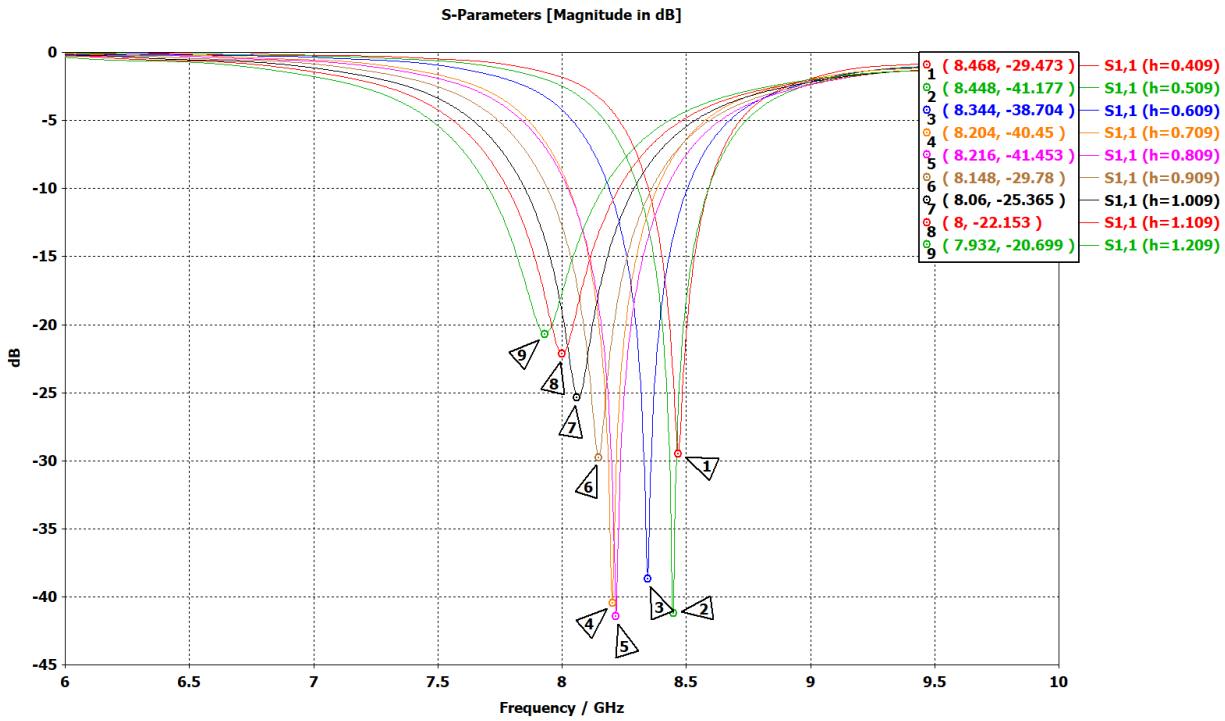

Figure 6.3: Substrate thickness parametric study of a single element patch antenna.

The thickness has also a significant influence into the resonant frequency, making us believe that in the programming of CST both thickness and length are assigned resonant modes into the simulation. Substrate thickness has also the same relationship of length for resonant frequency, as the lower the thickness the higher the resonant frequency (0.409 mm, 8.468 GHz), and the higher the thickness the lower the resonant frequency (1.209 mm, 7.932 GHz). It also has an influence in the magnitude with the highest values at the center of the data points (0.709 mm, 8.204 GHz, -40.45 dB and 0.809 mm, 8.216 GHz, -41.54 dB).

6.4 Feed Point Location Effect on Return Signal

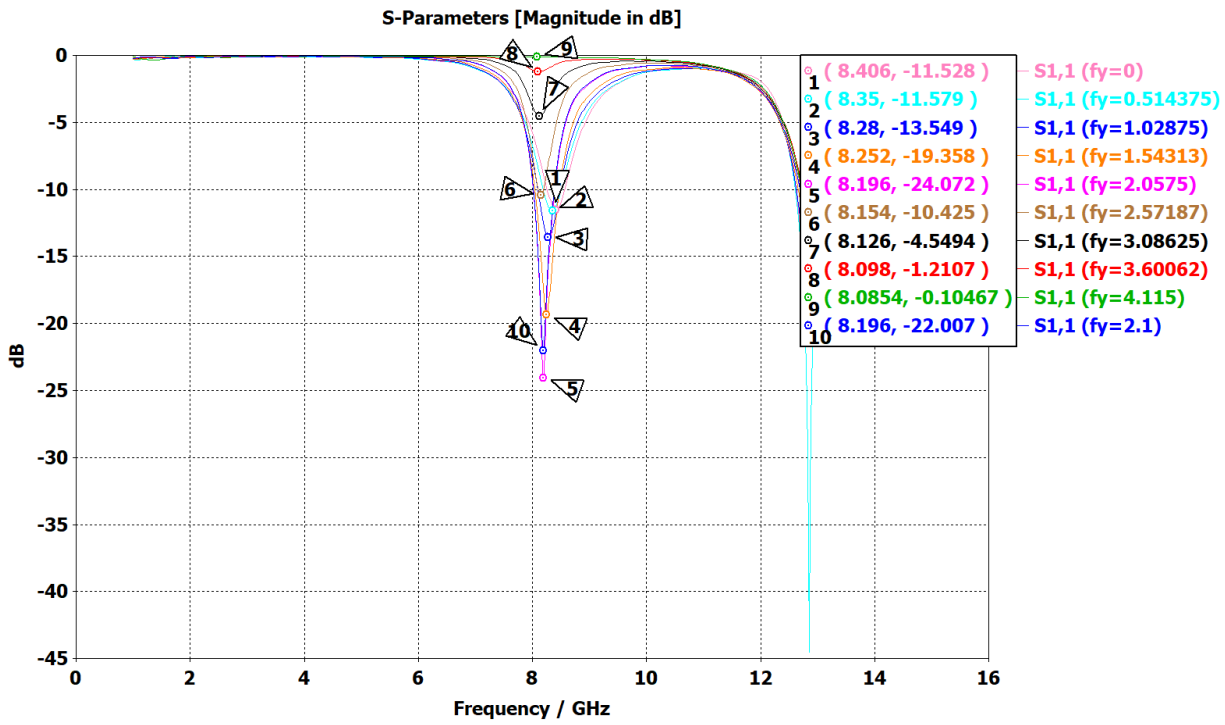

Figure 6.4: Feed point location parametric study of a single element patch antenna.

The feed point location is an interesting case of study, for one side if the feed point is located at a singular axis it would behave like the width's response, and for the other side if it's located at any quadrant, then it behaves totally different and it will be discussed in the following cases. Having a similar behaviour like the width, the feed point location has only influence on the magnitude of the return signal and in the resonant frequency response its negligent. The highest value for this parametric study is for (2.05 mm, 8.196 GHz, -24.07 dB). Having set this simulation for the feed point location starting at the edge of the patch antenna of the $\hat{y}$ or the length polarization up to the center of the patch antenna or $L/2$ we can see that it has a sinusoidal behaviour of cosine and that at the center of the antenna have an attenuated signal therefore zero output power is being transmitted. At the edge of the antenna since we have the maximum antenna's impedance and since it's not matched to the cables impedance we have some offset between the current and the voltage which is reflected at the return signal by not having as much magnitude.

6.5 Dielectric constant's Effect on Return Signal

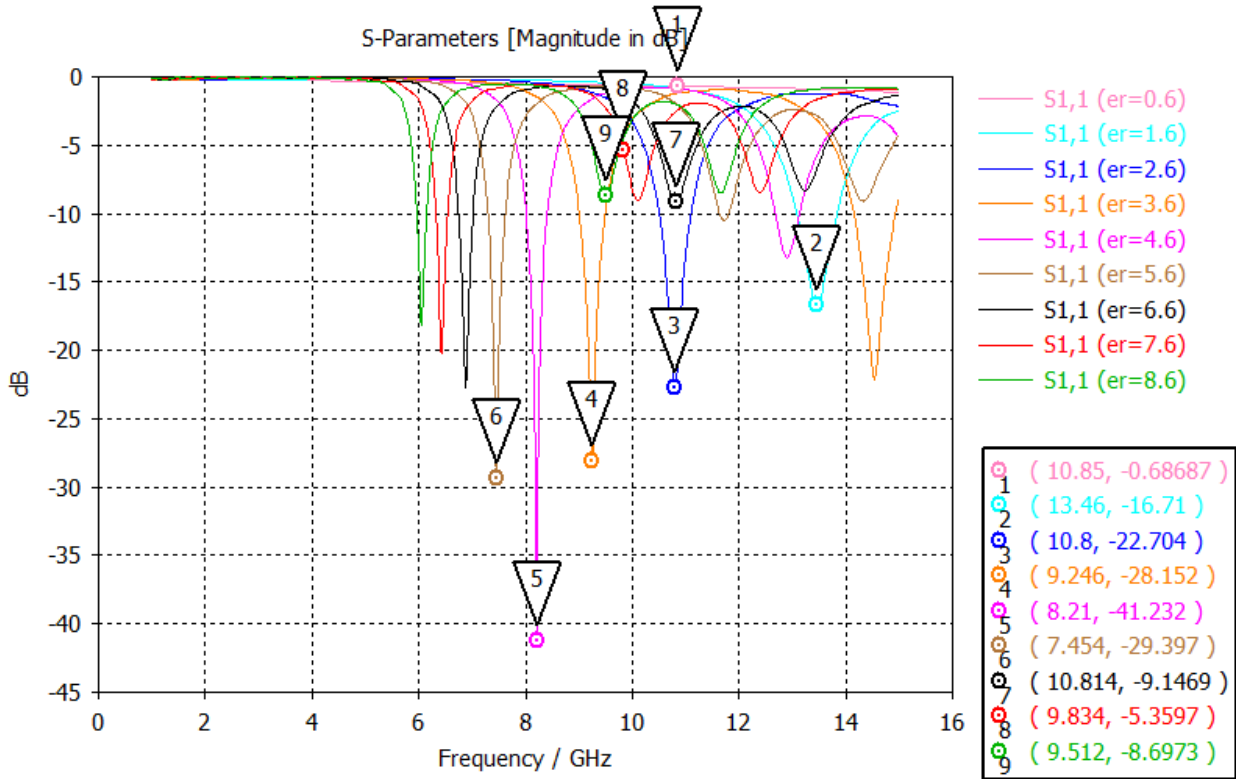

Figure 6.5: Dielectric constant parametric study of a single element patch antenna.

We can observe right away that the conventional commercial FR-4 with a dielectric constant of 4.6 has the highest magnitude of all of the other cases. However, we can note that there is an interesting effect when parametrizing the dielectric constant. Its interesting to note that the first curve with dielectric constant of 0.6 has a flat line across all frequency, meaning that it reflects all power at all frequencies making it a really bad for signal analysis. As we increase the dielectric constant we can see that the resonant frequency gets shifted towards the left until we reach our desired resonant frequency. We can also observe that for other dielectric constant other than of FR-4, there are two resonant frequencies within reasonable range.

6.6 Loss Tangent Effect on Return Signal

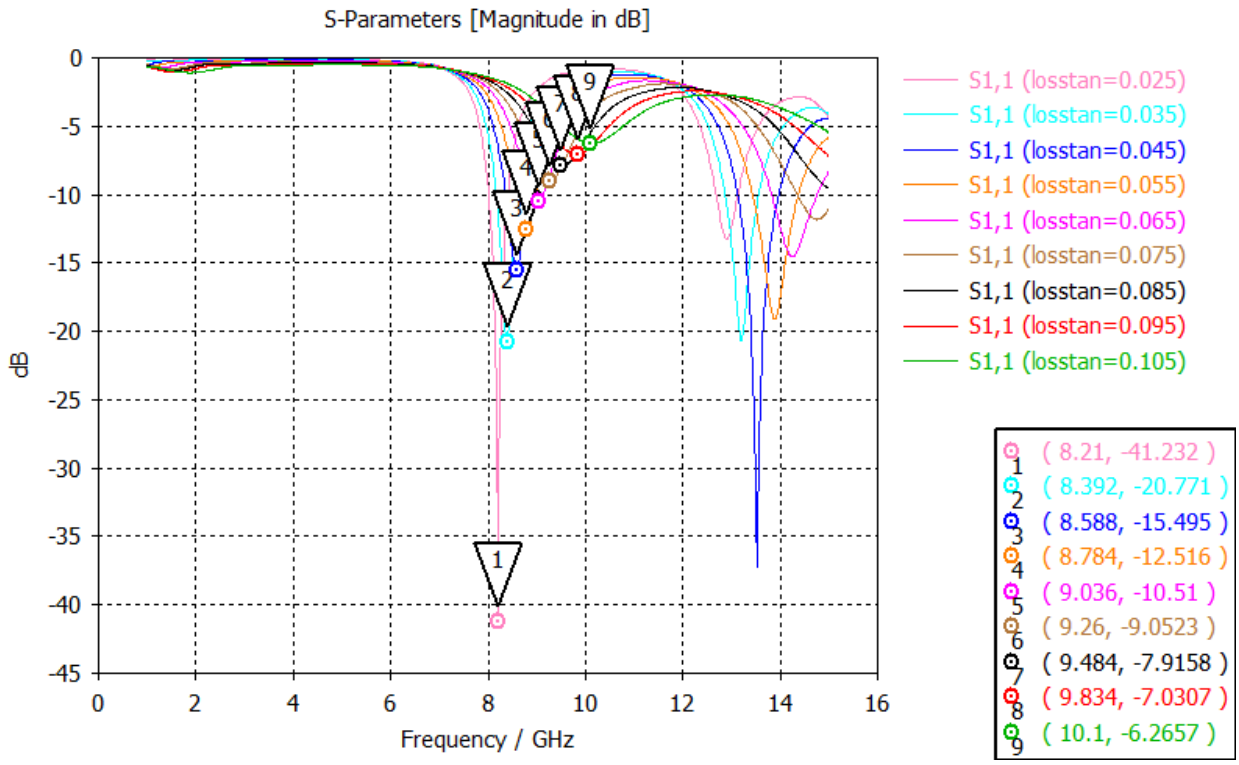

Figure 6.6: Loss tangent parametric study of a single element patch antenna.

When we are parametricing the loss tangent value we can observe that the resonant frequency gets shifted towards the right and the magnitude gets also attenuated. Interesting enough, curves other than our optimal case of 0.025, has a second resonant frequency at around 12-14 GHz.

6.7 Dual Resonant Frequency

For this subsection, we are going to parametrize the study of dual resonant frequency patch antennas by introducing several formulae for feed point location retrieved from several sources. For the $\hat{y}$ axis we are going to use the following:

$$y_{o,1} = \frac{L_p}{2\sqrt{\varepsilon_r}} \tag{6.1}$$

$$y_{o,2} = \frac{L_p}{2\sqrt{\varepsilon_{reff}(L_p)}} \tag{6.2}$$

$$y_{o,3} = \frac{L_p}{\pi} \arccos \sqrt{\frac{Z_0}{Z_{edge}}} \tag{6.3}$$

And for the $\hat{x}$ axis we are going to use the following:

$$x_{o,1} = \frac{W_p}{2\sqrt{\varepsilon_r}} \tag{6.4}$$

$$x_{o,2} = \frac{W_p}{2\sqrt{\varepsilon_{reff}}(L_p)} \tag{6.5}$$

$$x_{o,3} = \frac{W_p}{\pi} \arccos \sqrt{\frac{Z_0}{Z_{edge}}} \tag{6.6}$$

With $Z_{edge} = 90\frac{\varepsilon^2}{\varepsilon - 1}(\frac{L_p}{W_p})^2\,[\Omega]$

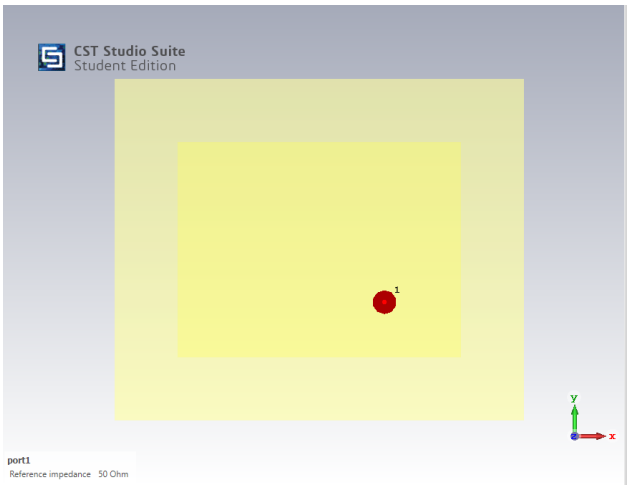

Figure 6.7: Dual resonant frequency parametric study of a single element patch antenna.

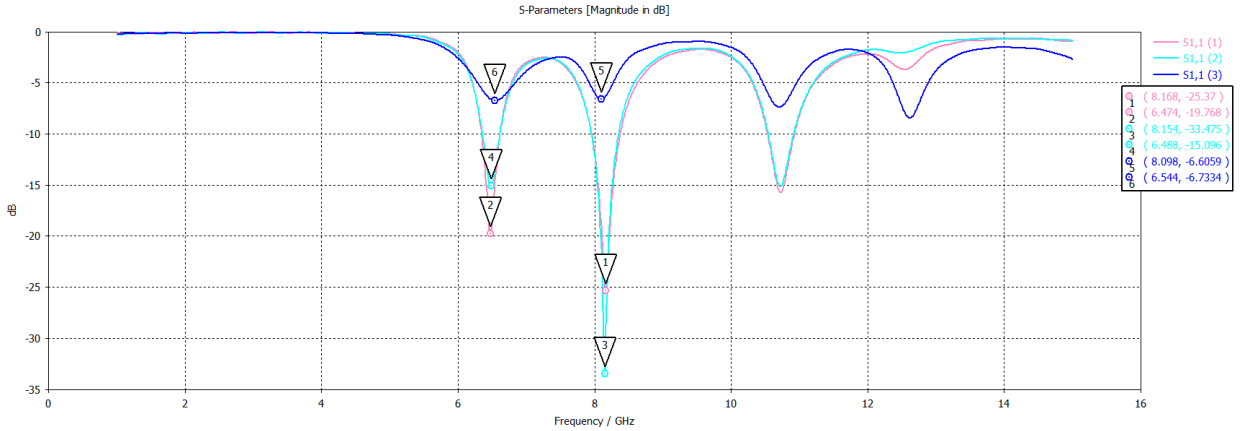

Figure 6.8: Dual resonant frequency parametric study of a single element patch antenna.

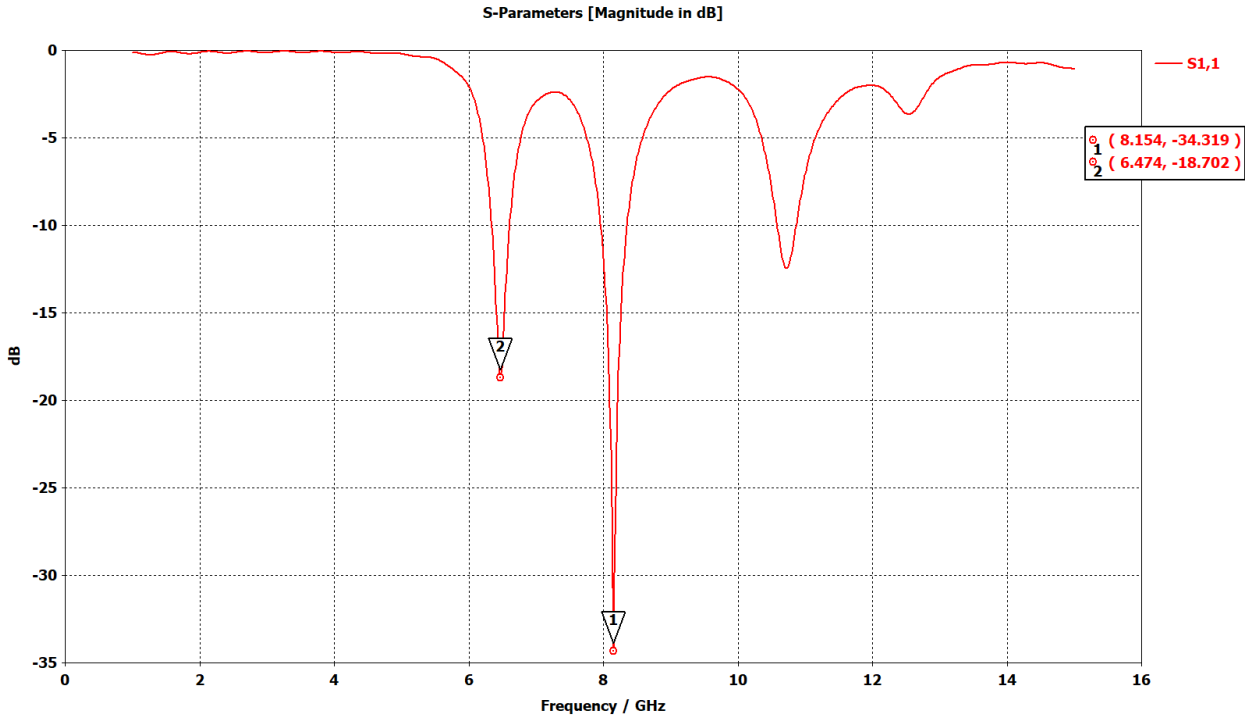

Figure 6.9: Dual resonant frequency parametric study of a single element patch antenna.

On this scenario we are going to place the feed point into the ($X1$,$Y2$) location as seen on figure 6.8. Analyzing this parametric study we can observe that 6.3 and 6.6 gives us the worst results (8.098 GHz, -25.37 dB) and (6.54 GHz, -6.73 dB) respectively. The optimal value to use for y_0 is equation 6.2 (8.154 GHz, -33.47 dB) and for x_0 the most optimal value would be using equation 6.4 (6.474 GHz, -19.768 dB). We can also observe that there are higher order of resonant modes in the result signal, proving that there are infinite number of resonant modes but the resonant frequency would be always increasing. Also we can see that by having the feed point location at a non-zero $x-y$ coordinates we get to have both the length and width polarization into a single signal.

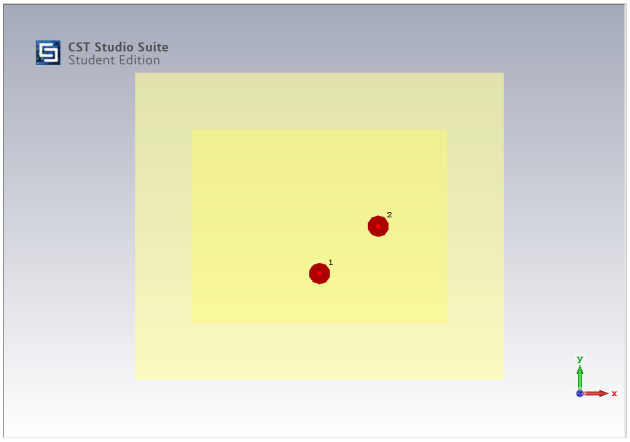

Figure 6.10: Dual resonant frequency parametric study of a single element patch antenna with two feeds.

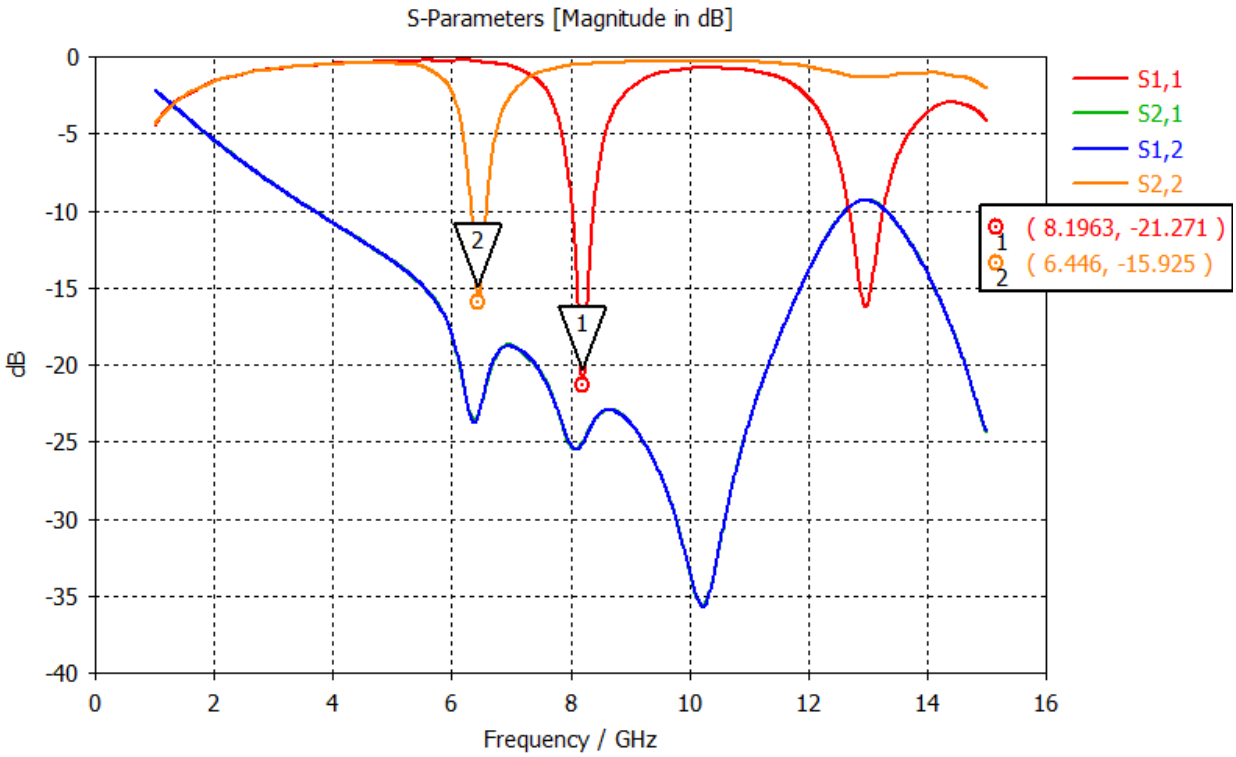

Figure 6.11: Dual resonant frequency S-Parameter parametric study of a single element patch antenna with two feeds.

This time we are going to introduce a second feed into the antenna and now we will have a system of $(0,Y_{o,2})$ and $(X_{o,1},0)$ feeds as we can observe on figure 6.10. Interesting enough we can observe that it has a similar behaviour as in the previous case but with a little less of magnitude on both feeds. On feed 1 we can see a resonant frequency of 8.19 GHz and and a magnitude of -21.27 dB. And for feed two we get a resonant frequency of 6.44 GHz and a magnitude of -15.92 dB. Since we have a system of two feeds in one antenna we get to have transmission coefficients, interesting enough both $S_{1,2}$ and $S_{2,1}$ are exactly the same. These curves represent the transmission signals going for both of these feeds and we can observe that its spectral magnitude is higher than the initial return loss signals and that it has two resonant frequencies at the same as its reflection coefficient counterparts.

CHAPTER VII

CONCLUSIONS

After retrieving the data for the two scenarios and their two sub-cases we've observed that by increasing the number of antennas into the simulation, for both scenarios, the resonant frequency is shifted to the left by a considerable amount. After doing to parametric study of a single patch antenna we were able to develop our own model to calculate the reflection coefficients of a singular patch antenna. We developed to models in which the return loss was accurately achieved. For the case of dual polarization, our needs to be refined so that we can attenuate the resonant mode reminder between our two target resonant frequencies.

Regarding the Wave Iterative Method, we think this is a promising model to do more specific and complex simulations. We found that the advantage of this model is that it reduces significantly the processing simulation time in comparison to CST and also it requires less computational power given the fact that we only used 100 pixels per simulation. This model was initially designed to work on IRIS antenna type so our contribution to this was to make it suitable for a patch antenna.

From the literature we found on this particular model we found some discrepancies between sources in how to approach this model, so we decided to make a combination of several sources to make our own variant. We were able to achieve the central goal of having an efficient return loss plot and surface plots of electric field and current distribution. From these we have two versions using different diffraction operators and we were able to see the importance if this metric.

We are excited for our future work for this investigation, our future tasks would be to upgrade the Wave Iterative Method to include transmission coefficients, and 2D/3D results for a phased array. We believe that to achieve that the diffraction operator is essential given the fact that it covers the geometrical information if the phased array.

BIBLIOGRAPHY

[1] . C. S. AKATIMAGOOL, S., *Wave iterative method for electromagnetic simulation.*, (2013).

[2] T. . B. H. AYARI, M.;AGUILI, *More efficiency of transverse wave approach (twa) by applying an-isotropic mesh technique (amt) for full-wave analysis of microwave planar structures.*, (2009).

[3] C. A. BALANIS, *Antenna Theory: Analysis and Design, 3rd Edition*, 2005.

[4] H. BAUDRAND, *The wave concept in electromagnetism and circuits: Theory and applications.*, 2016.

[5] P. BEVELACQUA, *Antenna theory*, 2009.

[6] S. BYRNES, *Most basic use of an impedance smith chart.*, 2012.

[7] T. GAMBLIN, *Mathematical construction and properties of the smith chart*, 2015.

[8] R. GARG, *Microstrip Antenna Design Handbook*, 2001.

[9] H. B. H. HAJLAOUI, A.; TRABELSI, *Periodic planar multilayered substrates analysis using wave concept iterative process.*, (2012).

[10] H. G. A. B. H. HAJLAOUI, A.; TRABELSI, *Analysis of novel dual-resonant and dual-polarized frequency selective surface using periodic contribution of wave concept iterative process: Ppms-wcip.*, (2003).

[11] P. INC., *Coaxial cable*, N.A.

[12] N. A. T. B. H. JARBOUA, I.; AMMAR, *Radiation pattern and scattering parameter for multilayer cylindrical loop antenna using the iterative method wcip.*, (2019).

[13] A. G. A. B. H. KADDOUR, M.; MAMI, *Analysis of multilayered microstrip antennas by using iterative method.*, (2003).

[14] T. NADER, *Microstrip patch antenna*, 2012.

[15] I. S. . A. S. NUANGPIROM, P., *Wave iterative method for patch antenna analysis.*, (2015).

[16] D. ORBAN, *The basics of patch antennas*, (2005).

[17] V. PARAFOROU, *Design and full-wave analysis of supershaped patch antennas*.

[18] I. N. P. A. S. SURASAK, I.; NATTAPONG, *The development of fast modal fourier transform for electromagnetic wave iterative computation.*, (2017).

[19] K. TAYLOR, *S-parameters, an introduction*, 2006.

[20] A. D. F. B. H. TITAOUINE, M.; GOMES, *Analysis of frequency selective surface on isotropic/anisotropic layers using wcip method.*, (2007).

[21] ——, *Analysis of shorted ring slots frequency selective surfaces using wcip method*, (2008).

[22] A. B. H. TRABELSI, H.; GHARSHALLAH, *Efficient analysis of via hole grounds by using the iterative method*, (2004).

BIOGRAPHICAL SKETCH

Luis Mario Bres Castro was awarded his Master of Science in Physics from the University of Texas Rio Grande Valley in May 2021. Luis completed his Bachelor's Degree of Science in Physics at the University of Texas Rio Grande Valley in December 2018. Throughout his academic career Luis was part of the internship at the National Radio Astronomy Observatory. Luis was part of the Arecibo Remote Command Center for over 5 years where he has worked in antenna simulation research.

To contact email: luis.bres95@gmail.com